SHARING

SELF-ORGANIZED HETEROGENEOUS ADVANCED RADIO NETWORKS GENERATION

D5.3

Performance assessment and comparison of the most promising techniques in relay-aided networks

Date of delivery	XX/XX/201X
Contractual date of delivery	31/12/2015
Project number	C2012/1-8
Editor(s)	Raymond Knopp (EUR), Hicham Anouar (TCS)
Author(s)	Dorin Panaitopol (TCS), Hicham Anouar (TCS), Antonio Cipriano (TCS), Jean-Marc Conrat (OLABS), Issam MAAZ (OLABS), Yi Yuan (OLABS), Zeina Mheich (CEA), Valentin Savin (CEA), Martina Cardone (Eurecom), Raymond Knopp (Eurecom), Robin Thomas (Eurecom)
Dissemination level	PU
Workpackage	5
Version	1.0
Total number of pages	105

Abstract:

This deliverable has two objectives. The first one is to compile the simulation results obtained after the deliveries of D5.1 and D5.2. The second objective is to compare the most promising innovations of each task in WP5 in order to identify the one that would best fit in some specific scenarios. In particular, we first identify two Layer 1 collaborative relaying strategies for standardization of 5G cellular networks. We then consider two innovations for improving spectral-efficiency in clustered multi-hop networks: two-way relaying strategies for bi-directional services and opportunistic scheduling. We then consider propagation measurements for realistic relay deployments which are coupled with numerical analysis of throughput and coverage extensions improvements provided by relay deployment. Finally, we consider simulation results for the novel D2D resource allocation strategies introduced in D5.2.

Keywords: Physical Layer Relaying, LDPC, Clustered-Multihop Networks, Opportunistic Scheduling, Channel Measurements, D2D communications.

Document Revision History

Version	Date	Author	Summary of main changes
0.1	16/12/15	Hicham Anouar (TCS)	Creation of the Table of Contents (ToC) and content from TCS on T5.3
0.2	13/01/16	Hicham Anouar (TCS)	Add of sections 2.1, 2.2 and 2.4
0.3	29/01/16	Jean-Marc Conrat (Orange)	Add sections 2.5
0.4	01/02/16	R Knopp (EURE)	Section 2.2, Reformatting of entire document, Introduction and conclusion, Abstract, Executive Summary
0.5	05/02/16	C. Conrat (Orange)	Moved references from Section 2.5 to end
0.6	06/02/16	R. Knopp (EURE)	Cleaned up global references (removed irrelevant ones)
0.7	8/02/2016	S.Mayrargue (CEA)	Add Section 2.3
0.8	10/02/2016	R. Knopp (EURE)	Add Section 3.1, updates to Executive Summary, Introduction, conclusion
0.9	11/02/2016	D. Panaitopol (TCS)	Minor updates in Section 3

TABLE OF CONTENTS

LIST OF FIGURES

LIST OF TABLES

EXECUTIVE SUMMARY

This deliverable compiles the simulation results obtained after the deliveries of D5.1 and D5.2. In addition, it also compares the most promising innovations of each task in WP5 in order to identify the one that would best fit in some specific scenarios.

We begin with Advanced Relaying techniques starting with physical layer relaying in where the performance of a novel cooperative coding scheme to communicate efficiently over multiple-relay fading channels is presented. The particularity of the approach is to rely on non-binary Low Density Parity Check (LDPC) codes at the source, coupled with non-binary repetition codes at the relays. A simple joint decoding strategy is used at the receiver end, so that the decoding complexity is not increased compared to a system without relays, while preserving the coding gain brought by re-encoding the signal at the relays. We show by simulations that the proposed scheme allows maintaining a constant gap to the outage probability of the cooperative system, irrespective of the number of relays. We then recall a three-message half-duplex single-relay scheme described in D5.1 whose key characteristic, in comparison to the one that is currently standardized by 3GPP for 4G, is firstly the use of physical-layer relaying. The relay station decodes information in a first phase and collaboratively aids the transmission with the source in the second phase. In LTE, multi-round transmission using HARQ is already the standard means for transmission and the method here simply puts the relay into the protocol. Secondly, in D5.1 we showed that the distributed three-message superposition coding approach used in the novel scheme achieves full degrees of freedom with half-duplex relaying. We provide new simulation results for dual-antenna receivers using more realistic channel models. We show that capacity is close to double in all cases in comparison to the current relaying strategy standardized (but unused) by 3GPP for 4G. As a main conclusion, we suggest that relaying such as this be reconsidered during the standardization phase of 5G. To this end, we discuss consequences on low-layer signalling requirements. Lastly, we investigate a code-dependent unequal power allocation method for Gaussian channels using irregular LDPC codes. This method allocates the power for each set of coded bits depending on the degree of their equivalent variable nodes. We propose a new algorithm to optimize the power allocation vector using density evolution algorithm under the Gaussian approximation. We show that unequal power allocation can bring noticeable gains on the threshold of some irregular LDPC codes with respect to the classical equal power allocation method depending on the code and the maximum number of decoding iterations.

We then switch to clustered mesh networks for Professional Mobile Radio (PMR) systems. In this context, in the particular case of fast deployable systems e.g. for crisis management, there can be absence of wired backhaul between the cells, called here clusters, and hence inter-cluster communications are taken in charge by some relay nodes called bridging mesh routers (MR). Since the back-bone traffic is going through those relay nodes, and part of it may be bidirectional, a two-way relaying (TWR) technique was investigated. Many works have been done in the open literature on the two-way relaying technique which promises interesting throughput gains. Here we are interested in comparing it to a more traditional decode-and-forward strategy in two main deployment scenarios, a small town with low buildings and a more populated city with higher buildings. The aim is to understand when it is worth considering using TWR. To this end, TWR is compared with a traditional Decode-and-Forward strategy for two main deployment scenarios:

- A scenario with a smaller frequency bandwidth for MR, a larger inter-site distance (ISD) and a lower location variability (corresponding to a smaller city for example, with lower number of users and lower roof-top height);
- A scenario with a larger frequency bandwidth for MR, a smaller ISD and a higher location variability (corresponding to a more populated city for example, with higher number of users and higher roof-top height – predominant NLOS scenario).

These categories have been defined by taking into account architecture opportunities and real-deployment situations. Real 3GPP and ITU parameters and system constraints have been also considered: the 700 MHz band was considered for simulations since it is one of the main candidate bands for deployment of the future broadband PMR networks. Scenarios A and B show that TWR provides better throughput than DF, for any possible position of a MR. TWR typically doubles the throughput at the best MR position. In scenario A, TWR achieves significant throughput gains only for certain distances (typically the MR must be placed in between the served nodes). However, for more

dense urban deployments like scenario B, throughput gains are weakly sensitive to the MR position, which is a desired feature in rapidly deployable PMR systems. It is also shown that DF is more robust than TWR in terms of end-to-end PER (e.g. DF has better or equal PER than TWR, depending on the MR position). A best-case scenario for a PMR deployment in the case of voice services is also considered. In this case it is showed that for long-distance robust communications (e.g. up to 5 km) where maximum limit for the achievable throughput is not of interest, the DF technique is an interesting approach.

Resource allocation for multi-hop communications inside a cell or cluster is considered for applications to PMR context. In PMR systems relaying and direct communications between users are features which are particularly appreciated by the customers since they are included by the legacy PMR standards. In this section a wireless communication system consisting in a single cluster having multiple users is considered. The study focus on efficient and fair opportunistic scheduling of delay tolerant traffics in clustered/cellular environment with dynamic relaying. A wide range of nowadays applications generate this type of traffic, i.e. email, internet browsing, asynchronous file transfer, etc. They are generally classed as requiring a best effort service and give more flexibility to the system to handle them. The work extends three traditional scheduling policies to this new framework. In order to differentiate the impact of relaying on performance a comparison is made among the case when all the communications pass mandatorily through the base station (also named cluster head in mesh deployments), which is the standard cellular configuration, the case in which also direct communications between users are allowed, and finally the case in which any user can be a relay.

We compare the performance of relay-assisted communication in terms of throughput with the capacity of the direct link using empirical path loss models and measured values. The measurements are based on an extensive campaign extracted previously. One set of measurements is focused on the backhaul link whereas another on the access link. The comparison between relay-assisted and direct communication is performed for different relay antenna heights and positions. The paper is divided in main parts, firstly it describes the simulation setup and secondly reports on simulation results to provide significant conclusions on relay deployment with decode-and-forward relaying namely that the direct link capacity can be improved by a relay-assisted communication when a full-duplex relay technology is used. No significant improved with simple decode-and-forward half-duplex relays. The capacity gain provided by the relay reaches more than 30 % depending on the antenna relay height and location. The analysis assumed omnidirectional antenna at RS and was performed at 2.2 GHz. Future work will analyse the frequency dependency of relay performances. Higher frequencies would allow the use of antenna array with a limited physical size but able to generate high gain directional beam enhancing the backhaul and access link capacities. But the actual benefits of directional antennas depend on the received signal spatial distribution.

We provide extensive simulation results for some of the resource allocation strategies described in D5.2 with respect to D2D communications where we provided a feasibility study of cellular-D2D reuse of radio resource, i.e. simultaneous use for cellular and D2D links, in the context of an LTE network. W review the results of simulations based on real constraints from recent 3GPP standardization activities. This work investigates the conditions for such an allocation scheme to serve the expected Quality of Service (QoS) on both cellular and D2D links. Interference constraints have to be identified and new interference control techniques have to be implemented along with a possible associated LTE system design.

1 INTRODUCTION

This deliverable concerns results has two objectives. Firstly is to compile the simulation results obtained after the deliveries of D5.1 and D5.2. The second objective is to compare the most promising innovations of each task in WP5 in order to identify the one that would best fit in some specific scenarios.

Section 2 is devoted to Advanced Relaying techniques. We first start with physical layer relaying in section 2.1 where the performance of a novel cooperative coding scheme to communicate efficiently over multiple-relay fading channels is presented. The particularity of the approach is to rely on non-binary Low Density Parity Check (LDPC) codes at the source, coupled with non-binary repetition codes at the relays. A simple joint decoding strategy is used at the receiver end, so that the decoding complexity is not increased compared to a system without relays, while preserving the coding gain brought by re-encoding the signal at the relays. We show by simulations that the proposed scheme allows maintaining a constant gap to the outage probability of the cooperative system, irrespective of the number of relays.

In Section 2.1, we investigate an unequal power allocation scheme for irregular LDPC codes. We give unequal power to different bits within same variable node degree in the Tanner graph of the irregular LDPC code and investigate the code's asymptotic performance using density evolution algorithm. The power allocation vector is chosen in order to maximize the noise threshold of the irregular LDPC code family. We propose an algorithm to solve this optimization algorithm, which is based on a modified density evolution algorithm using Gaussian approximation. We compare between the performances of unequal power allocation with that of equal power allocation for point-to-point channel and relay channel.

Section 2.2 recalls the single-relay scheme described in D5.1 whose key characteristic, in comparison to the one that is currently standardized by 3GPP for 4G, is firstly the use of physical-layer relaying. The relay station decodes information in a first phase and collaboratively aids the transmission with the source in the second phase. In LTE, multi-round transmission using HARQ is already the standard means for transmission and the method here simply puts the relay into the protocol. Secondly, in D5.1 and more completely in [6] we showed that the distributed three-message superposition coding approach used in the novel scheme achieves full degrees of freedom with half-duplex relaying. Here we provide new simulation results for dual-antenna receivers using more realistic channel models. We show that capacity is close to double in all cases in comparison to the current relaying strategy standardized (but unused) by 3GPP for 4G. We provide conclusions regarding the applicability of these results for 5G standardization and described some consequences on low-layer signaling requirements.

In Section 2.3, we investigate a code-dependent unequal power allocation method for Gaussian channels using irregular LDPC codes. This method allocates the power for each set of coded bits depending on the degree of their equivalent variable nodes. We propose a new algorithm to optimize the power allocation vector using density evolution algorithm under the Gaussian approximation. We show that unequal power allocation can bring noticeable gains on the threshold of some irregular LDPC codes with respect to the classical equal power allocation method depending on the code and the maximum number of decoding iterations.

Section 2.4 focuses on clustered mesh networks for PMR systems. In this context, in the particular case of fast deployable systems e.g. for crisis management, there can be absence of wired backhaul between the cells, called here clusters, and hence inter-cluster communications are taken in charge by some relay nodes called bridging mesh routers. Since the back-bone traffic is going through those relay nodes, and part of it may be bidirectional, a two-way relaying technique was investigated. Many works have been done in the open literature on the two-way relaying technique which promises interesting throughput gains. Here we are interested in comparing it to a more traditional decode-and-forward strategy in two main deployment scenarios, a small town with low buildings and a more populated city with higher buildings. The aim is to understand when it is worth considering using two-way relaying.

Section 2.5 deals with resource allocation for multi-hop communications inside a cell or cluster, for applications to PMR context. In PMR systems relaying and direct communications between users are features which are particularly appreciated by the customers since they are included by the legacy PMR standards. A wireless communication system consisting in a single cluster having multiple users is considered. The study focus on efficient and fair opportunistic scheduling of delay tolerant traffics in

clustered/cellular environment with dynamic relaying. A wide range of nowadays applications generate this type of traffic, i.e. email, internet browsing, asynchronous file transfer, etc. They are generally classed as requiring a best effort service and give more flexibility to the system to handle them. The work extends three traditional scheduling policies to this new framework. In order to differentiate the impact of relaying on performance a comparison is made among the case when all the communications pass mandatorily through the base station (also named cluster head in mesh deployments), which is the standard cellular configuration, the case in which also direct communications between users are allowed, and finally the case in which any user can be a relay. The joint scheduling and relaying is based on a dynamic max-min decision rule of the best relay for different opportunistic schedulers. The considered opportunistic schedulers are Multiuser Diversity Scheduling (MUDS), Proportionally Fair Scheduling (PFS), and Maximum Proportionally Fair Scheduling (MPFS). Simulation results show that increasing the number of possible relays increases the spectral efficiency of the three schemes and help also enhancing the fairness of PFS and MPFS.

The final contribution on advanced relaying in Section 2.5 compares relay-assisted communication throughput with the throughput provided by the direct link using empirical data collected from an extensive measurement campaign. Path loss models or measured values used for the analysis are derived from the measurements. One set of measurements is focused on the backhaul link whereas another on the access link. The comparison between relay-assisted and direct communication is performed for different relay antenna heights and positions.

In Section 3 we provide extensive simulation results for some of the resource allocation strategies described in D5.2 with respect to D2D communications where we provided a feasibility study of cellular-D2D reuse of radio resource, i.e. simultaneous use for cellular and D2D links, in the context of an LTE network. W review the results of simulations based on real constraints from recent 3GPP standardization activities. This work investigates the conditions for such an allocation scheme to serve the expected Quality of Service (QoS) on both cellular and D2D links. Interference constraints have to be identified and new interference control techniques have to be implemented along with a possible associated LTE system design.

2 ADVANCED RELAYING TECHNIQUES

Section 2.1 presents updated results for the cooperative coding scheme to communicate efficiently over multiple-relay fading channels with applications to OFDM or narrowband communications studied in D5.1. The presented approach couples non-binary Low Density Parity Check (LDPC) codes at the source with non-binary repetition codes at the relays. When the number of relays increases, the existing methods suffer from a large increase of decoding complexity, while the coding gain they present becomes increasingly less important. Here, the final goal is to avoid the previous drawbacks by proposing an effective yet computationally affordable relaying and coding / decoding strategy.

2.1 Non-binary LDPC code design for multi-relay scenarios

In this section, the performances of a novel cooperative coding scheme to communicate efficiently over multiple-relay fading channels are presented. The particularity of the approach is to rely on non-binary Low Density Parity Check (LDPC) codes at the source, coupled with non-binary repetition codes at the relays. A simple joint decoding strategy is used at the receiver end, so that the decoding complexity is not increased compared to a system without relays, while preserving the coding gain brought by re-encoding the signal at the relays. We show by simulations that the proposed scheme allows maintaining a constant gap to the outage probability of the cooperative system, irrespective of the number of relays.

2.1.1 Non-Binary LDPC Codes and Decoding

We denote by GF(q) the Galois field with q elements. A NB-LDPC code is defined by a sparse parity-check matrix H, with M rows and N columns, whose entries are taken from GF(q). We shall assume that H is full rank, hence the coding rate is $R = K/N$, where $K = N - M$ is the number of source symbols. A NB-LDPC code can be advantageously represented by a bipartite (Tanner) graph containing N symbol-nodes and M constraint-nodes, associated respectively with the N columns and M rows of H. A symbol-node and a constraint-node are connected by an edge if and only if the corresponding entry of H is non-zero. Each edge of the graph is further assumed to be "labelled" by the corresponding non-zero entry.

The Belief-Propagation (BP) decoding passes messages along the edges of the graph, in both directions, which are iteratively updated by Bayesian rules. In the non-binary case, each message is a probability distribution vector on GF(q), which gives the probabilities of the incident symbol-node being equal to each of its possible values. These probability distributions are iteratively updated until a codeword has been found or a maximum number of iterations has been reached.

2.1.2 Cooperative System Description

We assume that the source broadcasts a NB-LDPC codeword to the destination and a given number N_r of relays. Parameters of the different links in the system will be indicated by using subscripts SD, SR_i, and R_iD, with obvious meaning. We assume QAM signalling constellations of order M_{SD}, M_{SR_i}, and $M_{\mathrm{R}_i\mathrm{D}}$. Since relays and destination receive the same modulated signal broadcasted by the source, we have by construction $M_{\mathrm{SD}} = M_{\mathrm{SR}_i}$, $\forall i = 1,\ldots,N_r$.

Our cooperative coding scheme, depicted in Figure 1. In the case of two relays, can be described as follows:

[S] The source encodes the packet of information bits, generating a NB-LDPC codeword c (red filled circles in Figure 1). It modulates c with the M_{SD}-QAM constellation and broadcasts the modulated symbols x to both relays and destination.

[R_i] Each relay R_i decodes the received signal, so that to correct the transmission errors on c. If decoding fails (e.g. using a CRC check or with syndrome check inside the LDPC decoder), the relay does not transmit any information to the destination. Otherwise, it generates a new sequence $c^{(i)}$ of non-binary symbols using the *non-binary repetition* coding (blue or green filled circles in Figure 1). Vector $c^{(i)}$ needs not be of the same size as the original codeword c, since the coding rates

for the links relay-destination are typically higher. The vector $c^{(i)}$ is modulated using the $M_{\mathrm{R}_i\mathrm{D}}$-QAM constellation, and the modulated symbols $x^{(i)}$ are then sent to the destination.

[D] The destination receives noisy versions of x and $x^{(i)}$ (from both source and relays), and performs a joint iterative decoding using only the parity check matrix *H* of the NB-LDPC code broadcasted by the source.

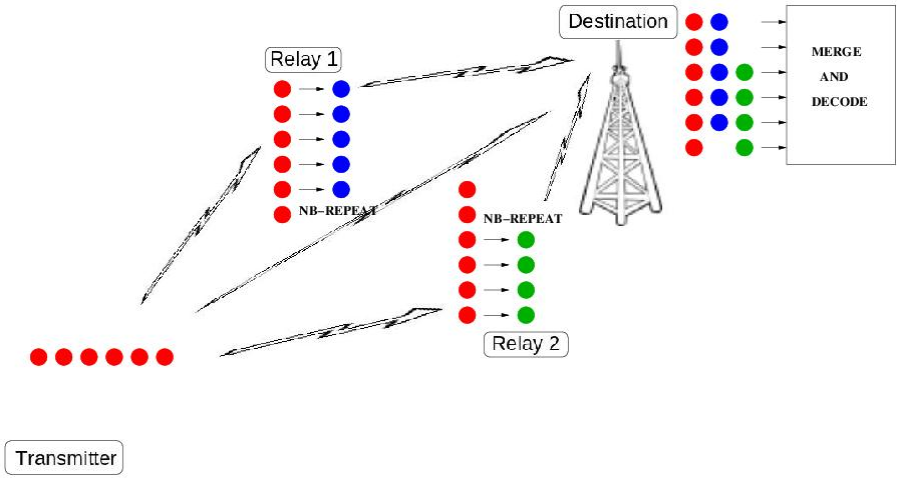

Figure 1: Cooperative coding using non-binary repetition coding. Circles: symbols transmitted by the source or the relays; Red: symbols of the source; Blue: symbols of the first relay (NB-repetition versions of all or part of the red symbols); Green: as above, but for the second relay.

2.1.3 Performance Evaluation

2.1.3.1 Cooperation scenario

The performance of the proposed cooperative coding scheme has been assessed by Monte-Carlo simulations under the following scenario. The source broadcasts a NB-LDPC code with $N = 2K$ (rate $K = 1/2$). Each relay decodes the received signal, then computes an exact number of *K* non-binary repetition symbols, which are sent to the destination. Whether the relays operate in the half-duplex or in the full-duplex mode is out of the scope of this work, however we mention that in our cooperation scenario both modes are possible. We consider that the source and the relays use multicarrier modulation with Orthogonal Frequency-Division Multiplexing (OFDM), and that the different signals, from the source and the relays, can be separated at the destination. This can be done by using different multiple access methods, in which the source and the relays are separated either in time, in frequency, or by using spatial diversity. Finally, we shall further assume that the signals transmitted by the source and the relays use the same QAM modulation, hence $M_{\mathrm{SD}} = M_{\mathrm{R}_i\mathrm{D}}$, and the transmission of the *N* coded symbols at the source and of the *K* non-binary repetition symbols at the relays takes the same period of time. Therefore, we assume that the source transmits on two frequency Physical Resource Blocks (PRBs), while each relay transmits on one separate frequency PRB (as a side note, notice that the number of relays is limited by the number of PRBs). In case of Spatial Division Multiple Access (SDMA), relays can transmit in any of the frequency PRB allocated to the source, which ensures an efficient use of the frequency spectrum.

According to the above scenario, the wireless channels can be modelled as block-fading channels, with flat Rayleigh fading, constant on each block and i.i.d. on different. The *N* coded symbols broadcasted by the source span two fading blocks, while the *K* repetition symbols transmitted by each relay span exactly one fading-block. Consequently, the number of fading blocks is given by $n_f = 2 + N_r$. For each fading block $j = 1, \ldots, n_f$, the baseband equivalent channel model is given by:

$$y_i^{(j)} = \sqrt{\rho^{(j)}}\, f^{(j)} x_i^{(j)} + z_i^{(j)},$$

where $x_i^{(j)}$ and $y_i^{(j)}$ denote the i^{th} QAM symbol transmitted in block *j* and the corresponding received symbol, $f^{(j)}$ is the fading coefficient of block *j*, and $z_i^{(j)} \approx CN(0,1)$ is the i.i.d. circular complex Gaussian noise. We assume that the QAM-constellation has unit energy and that the fading is normalized on each block, *i.e.* $\mathrm{E}\left[|f^{(j)}|^2 \right]=1$. It follows that $\rho^{(j)}$ is the average received SNR on block *j*, thus, $\rho^{(1)} = \rho^{(2)} = \mathrm{SNR}_{\mathrm{SD}}$ and $\rho^{(2+i)} = \mathrm{SNR}_{\mathrm{R}_i\mathrm{D}}$. We shall assume that $\rho^{(j)}$ and $f^{(j)}$ are perfectly known at the receiver.

For a given set of SNR values $\boldsymbol{\rho} = (\rho^{(1)},\ldots,\rho^{(n_f)})$, we denote by $I_{\boldsymbol{\rho}}(\mathbf{f})$ the mutual information between channel input and output, assuming that the fading coefficients are given by $\mathbf{f} = (f^{(1)},\ldots,f^{(n_f)})$ and that the channel input is uniformly distributed over the complex QAM constellation. Hence, $I_{\boldsymbol{\rho}}(\mathbf{f})$ takes values in $[0,m]$, where $m = \log_2(M_{\mathrm{SD}}) = \log_2(M_{\mathrm{R}_i\mathrm{D}})$ is the number of bits per QAM symbol. Let R_d be the *overall coding rate* of the cooperative system, defined as the ratio between the number of information symbols *K* and the number of non-binary symbols received at the destination both from the source and the relays. According to the previous settings $R_d = 1/n_f$. The *outage probability*, given by:

$$P_{out}(\boldsymbol{\rho}, R_d) = \Pr\left(I_{\boldsymbol{\rho}}(\mathbf{f}) < mR_d \right)$$

is the probability of the instantaneous mutual information $I_{\boldsymbol{\rho}}(\mathbf{f})$ being less than the information rate value mR_d. Since this probability is non-zero, it follows that the Shannon capacity of the channel is 0. As a consequence, the performance of a code over the block fading channel is usually evaluated in terms of the SNR gap to the outage probability. If this gap is maintained constant for arbitrarily large SNR values, the code is said to be *full-diversity*.

2.1.3.2 Simulation Results

A class of full-diversity LDPC codes over block-fading channels, referred to as *root-LDPC* codes, was proposed in [1]. Since the *N* coded symbols transmitted by the source span two fading blocks, for the NB-LDPC code at the source we chose a rate 1/2 root-NB-LDPC code with (d_v = 2, d_c = 2), defined over GF(64). Namely, the bipartite graph of the NB-LDPC code was designed according to the approach proposed in [1], while the non-zero entries on each row of the parity-check matrix were randomly selected among the four sets of "best rows" given in Table 1. The code has *K* = 50 information symbols, corresponding to 300 information bits.

Table 1: Best rows with $d_c = 4$, for GF(64) and GF(256)

GF(64)	$(\alpha^0,\alpha^9,\alpha^{26},\alpha^{46})$	$(\alpha^0,\alpha^{17},\alpha^{26},\alpha^{43})$	$(\alpha^0,\alpha^{17},\alpha^{37},\alpha^{54})$	$(\alpha^0,\alpha^{20},\alpha^{37},\alpha^{46})$
GF(256)	$(\alpha^0,\alpha^8,\alpha^{173},\alpha^{183})$	$(\alpha^0,\alpha^{10},\alpha^{82},\alpha^{90})$	$(\alpha^0,\alpha^{72},\alpha^{80},\alpha^{245})$	$(\alpha^0,\alpha^{165},\alpha^{175},\alpha^{247})$

We consider here the case of 4 relays: R_1, …, R_4. The non-binary symbols transmitted by both the source and the relays are modulated using QPSK modulation. The Frame Error Rate (FER) performance of the root-NB-LDPC code broadcasted by the source is shown in Figure 2, and corresponds to the case when no relay is activated (the right-most curve). Consequently, we shall assume that $\mathrm{SNR}_{\mathrm{SR}_i} > 24$ dB, for each relay R_i, such that the probability that the relay fails decoding the signal broadcasted by the source is less than 10^{-4}.

"direct" link (source-to-destination):

$SNR_{\mathrm{R}_1\mathrm{D}} = SNR_{\mathrm{SD}} + 6$ dB, $SNR_{\mathrm{R}_2\mathrm{D}} = SNR_{\mathrm{SD}} + 4$ dB, and $SNR_{\mathrm{R}_3\mathrm{D}} = SNR_{\mathrm{R}_4\mathrm{D}} = SNR_{\mathrm{SD}} + 2$ dB.

The *K* symbols transmitted by R_1 and R_3 are non-binary repeated versions of the *K* information symbols, while the *K* symbols transmitted by R_2 and R_4 are non-binary repeated versions of the *K* parity symbols.

The non-zero field values used at the relays for repetition coding are chosen according to Table 2. Specifically, R_1 and R_2 use $h^{(1)} = \alpha^{26}$ (together, they send to the destination a first repeated version of the *N* coded symbols), while R_3 and R_4 use $h^{(2)} = \alpha^{41}$ (they send to the destination a second repeated version of the *N* coded symbols).

Table 2 : Optimum values used at the relays for repetition coding

Relay #	1	2	3	4	5	6	7	8
GF(64)	α^{26}	α^{41}	α^{52}	α^{6}	α^{56}	α^{17}	α^{50}	α^{11}
$D_{\min}$	8	14	20	25	31	37	43	49
GF(256)	α^{15}	α^{165}	α^{71}	α^{150}	α^{128}	α^{122}	α^{113}	α^{104}
$D_{\min}$	10	17	24	32	39	46	54	62

Figure 2 shows the FER performance of the proposed cooperative coding scheme in case that 1, 2 or 4 relays are activated. For each case, we plotted the corresponding outage probability (dotted curves, asterisk markers) and the FER of the proposed cooperative coding scheme with optimized non-binary repetition coefficients (solid curves, full markers). For comparison purposes, we have also plotted the FER of the proposed cooperative coding scheme with classical repetition coding (same *optimized* NB-LDPC code at the source, but $h^{(1)} = h^{(2)} = 1$ dotted curves, empty markers). It can be seen that the proposed coding scheme achieves full-diversity in every case, hence fully exploiting the spatial diversity brought by the existence of relays. When no relay is activated, the gap between the FER of the NB-LDPC code used at the source and the outage probability is about 1 dB. More important, the non-binary repetition coding proves to be strong enough to maintain the same gap to the outage probability, irrespective of the number of activated relays.

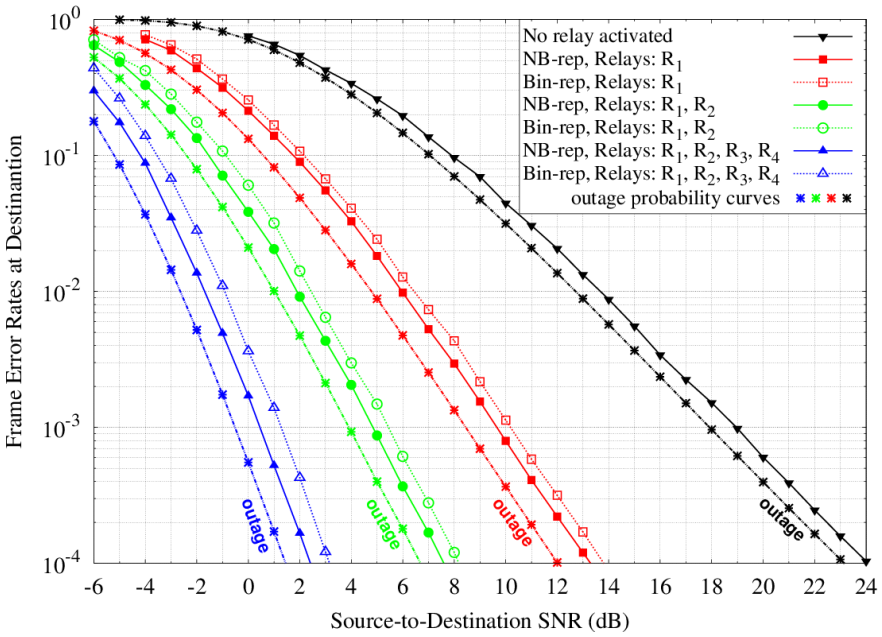

Figure 2 : FER performance of the proposed cooperative coding scheme

2.1.4 Discussion and Conclusion

We have introduced and optimized a new cooperative coding scheme based on NB-LDPC coding at the source and NB-repetition coding at the relays. For cooperative systems with block-fading wireless channels, we showed that the proposed scheme achieves full diversity, with constant gap to the outage probability of the system, irrespective of the number of relays. Additionally, our scheme is independent of the channel model or of the order of the modulation used for each link in the system, which allows preserving all the advantages shown in this contribution with advanced link-adaptation and channel estimation techniques.

As future work, we will investigate the use of Network-Coding (NC) at the relays, in case that two or more users use the same relays to communicate with the final destination. The use of NC is mainly aimed at reducing the traffic load on the relay-to-destination links, while providing the users with significant diversity gain brought by the use of several relays.

2.2 LTE-Advanced collaborative relaying

In D5.1 and [2]-[9] we described several collaborative relaying strategies for which an information-theoretic analysis was undertaken to gain insight into the most promising transmission methods without having to analyse a particular practical embodiment. One particular example [6][7] that was studied with respect to practical feasibility is recalled in Figure 3. Here a wireless relay station is used to collaboratively aid transmission from the so-called *Donor eNodeB* to the UE. The key characteristic of this type of relaying strategy, in comparison to the one that is currently standardized by 3GPP for 4G is firstly the use of physical-layer relaying. The relay station decodes information in a first phase and collaboratively aids the transmission with the source in the second phase. In LTE, multi-round transmission using HARQ is already the standard means for transmission and the method here simply puts the relay into the protocol. Secondly, in D5.1 and more completely in [6] we introduced a distributed three-message superposition coding approach which achieves full degrees of freedom with half-duplex relaying. It should be noted that current standardized schemes are limited to a single-level of coding (classical decode-and-forward relaying) are a vastly sub-optimal from the perspective of spectral-efficiency. The proposed method uses a superposition of two messages in the first phase, with retransmission of one of the two in second phase by both the eNodeB and the relay overlaid with a third message from the eNodeB. This is essentially the same way MIMO transmission (transmission modes 3,4) is performed in current networks, although in a distributed fashion, and is fully compatible with the coded-modulation strategy used in 4G.

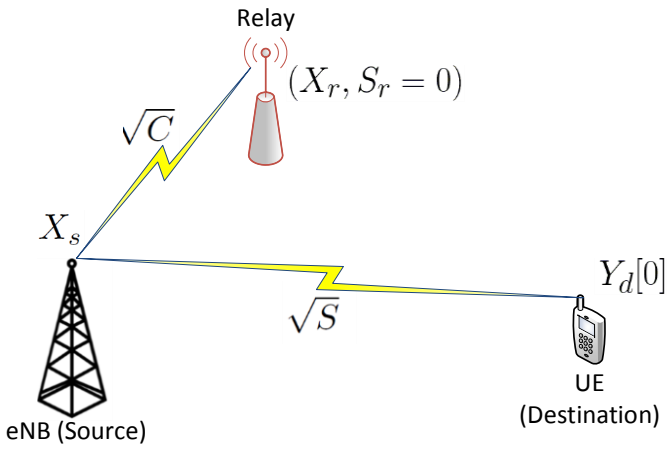

(a) Phase I

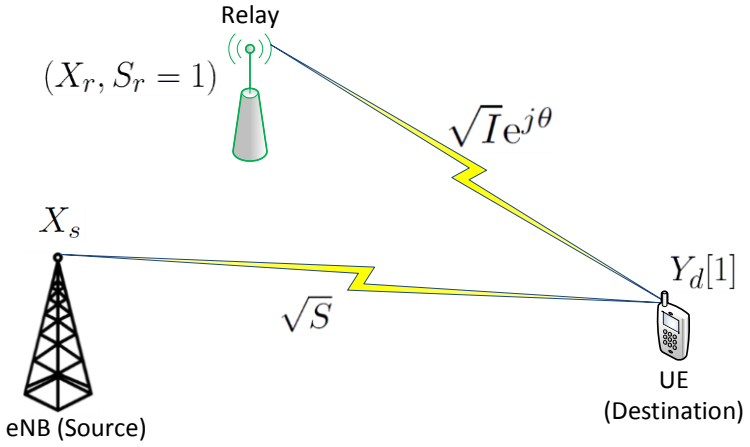

(b) Phase II

Figure 3: Collaborative Single-Relay Scenario

2.2.1 Updated Simulation Results

The main update on the simulated analysis of the considered transmission strategy with respect to the results presented in D5.1 is the evaluation with multi-antenna receivers (single-input multi-output or SIMO) at the UE using more realistic channel models. These are reported in the following figures and compare the performance of the proposed scheme with analytical bounds and a baseline scheme representing classical decode-and-forward relaying which is the currently standardized technique in 4G. Firstly we show the case for line-of-sight channels in Figure 4 and Figure 5 and secondly for typical-urban and pedestrian channels in Figure 6 and Figure 7. We see that for line-of-sight channels there is a very significant improvement in spectral-efficiency in comparison to the baseline strategy (on the order of a factor 2 improvement for all operating received signal-to-noise ratios). For convenience we also show comparisons with theoretical (asymptotic) performance of the protocol using infinite block-length codes and ideal channel estimation. The simulated curves make use of imperfect channel estimates which explains 2-3 dB gap with respect to the theoretical bounds. For the case with ETU (typical urban) and EPA (pedestrian) channels we have a somewhat reduced performance improvement, although still very significant (greater than a factor 1.5).

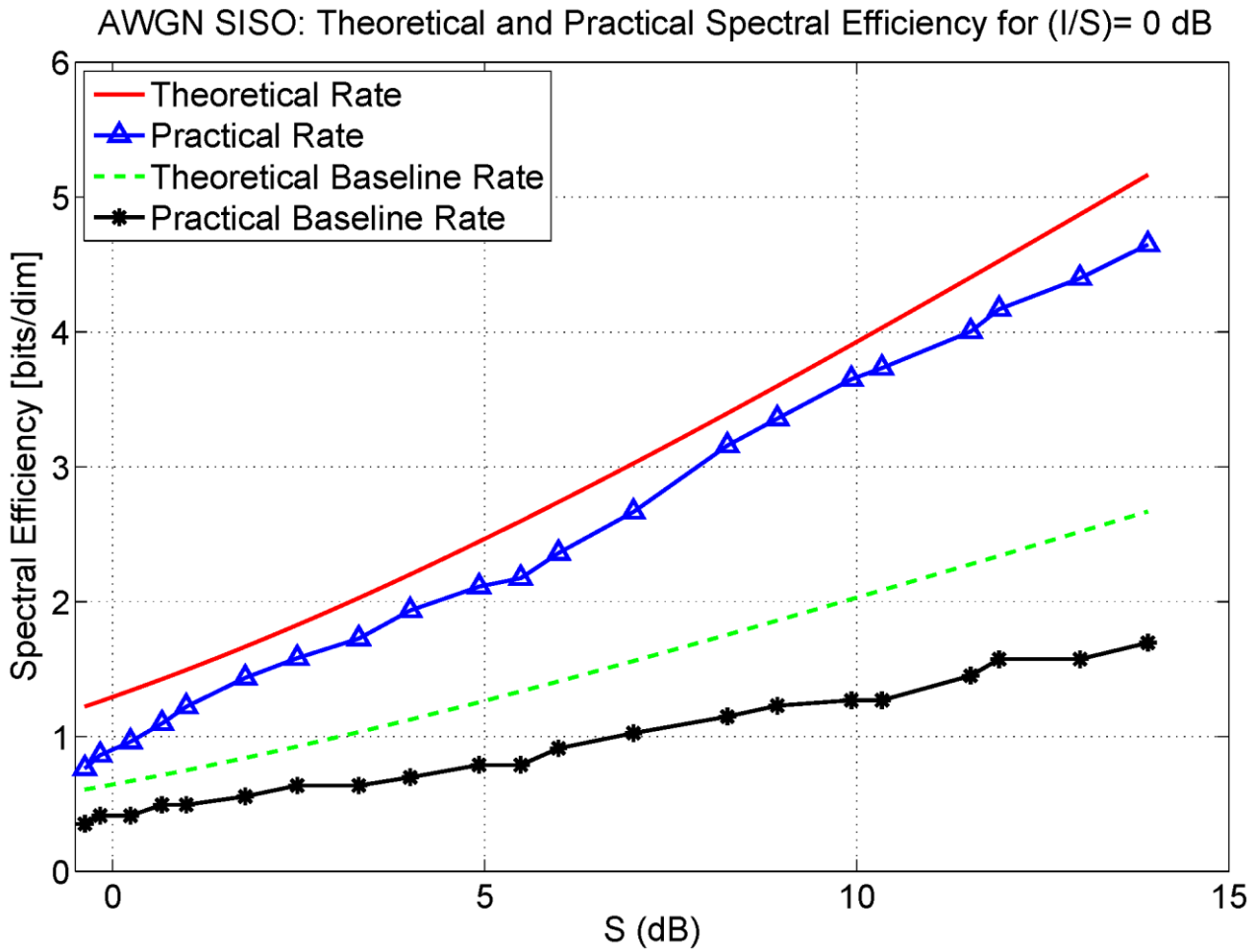

Figure 4: SIMO Rates (2 UE RX antennas) for Line-of-Sight Channels (Direct path to Relay path loss of 0 dB). Note: each point on simulated curves corresponds to a different set of MCS (MCS 0-20 on the first codeword of Phase 1)

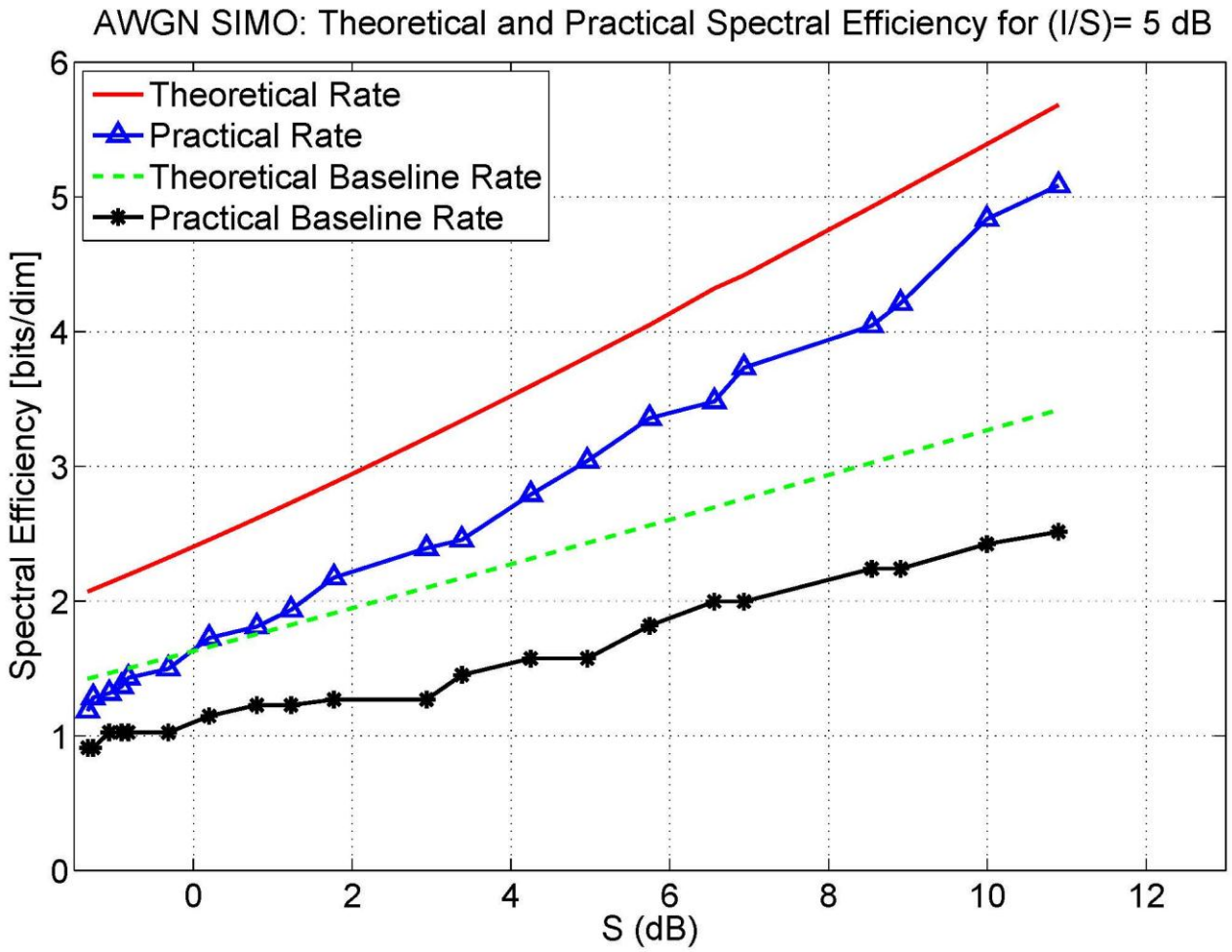

Figure 5: SIMO Rates (2 UE RX antennas) for Line-of-Sight Channels (Direct path to Relay path loss of 5 dB). Note: each point on simulated curves corresponds to a different set of MCS (MCS 0-20 on the first codeword of Phase 1)

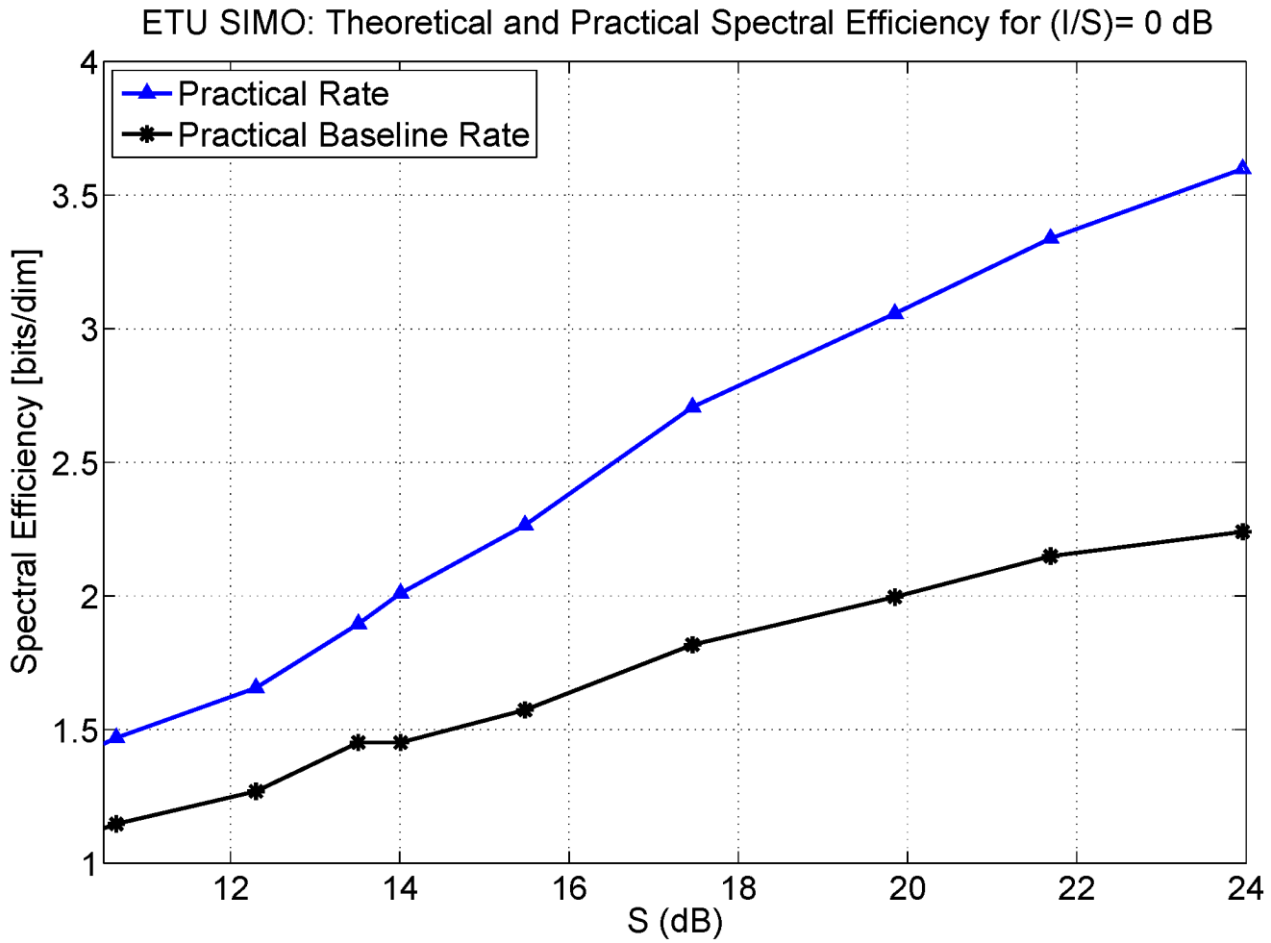

Figure 6: SIMO Rates (2 UE RX antennas) for 3GPP-ETU Channel (Direct path to Relay path loss of 0 dB). Notes: each point on simulated curves corresponds to a different set of MCS (MCS 0-9 on the first codeword of Phase 1). The channel between the Donor eNodeB and the Relay station is assumed to be a line-of-sight channel.

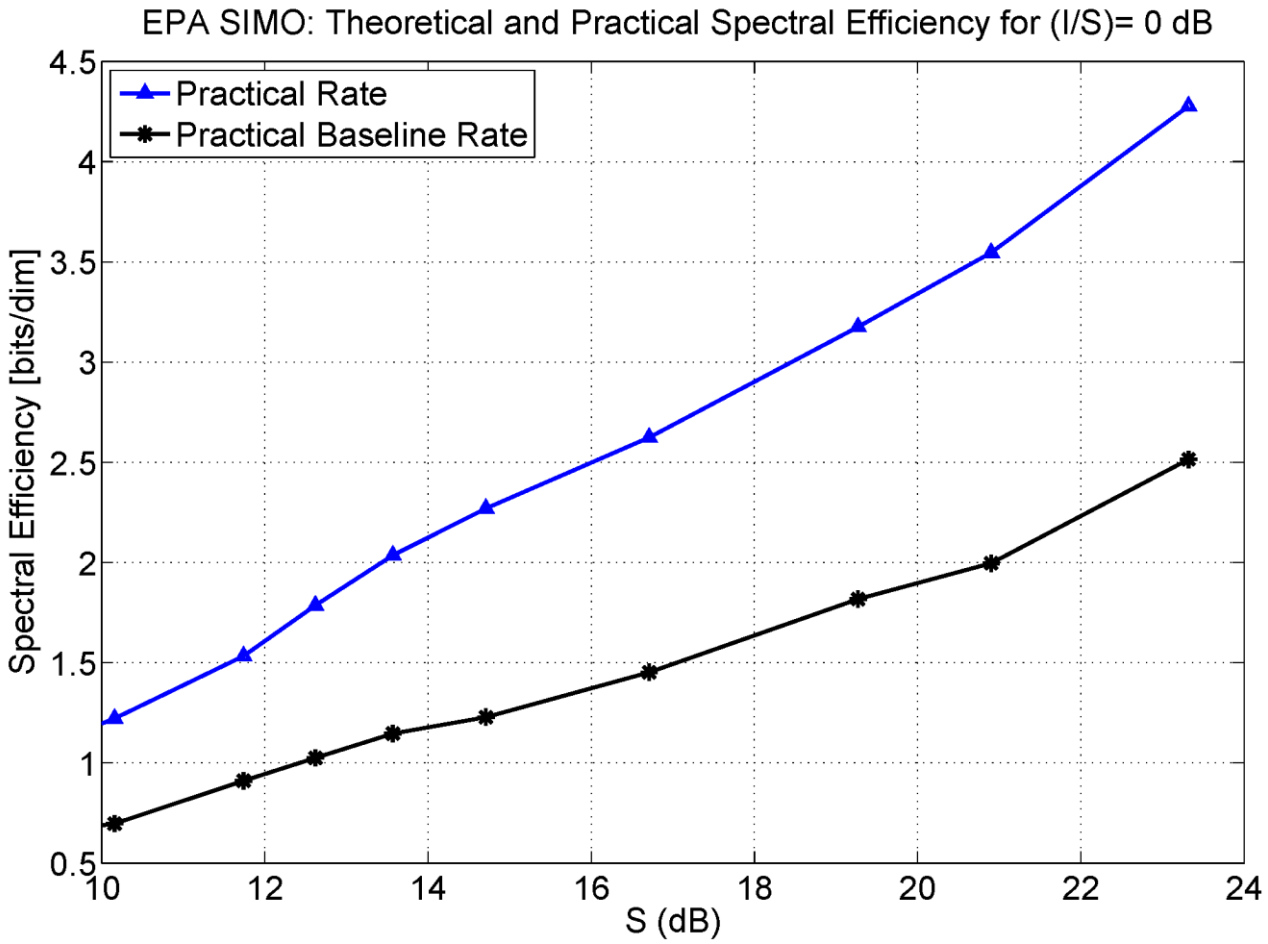

Figure 7: SIMO Rates (2 UE RX antennas) for 3GPP-EPA Channel (Direct path to Relay path loss of 0 dB). Notes: each point on simulated curves corresponds to a different set of MCS (MCS 0-9 on the first codeword of Phase 1). The channel between the Donor eNodeB and the Relay station is assumed to be a line-of-sight channel.

2.2.2 Main conclusions on the use of such techniques

General conclusions

The gains in spectral efficiency afforded by the relaying techniques summarized in the previous subsection are substantial. Operators have lacked a business case for the deployment of relays because of marginal benefits for relatively high deployment costs (on the order of a 20% improvement, see [10][27]). The results in D5.1 and extended here along with those in Section 2.6 highlight the fact that spectral efficiency gains of conventional decode-and-forward relaying are not cost effective. For this reason, the results presented here should be used to reconsider the case of relay stations for future 5G deployments where new layer 1-2 signalling can be envisaged to reap the benefits from physical-layer relaying. This may prove to be even more effective in millimetre-wave deployments where predominantly line-of-sight links are required and wired access-points will be extremely costly to deploy massively. In this case we would have a few Donor eNodeB with an optical backbone to the core network and many wireless relay stations using physical layer relaying to their proximity when possible. For UEs in line-of-sight with both there will be substantial benefits as described by these results. We have only considered a practical extension of the single-relay scenario, although our more fundamental results also show that multi-relaying can be beneficial as well.

Some Practical Issues

From a purely practical standpoint, two main issues related to low-layer signalling need to be addressed for such techniques to be viable for future (e.g. 5G) standardization. The first pertains to timing advance of the relay transmission. In a conventional OFDM system, the receiver synchronizes its reception to

the start of OFDM symbols and this synchronization must be accurate enough so that the entire channel response falls within the duration of the cyclic-prefix. Otherwise, inter-symbol interference will significantly degrade the performance of the receiver. In the context of the physical-layer relaying scheme, the received signal in the second phase of the protocol is jointly transmitted from the eNodeB and the relay station. These two signal components must arrive more or less synchronized in order for the receiver to be able to receive the OFDM waveform without too much trouble. This clearly requires some form of timing adjustment since the path from the source to destination going through the relay is longer than the direct path. The relay will adjust its timing to the received signal from the eNodeB (phase 1) and must advance the signal for each UE that it is serving according to the difference in path delay between the direct path and the path going through it to the destination. This will clearly require additional signalling. The second main issue is related to signalling in support of HARQ. In the first phase of the protocol, separate ACK/NAK signals need to be conveyed from the relay (for two messages) and the destination (for one message). Similarly, in the second phase, two ACK/NAK signals must be sent to the source from the destination and one to relay from the destination. This will clearly require significant modifications in low-layer signalling, but a feasible solution can surely be found.

2.3 Code-Aware Power Allocation for Irregular LDPC Codes

The Shannon capacity of the power constrained point-to-point Gaussian channel is achieved using independent and identically distributed (i.i.d.) symbols. Therefore, unequal power allocation (UPA) does not increase capacity. However, Shannon did not provide any practical coding/decoding scheme to achieve this capacity. Nowadays, there are powerful codes approaching this capacity as LDPC codes. It was shown in [10] that irregular LDPC codes perform better than regular ones in terms of threshold. In irregular LDPC codes, the variable nodes do not have the same degree and thus are not equally protected. Thus we expect that the performance of the code will be affected if the power allocated for some set of symbols associated to variable nodes of a certain degree is different from that allocated for a set of symbols associated to variable nodes of an another degree. Therefore, it is not known whether power allocation is also optimal for practical irregular LDPC codes. This will be the subject of investigation in our work.

In [11], the authors investigate the unequal power allocation problem for irregular LDPC codes for point-to-point Gaussian channels. They obtained up to 0.25 dB of gain with respect to equal power allocation (EPA) method. However, the authors use Monte-Carlo simulations in order to optimize the power allocation vector, which is time-consuming. In this work, we propose a new algorithm to optimize the power allocation vector such that the noise threshold of the existing irregular LDPC code family is maximized. Hence, we propose a modified density evolution algorithm using Gaussian approximation [12] when the unequal power allocation method is used at the transmitter. We apply this algorithm for the Gaussian point-to-point channel and the Gaussian relay channel.

2.3.1 LDPC codes and density evolution

This section recalls some of the basics about LDPC codes. We consider the point-to-point Gaussian channel case. At the source side, a message of k information bits is encoded by an LDPC encoder to a n-bit codeword. When the transmitter uses an equal power allocation strategy, the coded bits are modulated using a BPSK constellation, such that the bits 0 and 1 are mapped into $+1$ and -1 respectively. The resulting sequence after modulation is denoted by $x^n = [x_1, \cdots, x_n]$. The symbols $x_i, i \in \{1, \cdots, n\}$ are transmitted over a discrete-time memoryless additive white Gaussian noise (AWGN) channel. The channel output corresponding to the input x is $y = x + z$, where z is a noise following a normal distribution of zero mean and of variance σ^2.

Consider an LDPC code characterized by a Tanner graph H, with n variable nodes and m check nodes ($m = n - k$). An irregular LDPC code is characterized by bit nodes and check nodes with varying degrees. The fraction of edges which are connected to degree-i variable nodes is denoted λ_i, and the

fraction of edges which are connected to degree-i check nodes, is denoted ρ_i. The functions $\lambda(x)=\sum_{i=2}^{d_v}\lambda_i x^{i-1}$ and $\rho(x)=\sum_{i=2}^{d_c}\rho_i x^{i-1}$ are defined to describe the degree distributions from the perspective of Tanner graph edges. By definition $\lambda(1)=1$ and $\rho(1)=1$. An alternative characterization of the degree distribution for the variable nodes $\Lambda(x)=\sum_{i=2}^{d_v}\Lambda_i x^i$, from the perspective of Tanner graph nodes, will be used also in this paper. Here, Λ_i designates the fraction of degree-i variable nodes. The decoding algorithms used to decode LDPC codes are collectively called message-passing algorithms since they operate by the passing of messages along the edges of a Tanner graph. Under a message-passing algorithm, variable nodes and check nodes exchanges messages iteratively. Each node processes the received messages on the edges connected to it and sends messages back to its neighbors such that the output message is a function of all incoming messages to the node except the incoming message on the edge where the output message will be sent. The sum-product decoding is a message-passing algorithm in which the messages are log likelihood ratios (LLR) and the calculations at the variable and check nodes are performed using sum and product operations. Hence, a message can be written as the LLR of the equally probable random variable $x\in\{+1,-1\}$:

$$\mathrm{LLR}=\log\frac{p(x=+1\,|\,w)}{p(x=-1\,|\,w)}, \tag{1}$$

where w is a random variable describing all the information incorporated into this message. The sum-product algorithm iteratively computes an approximation of the maximum a posteriori (MAP value) for each code bit. However, the a posteriori probabilities returned by the sum-product decoder are only exact MAP probabilities if the Tanner graph is cycle free. Under the "cycle free assumption", the analysis of the decoding algorithm is straightforward because the incoming messages to every node are independent. In sum-product decoding the extrinsic message from a check node to a variable node, u, at the ℓ th iteration, is

$$u^{(\ell)}=2\cdot\tanh^{-1}\Big(\prod_{j=1}^{d_{c-1}}\tanh\frac{v_j^{(\ell)}}{2}\Big), \tag{2}$$

where d_c is the check node degree and $v_j, j=1,\cdots,d_c-1$ are the received messages from all neighbors of the check node except the variable node that gets the message u. The message from a variable node to a check node, v at the ℓ th iteration is equal to

$$v^{(\ell)}=\sum_{i=1}^{d_v-1}u_i^{(\ell-1)}+u_0, \tag{3}$$

where d_v is the variable node degree, $u_i, i=1,\cdots,d_v-1$ are the received messages from all neighbours of the variable node except the check node that gets the message v with $u_i^{(0)}=0$ and u_0 is the input a priori LLR of the output bit associated with the variable node. For an AWGN channel the a priori LLRs are given by $u_0=\frac{2}{\sigma^2}y$. The total LLR of the i-th bit is $\mathrm{LLR}_i^{(\ell)}=\sum_{i=1}^{d_v}u_i^{(\ell)}+u_0$. The i-th bit is decided to be a 0 if $\mathrm{LLR}_i>0$, and 1 otherwise. The decoding process ends when the decoded sequence is a codeword or until the maximum number of iterations is reached.

Density evolution is an algorithm for which the PDFs evolution of the exchanged messages is tracked through the message-passing algorithm. It determines the behaviour of an ensemble of Tanner graphs if the channel is memoryless and under the assumption that the Tanner graphs are all cycle free. Due to the symmetry of the channel and the decoder, the density evolution equations can be derived without loss of generality by assuming that all-zero codeword is sent through the channel ($x_i=+1,\forall i\in\{1,\cdots,n\}$). Thus, negative messages indicate errors. In particular, the evolution of the error probability can be determined, via density evolution, as a function of the iteration number of the message-passing decoding algorithm. The density evolution algorithm enables to compute the *noise*

threshold of a family of LDPC codes which is the maximum level (e.g. variance) of channel noise such that the probability of error converges to zero as the number of iterations tends to infinity.

Chung *et al.* investigated in [12] the sum-product decoding of LDPC codes using a Gaussian (for regular LDPC codes), or a Gaussian mixtures (for irregular LDPC codes), approximation for message densities (of u and v) under density evolution to simplify the analysis of the decoding algorithm and the design of irregular LDPC codes for AWGN channels. The authors show that the mean of a Gaussian density, which is a one-dimensional quantity, can act as faithful surrogate for the message density, which is an infinite-dimensional vector..

In order to present some results of [12]on the density evolution using Gaussian approximation, assume that the all-zero codeword is sent through the channel. Thus, the LLR message $u_0 = \frac{2}{\sigma^2} y$ from the channel is Gaussian with mean $\frac{2}{\sigma^2}$ and variance $\frac{4}{\sigma^2}$. The *symmetry condition* for a Gaussian variable with mean m and variance σ^2 reduces to $\sigma^2 = 2m$, thus we need only to keep the mean during the density evolution process. We denote the means of the messages u and v by m_u and m_v respectively. The Gaussian approximation method in [12] for irregular LDPC codes assumes that the individual output of a variable or a check node is Gaussian. Thus, the mean of the output of a variable node of degree i at the ℓ th iteration, $m_{v,i}^{(\ell)}$, is given by

$$m_{v,i}^{(\ell)} = m_{u_0} + (i-1)m_u^{(\ell-1)}, \tag{4}$$

where m_{u_0} and $m_u^{(\ell-1)}$ are the means of u_0 and $u^{(\ell-1)}$ respectively. Therefore, a message v sent by the variable node to its neighbours check nodes at the ℓ th iteration has a density function $f_v^{(\ell)}$ following a Gaussian mixture:

$$f_v^{(\ell)} = \sum_{i=2}^{d_v} \lambda_i N(m_{v,i}^{(\ell)}, 2m_{v,i}^{(\ell)}) \tag{5}$$

Using (2), the authors demonstrate also in [12] that the mean of the Gaussian output message $u_j^{(\ell)}$ of a degree-j check node at the ℓ th iteration, $m_{u,j}^{(\ell)}$ can be written as:

$$m_{u,j}^{(\ell)} = \phi^{-1}(1-[1-\sum_{i=2}^{d_v} \lambda_i \phi(m_{v,i}^{(\ell)})]^{j-1}), \tag{6}$$

where

$$\phi(x) = \begin{cases} 1 - \frac{1}{\sqrt{4\pi x}} \int_R \tanh\frac{u}{2} e^{-\frac{(u-x)^2}{4x}} du & \text{if } x > 0 \\ 1, & \text{if } x = 0. \end{cases} \tag{7}$$

Hence, the mean of $u^{(\ell)}$ at the ℓ th iteration, $m_u^{(\ell)}$, is obtained by linearly combining $m_{u,j}^{(\ell)}$ with weights $\rho_j, 2 \le j \le d_c$:

$$m_u^{(\ell)} = \sum_{j=2}^{d_c} \rho_j \phi^{-1}(1-[1-\sum_{i=2}^{d_v} \lambda_i \phi(m_{v,i}^{(\ell)})]^{j-1}). \tag{8}$$

The noise threshold σ^* is the supremum of all $\sigma \in R^+$ such that $m_u^{(\ell)} \to \infty$ as $\ell \to \infty$. In [12], the functions $h_i(s,r)$ and $h(s,r)$ are defined as:

$$h_i(s,r) = \phi(s + (i-1)\sum_{j=2}^{d_c} \rho_j \phi^{-1}(1-(1-r)^{j-1})), \tag{9}$$

$$h(s,r) = \sum_{i=2}^{d_v} \lambda_i h_i(s,r). \tag{10}$$

Equation (8) is written equivalently in [12] as

$$r_\ell = h(s, r_{\ell-1}), \tag{11}$$

where $s = m_{u_0} = \frac{2}{\sigma^2}$, and $r_0 = \phi(s)$. It is demonstrated in [12] that the convergence condition is equivalent to $r_\ell \to 0$ when $\ell \to \infty$ and is satisfied iff $r > h(s,r), \forall r \in (0, \phi(s))$.

2.3.2 Unequal power allocation

2.3.2.1 Problem formulation

Given an irregular LDPC code with a variable node degree distribution $\Lambda(x) = \sum_{i=2}^{d_v} \Lambda_i x^i$, we denote by P_i the power allocated at the transmitter to a symbol associated to a variable node of degree i. Thus $P_i > 0$ if $\Lambda_i > 0$ Bits 0 and 1 are mapped into $+\sqrt{P_i}$ and $-\sqrt{P_i}$ respectively. We assume that the destination is aware of the power allocation strategy at the source. Without loss of generality, we assume a total power constraint $P = 1$. The power constraint at the transmitter can be written as $\sum_{i=2}^{d_v} \Lambda_i P_i = 1$. In this work, we propose to choose $P_i, i \in \{2, \cdots, d_v\}$ in order to optimize the threshold of the irregular LDPC code family under consideration via density evolution. This is because density evolution, using Gaussian approximation, is a simple tool to evaluate the asymptotic performance of a family of LDPC codes. For convenience, we denote by $\mathbf{P}$ the vector whose elements are $P_i, i \in \{2, \cdots, d_v\}$. Thus, the optimization problem under consideration is the following:

$$\begin{aligned} \sigma_{th} &= \max_{\mathbf{P}} \sigma^*(\mathbf{P}) \\ \text{subject to} \quad & \sum_{i=2}^{d_v} \Lambda_i P_i = 1, \end{aligned} \tag{12}$$

where $\sigma^*(\mathbf{P})$ is the noise threshold for a given $\mathbf{P}$. When a 0-bit is transmitted with a power P_i, the mean of the message from the channel, $m_{u_{0i}} = \frac{2}{\sigma^2} P_i$ is varying with the node degree unlike the case with equal power allocation. We can easily extend the equations of the evolution of message means using Gaussian approximation in (4)-(11) to the case with unequal power allocation at the transmitter. Therefore, we can demonstrate that these equations become:

$$m_{v,i}^{(\ell)} = m_{u_{0i}} + (i-1) m_u^{(\ell-1)}, \tag{13}$$

$$m_v^{(\ell)} = \sum_{i=2}^{d_v} \lambda_i m_{v,i}^{(\ell)}, \tag{14}$$

$$m_{u,j}^{(\ell)} = \phi^{-1}(1 - [1 - \sum_{i=2}^{d_v} \lambda_i \phi(m_{v,i}^{(\ell)})]^{j-1}), \tag{15}$$

$$m_u^{(\ell)} = \sum_{j=2}^{d_c} \rho_j \phi^{-1}(1 - [1 - \sum_{i=2}^{d_v} \lambda_i \phi(m_{v,i}^{(\ell)})]^{j-1}). \tag{16}$$

$$h_i(s_i, r) = \phi(s_i + (i-1) \sum_{j=2}^{d_c} \rho_j \phi^{-1}(1 - (1-r)^{j-1})), \tag{17}$$

$$h(\mathbf{s}, r) = \sum_{i=2}^{d_v} \lambda_i h_i(s_i, r). \tag{18}$$

$$r_\ell = h(\mathbf{s}, r_{\ell-1}), \tag{19}$$

where $s_i = m_{u_{0i}} = \frac{2}{\sigma^2} P_i$, $\mathbf{s} = \{s_i\}$, and $r_0 = \sum_{i=2}^{d_v} \lambda_i \phi(s_i)$. The convergence condition to the threshold is the same of [12]. Therefore, for a given vector $\mathbf{P}$, the threshold $\sigma^*(\mathbf{P})$ is the supremum of all $\sigma \in R^+$ such that $r_\ell \to 0$ as $\ell \to \infty$.

2.3.2.2 Proposed solution

In order to solve the optimization problem in (12), we propose an algorithm with less complexity comparing to exhaustive search, in which the number of optimization variables is independent of the LDPC code. The proposed solution is inspired from the expression of r_ℓ in (19). Indeed, we rewrite r_ℓ as

$$r_\ell(\mathbf{P}, \sigma) = \sum_{i=2}^{d_v} \lambda_i \phi\left(\frac{2}{\sigma^2} P_i + (i-1)k_{\ell-1}\right), \tag{20}$$

where $k_{\ell-1} = \sum_{j=2}^{d_c} \rho_j \phi^{-1}(1-(1-r_{\ell-1})^{j-1}) \in (0, r_0)$. We recall that $\phi(x)$ is continuous and monotonically decreasing on $[0, +\infty)$, with $\phi(0) = 1$ and $\phi(\infty) = 0$ [12]. Hence $r_\ell \geq 0$. Since the convergence condition to the threshold requires that $r_\ell \to 0$ when $\ell \to \infty$, we consider the parametric family of functions $\{f_k, k \geq 0\}$ with parameter k, where f_k is defined by

$$f_k(\sigma, \mathbf{P}) = \sum_{i=2}^{d_v} \lambda_i \phi\left(\frac{2}{\sigma^2} P_i + (i-1)k\right), \tag{21}$$

and for a fixed σ, we look only for the vectors $\mathbf{P}$ which are the minima of $\{f_k\}_{k \geq 0}$. Therefore, for a fixed σ and k, we consider the following optimization problem

$$\mathbf{P}^*(\sigma, k) = \arg\min_{\mathbf{P}} f_k(\sigma, \mathbf{P})$$
$$\text{subject to} \quad \sum_{i=2}^{d_v} \Lambda_i P_i = 1. \tag{22}$$

Then, we define $r(k, \sigma) = r_\infty(\mathbf{P}^*(\sigma, k), \sigma)$ which can be calculated using (20). For a fixed k, the threshold $\sigma^*(k)$ is defined as the maximal value of σ such that $r(k, \sigma) \to 0$. Finally, k is chosen to maximize the threshold, thus we denote

$$k^* = \arg\max_k \sigma^*(k). \tag{23}$$

For a given k and σ, we should solve the optimization problem in (22). The expression of $\phi(x)$ in (7) makes very difficult to have a closed form expression of $\mathbf{P}^*(\sigma, k)$. In [12] the following approximation of $\phi(x)$ is used $\phi(x) \sim e^{-\alpha x^\gamma + \beta}$, where $\alpha = 0.4527$, $\beta = 0.0218$ and $\gamma = 0.86$. Even with this approximation, it is difficult to obtain an analytic solution for the optimization problem (22). Therefore, we propose to approximate $\phi(x)$ by a convex function of the form $\phi(x) \sim e^{-ax}$ with $a > 0$. Since the value for which the function ϕ should be evaluated in (21) depends on i and since e^{-ax} cannot approximate exactly $e^{-\alpha x^\gamma + \beta}$ for all values of x, a, we define a function $\phi_i(x) = e^{-a_i x}$ for each $i \in \{2, \cdots, d_v\}$ with $a_i > 0$. Thus, using the latter approximation, the optimization algorithm in (22) becomes:

$$\mathbf{P}^*(\sigma, k) = \arg\min_{\mathbf{P}} \sum_{i=2}^{d_v} \lambda_i \phi_i\left(\frac{2}{\sigma^2} P_i + (i-1)k\right)$$

$$\text{subject to} \quad \sum_{i=2}^{d_v} \Lambda_i P_i = 1. \tag{24}$$

Proposition 1 ; The solution of the optimization algorithm in (24) is

$$P_i^*(\sigma,k) = -\frac{(i-1)k}{k_0} - \frac{1}{a_i k_0}\log(\frac{\Lambda_i}{a_i \lambda_i k_0})$$

$$-\left(\frac{1}{a_i \sum_i \frac{\Lambda_i}{a_i}}\right)\left(-1 - k\sum_{i=2}^{d_v}(i-1)\frac{\Lambda_i}{k_0} - \sum_{i=2}^{d_v}\frac{\Lambda_i}{a_i k_0}\log\left(\frac{\Lambda_i}{a_i k_0 \lambda_i}\right)\right), \tag{25}$$

Where $k_0 = \frac{2}{\sigma^2}$ and $i \in \{2,\cdots,d_v\}$.

Proof. First, we form the Lagrangian of problem (24)

$$L(\mathbf{P},\theta;\sigma,k) = \sum_{i=2}^{d_v} \lambda_i \phi_i(\frac{2}{\sigma^2}P_i + (i-1)k) + \theta(\sum_{i=2}^{d_v}\Lambda_i P_i - 1). \tag{26}$$

where θ is the Lagrange multiplier. Since the objective function in problem (24) is convex and the constraint is affine, the KKT conditions guarantee the global optimality of the solution. Thus, the solution $(\mathbf{P}^*,\theta^*)$ of problem (24) verifies the following equations

$$\begin{cases} \frac{\partial L}{\partial P_i}(P_i^*) = -a_i k_0 \lambda_i e^{-a_i(k_0 P_i^* + (i-1)k)} + \theta^* \Lambda_i = 0, \qquad \forall i \in \{2,\cdots,d_v\} \\ \sum_{i=2}^{d_v} \Lambda_i P_i^* - 1 = 0. \end{cases} \tag{27}$$

For simplicity of notation, we drop the dependence of P_i^* on σ and k. From the first equation in (27), we get

$$P_i^* = -\frac{k(i-1)}{k_0} - \frac{\log(\frac{\theta^*\Lambda_i}{a_i\lambda_i k_0})}{a_i k_0}. \tag{28}$$

After substituting (28) in the equation $\sum_{i=2}^{d_v}\Lambda_i P_i^* - 1 = 0$, we get

$$\theta^* = e^{\frac{-k\sum_{i=2}^{d_v}(i-1)\Lambda_i - k_0 - \sum_{i=2}^{d_v}\frac{\Lambda_i}{a_i}\log\left(\frac{\Lambda_i}{a_i k_0 \lambda_i}\right)}{\sum_i \frac{\Lambda_i}{a_i}}} \tag{29}$$

Finally, after substituting (29) in (28), we get (25).

In order to determine the set $\{a_i\}_{i>1}$, we set $e^{-a_i x} = e^{-\alpha x^\gamma + \beta}$ where x is the value for which the function ϕ should be evaluated. Thus $a_i = \frac{-\alpha x^\gamma + \beta}{-x}$. Since we should evaluate $\phi_i(x)$ in (24) where $x = \frac{2}{\sigma^2}P_i + (i-1)k$ and that P_i is unknown, we set in our experiments $a_i = \frac{-\alpha \hat{x}^\gamma + \beta}{-\hat{x}}$ where $\hat{x} = \frac{2}{\sigma^2} + (i-1)k$.

The proposed solution is summarized in Algorithm 1.

Remark: In the optimization problem (24), we discarded the constraint $P_i \geq 0$. The solution obtained in **Proposition 1** can be written as $P_i^* = A_i + \frac{1}{k_0}B_i$ where $A_i > 0$ and $k_0 = 2/\sigma^2$. Thus if for some

$i \in \{2, \cdots, d_v\}$ and k, the obtained solution P_i^* is non-positive, we should decrease the value of σ while searching for the threshold, as stated in Algorithm 1.

Algorithm 1 Algorithm to solve (12)

$\epsilon \leftarrow 10^{-10}$, MaxIter $\leftarrow 10^4$.
for $k = 0 : k_{\max}$ **do**
  $\sigma_{\min} \leftarrow 0$, $\sigma_{\max} \leftarrow 10$
  $\sigma \leftarrow \frac{\sigma_{\max}+\sigma_{\min}}{2}$
  while $\sigma_{\max} - \sigma_{\min} > \epsilon$ **do**
    Compute $\mathbf{P}^*(\sigma, k)$ using Proposition 1
    if there exists at least one $P_i^* < 0$ **then** decrease $\sigma_{\max}$
    else
      $m_{u_{0i}} \leftarrow \frac{2}{\sigma^2} P_i^*(\sigma, k)$, for $i \in \{2, \cdots, d_v\}$
      for $\ell = 1 :$ MaxIter **do**
        Calculate $r_\ell = h(\mathrm{s}, r_{\ell-1})$ using (19)
        if $r_\ell < \epsilon$ **then** break
      if $r_\ell < \epsilon$ **then** $\sigma_{\min} \leftarrow \sigma$
      else $\sigma_{\max} \leftarrow \sigma$
      $\sigma \leftarrow \frac{\sigma_{\max}+\sigma_{\min}}{2}$
  Save $\sigma^*(k) = \sigma$
$\sigma_{\text{th}} \leftarrow \max_k \sigma^*(k)$

In Algorithm 1 "MaxIter" represents the maximum number of iterations that can be performed by the decoder. In our work, we will study also the unequal power allocation for decoders with limited number of iterations L. In this case, we set MaxIter$= L$ in Algorithm 1. Finally, we should note that the power allocation vector maximizing the noise threshold in Algorithm 1 to get zero error probability could achieve worst performance than equal power allocation for practical (low) bit error rate values (BER). Hence we propose to optimize the noise threshold $\sigma_{\text{th}}(\eta)$ for a target error probability η. Using the density evolution algorithm with Gaussian approximation, the error probability at the the L th iteration of the decoder, $P_e^{(L)}$, can be calculated. Therefore, for a target BER η, the convergence condition to the threshold $\sigma_{th}(\eta)$ becomes $P_e^{(L)} < \eta$, instead of $r_L \to 0$. [

2.3.3 Unequal power allocation for relay channels

In this section, we consider the Gaussian relay channel case. Indices s, r and d will refer to the source, the relay and the destination respectively. The relay uses the "amplify and forward" strategy. Without loss of generality, we consider an average power constraint at the source $P_s = 1$ and an average power constraint at the relay $P_r = 1$.

In the relay channel case, the source and the relay can use simultaneously different power allocation strategies but this makes the problem difficult to solve due to the large number of variables. Therefore, we will study in the following, a strategy where the source only uses an unequal power allocation strategy. The transmitted signal x_s by the source is given by $x_s = \sqrt{P_{si}}x$ where $x \in \{+1, -1\}$ and P_{si} is the power allocated at the source for a bit associated to variable node of degree i. We denote by $\mathbf{P_s}$ the vector whose elements are P_{si}, $i \in \{2, \cdots, d_v\}$. The received signal by the relay is $y_{sr} = \sqrt{P_{si}}x + z_{sr}$,$z_{sr} \sim \mathcal{N}(0, \sigma_{sr}^2)$. The transmitted signal by the relay is given by $x_r = f y_{sr}$, where $f = \frac{1}{\sqrt{P_s + \sigma_{sr}^2}} = \frac{1}{\sqrt{1+\sigma_{sr}^2}}$. The destination receives $y_{sd} = x_s + z_{sd}$ from the source $\left(z_{sd} \sim \mathcal{N}(0, \sigma_{sd}^2)\right)$ and $y_{rd} = x_r + z_{rd} = f\sqrt{P_{si}}x + f z_{sr} + z_{rd}$ from the relay $\left(z_{rd} \sim \mathcal{N}(0, \sigma_{rd}^2)\right)$. The destination, aware of the power

allocation strategy, can determine y'_{sd} and y'_{rd} as $y'_{sd}=\frac{y_{sd}}{\sqrt{P_{si}}}=x+z'_{sd}$, where $z'_{sd}=\frac{z_{sd}}{\sqrt{P_{si}}}\sim\mathcal{N}\left(0,\frac{\sigma_{sd}^2}{P_{si}}\right)$, and $y'_{rd}=\frac{y_{rd}}{f\sqrt{P_{si}}}=x+z'_{rd}$, where $z'_{rd}=\left(\frac{z_{sr}}{\sqrt{P_{si}}}+\frac{z_{rd}}{f\sqrt{P_{si}}}\right)\sim\mathcal{N}\left(0,\frac{\sigma_{sr}^2}{P_{si}}+\frac{\sigma_{rd}^2}{f^2P_{si}}\right)$. At the destination, the LLR message at a variable node of degree i from the relay channel is given by

$$u_{0i}=\log\frac{p(x=+1\,|\,y'_{sd},y'_{rd})}{p(x=-1\,|\,y'_{sd},y'_{rd})} \tag{30}$$

$$=\underbrace{\log\frac{p(y'_{sd}\,|\,x=+1)}{p(y'_{sd}\,|\,x=-1)}}+\underbrace{\log\frac{p(y'_{rd}\,|\,x=+1)}{p(y'_{rd}\,|\,x=-1)}} \tag{31}$$

$$= \quad u_{0i}^{s} \quad + \quad u_{0i}^{r} \tag{32}$$

where $u_{0i}^{s}=\frac{2y'_{sd}P_{si}}{\sigma_{sd}^2}$ and $u_{0i}^{r}=\frac{2y'_{rd}P_{si}}{\sigma_{sr}^2+\frac{\sigma_{rd}^2}{f^2}}$. Hence, when the all-zero codeword is assumed to be sent by the source, the mean of the LLR message u_{0i} is given by $m_{u_{0i}}=m_{u_{0i}^s}+m_{u_{0i}^r}$, where $m_{u_{0i}^s}=\frac{2P_{si}}{\sigma_{sd}^2}$ and $m_{u_{0i}^r}=\frac{2P_{si}}{\sigma_{sr}^2+\frac{\sigma_{rd}^2}{f^2}}$. In the relay channel case, we have three independent channels. Therefore, we should fix the SNR of two channels and find the power allocation vector which maximizes the noise threshold for the remaining channel. In this work, we consider the setting where the source and the relay know both the SNRs of the channels source-relay and source-destination. The power allocation vector at the source is optimized in order to maximize the threshold of the relay-destination channel. This optimization can be solved in the same manner as in the point-to-point case. Indeed, the Algorithm 1 can be extended for the relay channel case after replacing the expression of $m_{u_{0i}}$ in Algorithm 1 by its expression in the relay case depending on the strategy used. The output σ_{th} of Algorithm 1 will refer to $\sigma_{rd_{\text{th}}}$ in the relay case. Moreover, the Proposition 1 should be updated for the relay channel case in Algorithm 1. Hence, it is easy to demonstrate that the expression of P_{si}^{*} as function of k and the channel noise variances is obtained from Proposition 1 by replacing k_0 with $k_0=\frac{2}{\sigma_{sd}^2}+\frac{2}{\sigma_{sr}^2+\frac{\sigma_{rd}^2}{f^2}}$.

2.3.4 Simulation results and discussion

This section presents simulation results on unequal power allocation for irregular LDPC codes. Table 3 shows the SNR threshold of some irregular LDPC codes using Gaussian approximation with both equal power allocation and unequal power allocation. It gives also the power allocation function $P(x)$ obtained by Algorithm 1, for each code in Table 3, where $P(x)=\sum_i P_i x^{i-1}$ and P_i is the power allocated for the degree-i variable node. We observed in our simulations that our proposed algorithm gives the same threshold values as the exhaustive search method. We observe in Table 3 that a gain up to 0.22 dB can be obtained on the threshold with respect to equal power allocation strategy. However, for some codes EPA is optimal. We recall that the proposed power allocation method in Algorithm 1 relies on computing the threshold $\text{SNR}^{*}(k)$ for each parameter $k\geq 0$ and then to choose k^{*} which gives the better threshold (cf. (22) and 23). Figure 8 shows $\text{SNR}^{*}(k)$ as a function of k for the LDPC code of rate $1/2$ and $\Lambda(x)=0.5x^2+0.5x^4$. We observe that the SNR threshold decreases with k until k^{*}. Intuitively, k is small means that the density evolution algorithm is far from the convergence (cf. 20). Thus, the power allocation vector optimized for small values of k could be not the optimal power allocation vector when the density evolution algorithm is near convergence. Moreover, when k becomes large, the objective function to minimize in problem (24) decreases (since $\phi(x)$ is decreasing with x),

and the objective function becomes less dependent on the power allocation vector (since its value is close to zero when k is large). Thus there is a trade-off in the optimal value of k which minimizes the SNR threshold.

Remark: for k and σ fixed, the objective function to minimize in problem (24) can be written as $f(\mathbf{P}) = \sum_{i=2}^{d_v} \lambda_i f_i(P_i)$, where $f_i(P_i) = \phi_i(\frac{2}{\sigma^2} P_i + (i-1)k)$.

Table 3 Threshold in dB of some LDPC code families of rate $1/2$ with EPA and UPA for the binary-input AWGN point-to-point channel.

$\Lambda(x)$	$\mathbf{SNR}_{th}$ **EPA**	$\mathbf{SNR}_{th}$ **UPA**	$P(x)$
$0.5x^2 + 0.5x^4$	0.8733	0.8725	$0.9775x^2 + 1.0225x^4$
$0.5x^2 + 0.5x^6$	1.0854	0.9492	$0.8183x^2 + 1.1817x^6$
$0.5x^2 + 0.5x^8$	1.4520	1.2301	$0.8509x^2 + 1.1491x^8$

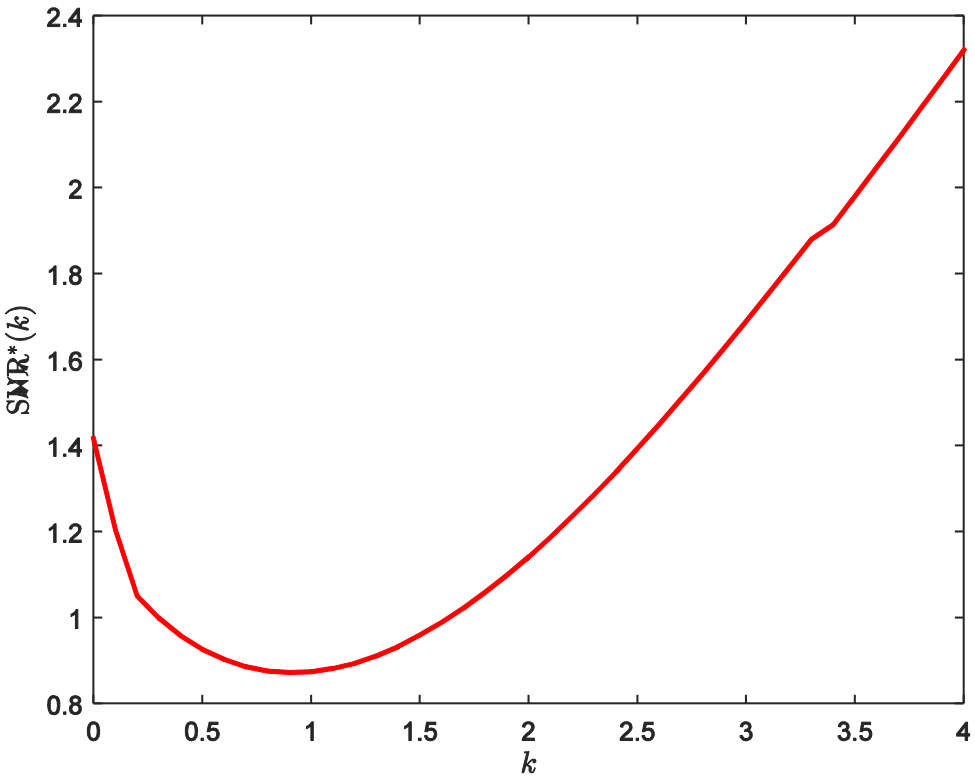

Figure 8 $\mathrm{SNR}^*(k)$ as a function of k, for the code of rate $1/2$ and $\Lambda(x) = 0.5x^2 + 0.5x^4$.

When the irregular LDPC code involves a degree i which is too large, $f_i(P_i)$ becomes too small and the value of P_i will not affect too much the value of the objective function. Thus, in our simulations, we define a "saturation" parameter K_{sat} and we set $f_i(P_i) = \phi_i(\frac{2}{\sigma^2} P_i + K_{\text{sat}})$, $\forall(i,k)$ such that $(i-1)k \geq K_{\text{sat}}$. This introduces an additional optimization variable in Algorithm 1 (K_{sat}), however, this value is optimized in our simulations one time for all the simulated codes.

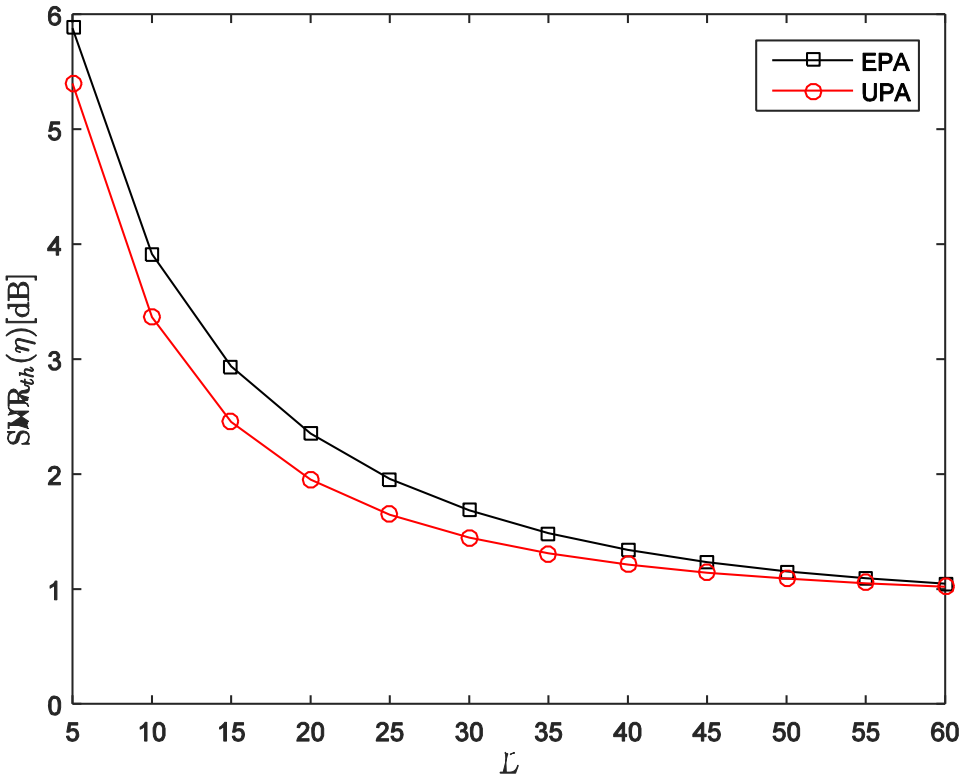

Figure 9 $\mathrm{SNR}_{\mathrm{th}}(\eta = 10^{-8})$ as a function of L, for the code of rate $1/2$ and $\Lambda(x) = 0.5x^2 + 0.5x^4$, in the point-to-point channel case.

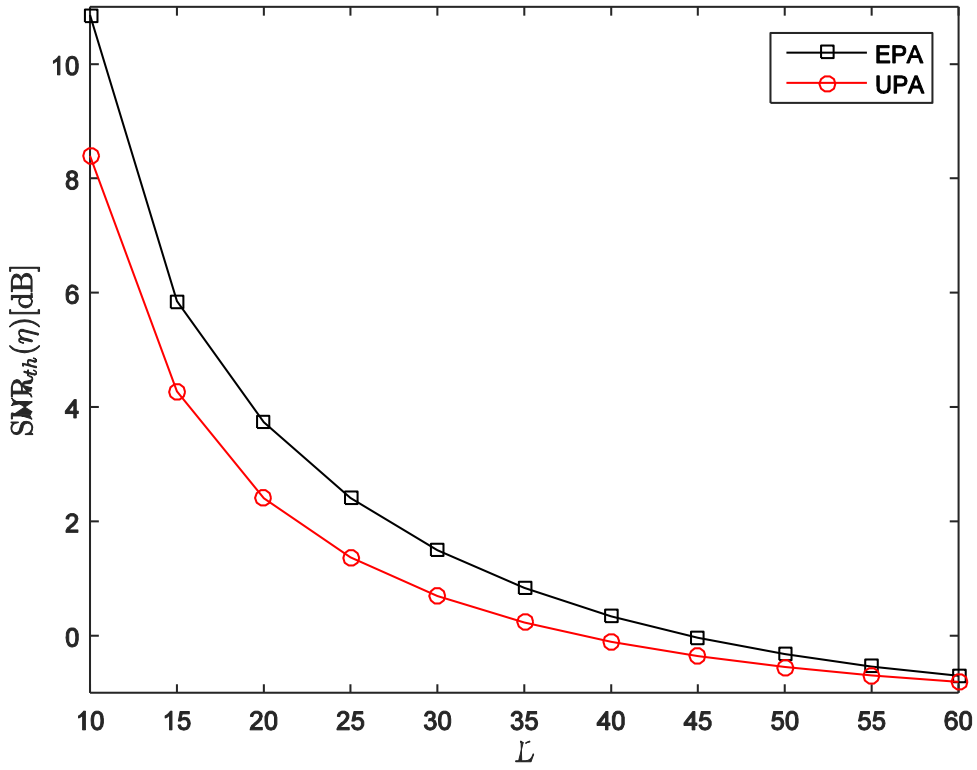

Figure 10 $\mathrm{SNR}_{rd\,\mathrm{th}}(\eta=10^{-8})$ as a function of L, for the code of rate $1/2$ and $\Lambda(x)=0.5x^2+0.5x^4$, in the relay channel case with $\sigma_{sd}=1.1$ and $\sigma_{sr}=0.7$.

Figure 9shows the SNR threshold as a function of the decoder maximum number of iterations L for a target BER less than 10^{-8}. We observe that a gain of 0.5 dB on the SNR threshold can be obtained by optimizing the power allocation with respect to equal power allocation. We should note that in this work, we optimize the power allocation for a given code but rather it is also possible to optimize the code degree distributions for a decoder of fixed number of iterations L and using EPA. Figure 10 shows the SNR threshold for the relay-destination channel as a function of the decoder maximum number of iterations L for a target BER less than 10^{-8}, when $\sigma_{sd}=1.1$ and $\sigma_{sr}=0.7$. The gain of the unequal power allocation method with respect to the equal power allocation seems to be more important for the relay case (up to 2.4 dB). This is because we have more degrees of freedom in the relay case where we can fix the SNR of two channels and determine the threshold for the remaining channel. When L increases, the gain brought by UPA decreases, as shown in

Figure 9 and Figure 10.

2.3.5 Conclusion

In this paper, we investigated an unequal power allocation method for irregular LDPC codes where the power allocated of a coded bit depends on the degree of its associated variable node in the Tanner graph. We proposed an algorithm to optimize the power allocation vector using a modified density evolution algorithm under the Gaussian approximation. Simulation results show that in some cases, the unequal power allocation leads to a gain on the threshold of the LDPC code compared to equal power allocation.

2.4 Two-way relaying for clusterized mesh networks

2.4.1 Scenario: Clustered wireless mesh networks based on LTE

This activity refers to wireless mesh network based on LTE for public safety applications. As explained in SHARING D2.2, the scenario is focused on a clustered wireless mesh network: the network is divided in clusters, mapping (or equivalent) to LTE macro cells (or micro cells, depending on the available transmit power, type of equipment, etc.). As seen further in Figure 11 and Figure 12 below, a mesh network has no longer a centralized structure such as for classic mobile communication networks, and can be easily deployable in an infrastructure-less environment. In this context, each user is controlled by a ClusterHead (CH) which is acting as a 3GPP eNodeB. Mesh Routers (MR) which may be found in mesh networks in between two cells are acting as 3GPP relays, and inherit relay and User Equipment (UE) procedures from LTE. Some MRs, connected to 2 or 3 clusters, are called bridging MRs and allow communications between the clusters. Common bridging MRs between the clusters can cooperate for improving performance (robustness, throughput, latency). Edge MRs are possibly present, if the wireless mesh network is not independent but is linked to other networks via other technologies.

Wireless mesh networks can come in different flavors. They can be used as a mesh extension of a traditional wired network, as shown in Figure 11. Red links show infrastructure links, meaning that traffic among clusters is transferred over these links.

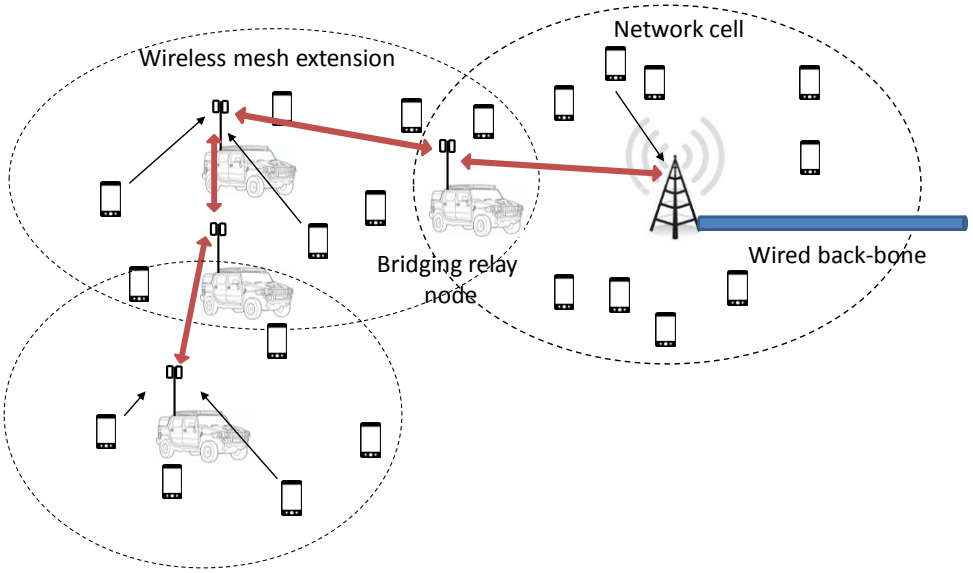

Figure 11: Wireless mesh extension

In crisis scenarios, it can be required to deploy a temporary wireless network quickly. Such a network is illustrated in Figure 12. In this configuration it can also be interesting to support connectivity while bridging nodes are still on-the-move at low vehicular speeds. Moreover, it would be interesting that isolated clusters (or cells) can be reached by relaying of UEs (see e.g. in Figure 12). This situation can happen, for example, when the relay is badly placed, in case of fast and unorganized deployment which can be required in certain situations. Therefore, as opposed to Figure 11, Figure 12 also defines a scenario where the function of the Mesh Router can be taken by mobile UEs.

In general, in such a network, a vehicular node can dispose of more power than a hand-held terminal. However, there is an interest also in having robust and interchangeable equipment. For instance if a CH is damaged or is out of service, it would be interesting that another node could take over its role.

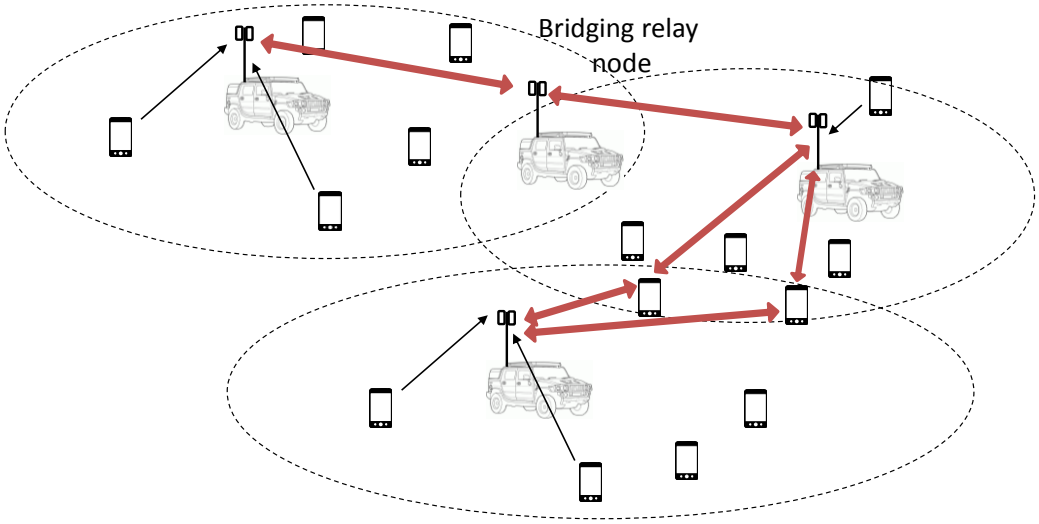

Figure 12: Quickly deployable mesh network

Notice that a very interesting point here, among others, is the inter-cluster communications which are indicated with red arrows. Similarly to Figure 11, inter-cluster links will enable communications between clusters, but the relays can also be UEs and not only relay nodes. These scenarios are also interesting for application in the Public Protection and Disaster Relief (PPDR) area. In the US, LTE has been identified as the technology for building up next generation of broadband radio system for PPDR applications, and 3GPP has already started working on adding features for implementing specific requirements linked to Private Mobile Radio (PMR), see for instance [17].

2.4.2 Relaying for inter-cluster communications

In an ideal situation with perfect channels, it is known that Two-Way Relaying (TWR) outperforms Decode-and-Forward (DF). This can be seen on top of Figure 13 where both schemes are represented. For TWR: 1) two users U1 and U2 are transmitting and are received at the same time (during reception phase) by the MR and 2) an eXclusive OR (XOR) operation is performed by MR on received data and retransmitted to both users U1 and U2 at the same time (during the broadcast phase). Compared to DF scheme, TWR uses 2 slots instead of 4 to transmit from U1 to U2 through MR and from U2 to U1 through the same MR.

In addition, in the bottom part of Figure 13, a real situation when some packets are not received is introduced. The main difference between the Simple TWR and Adaptive TWR is the following:

1. For simple TWR scheme, if one of the packets is not received, the MR discards the other packet since it cannot perform a XOR operation.
2. For adaptive TWR scheme, if one of the packets is not received, the MR forwards anyway the other packet (without performing XOR operation).

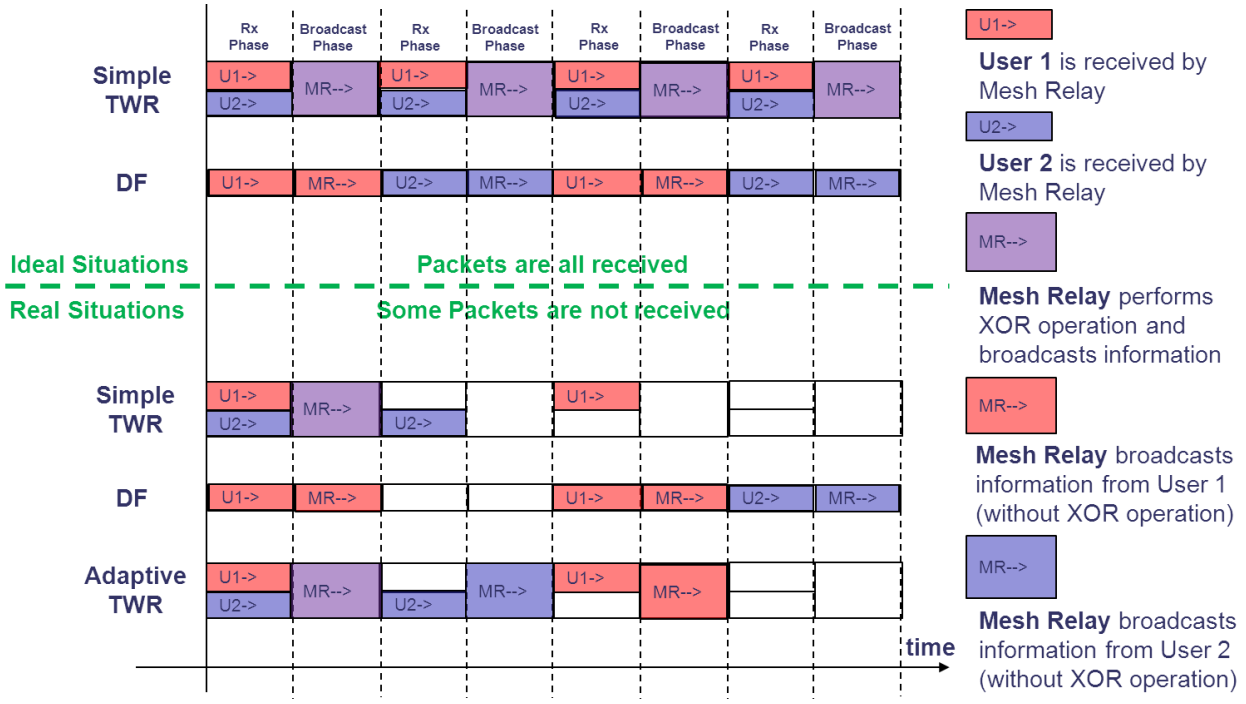

Figure 13: System Description of Simple Two-Way-Relaying Scheme, Decode-and-Forward Scheme, and Adaptive Two-Way-Relaying Scheme for Ideal and Real Situations

Adaptive TWR is better than simple TWR in terms of spectral efficiency. However, the advantage with respect to DF is not very clear since during the first slot, in TWR two users are simultaneously transmitting resulting in interference at MR level. Therefore, TWR theoretically can achieve higher throughput but in terms of PER (Packet Error Rate) DF may be better. The goal of the next sections is therefore to evaluate and compare these two schemes in terms of throughput and PER.

For this purpose, in Figure 14 we have represented the Key Performance Indicators (KPIs) and the system assumptions. At user level we are therefore interested to evaluate End-to-End throughput and End-to-End PER, while at relay level we are interested to evaluate total throughput and mean PER. The total distance between two users is considered to be equal to ISD (inter-site distance) or other. The distance between the first user (U1) and MR is *d*, and the distance between the second user (U2) and MR is ISD – *d*. A user uses 1 antenna in reception mode and 1 antenna in transmission mode but a MR uses 2 antennas in reception mode (in order to separate simultaneous transmission from the two users at the same time) and 1 antenna in transmission mode. For separating the two users several techniques can be employed, including Space-Division Multiple Access (SDMA), Successive Interference Cancellation (SIC) techniques or even linear equalization. In this deliverable we employ a linear space-time MMSE equalization technique implemented in frequency domain [19].

Another goal of this study is to evaluate the impact of MR position with respect to the position of users in terms of achievable throughput and PER for TWR and DF schemes. This would serve to evaluate for example which is the best position for a MR in order to satisfy Quality of Service (QoS) criteria and which is the maximum achievable distance for different channel models.

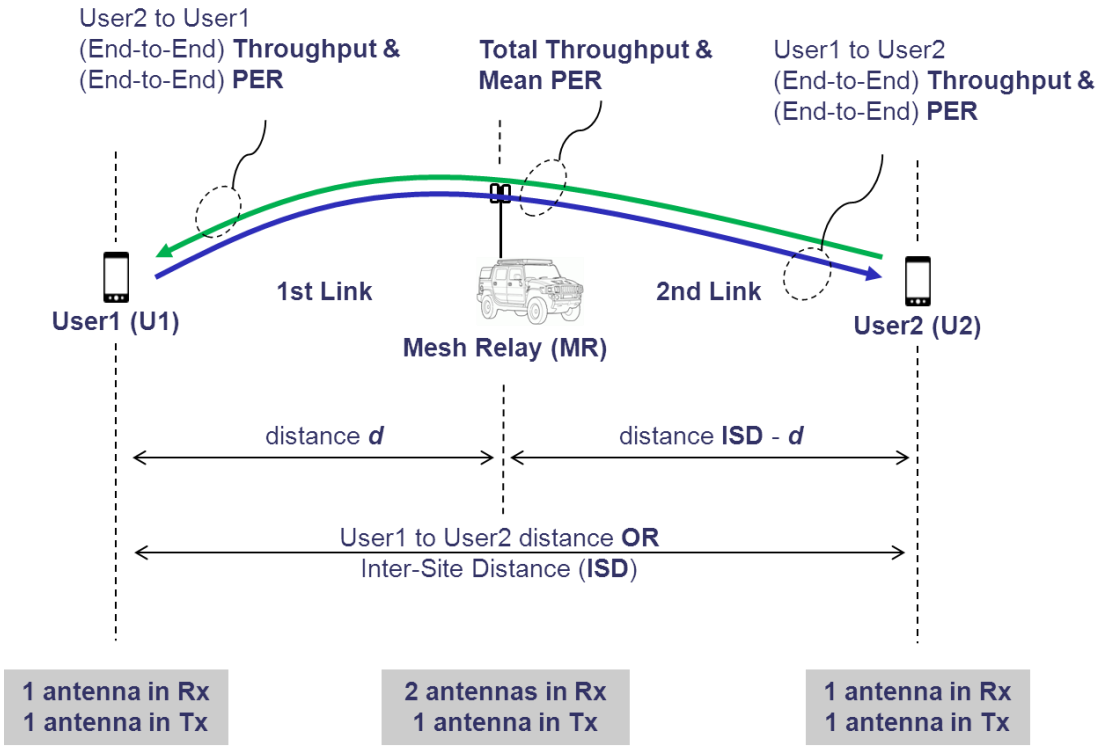

Figure 14: Simplified System Description and KPIs of Interest

2.4.2.1 Power Allocation for Relaying Schemes

A usually neglected assumption is the power constraint that has to be considered at relay and user level. In this work it is assumed that the power at relay level is bounded by a maximum transmission power and shared between the end-to-end links using the frequency resources at the same time. This effect can be seen as a compromise between the total achievable throughput and the total transmission distance:

1. a smaller-bandwidth MR (e.g. 1.4 MHz) can relay a lower number of connections but for the same maximum transmission power the communication distance is higher.
2. a larger-bandwidth MR (e.g. 5 MHz) can relay a higher number of connections but for the same maximum transmission power the communication distance is lower.

An illustrative example is given in Figure 15. This example is applicable to both TWR and DF schemes previously represented in Figure 13, and shows that there is a maximum transmission power to be transmitted by a user and a maximum transmission power to be transmitted by a MR.

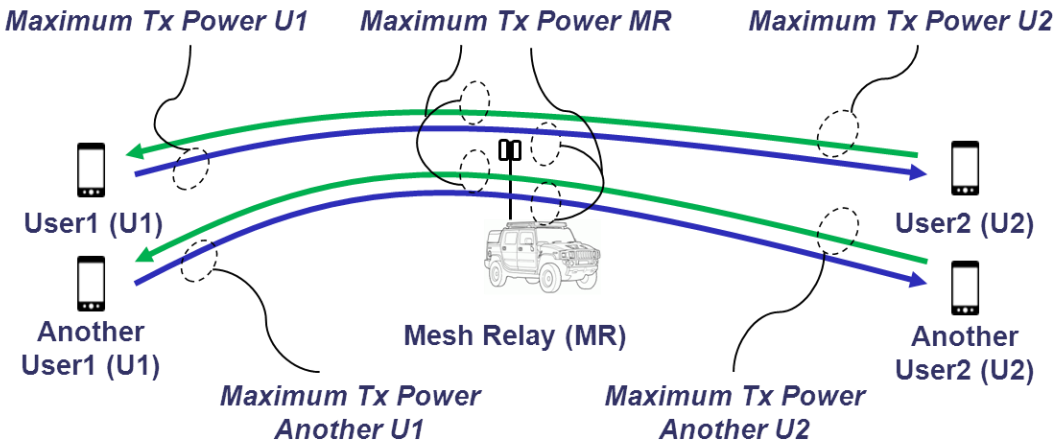

Figure 15: Power Constraint Representation for a Relaying Scheme

No matter if transmission takes place during the first slot or during the second slot, the MR has to support multiple End-to-End transmissions at the same time and therefore the maximum transmission power per link is constrained at MR level with respect to the number of links simultaneously being relayed and the service per each link.

From the point of view of the transmission scheme to be used (DF or TWR) there is no difference with respect to the transmitted power during the first slot or during the second slot per user or per relay. However, in terms of total (global) transmitted power, it is possible that TWR scheme consumes more instantaneous power since during the first slot the users (i.e. U1 & U2) can transmit simultaneously 2 different packets at the same time towards the MR. Similarly, in terms of (global) transmitted average power it is possible that DF scheme consumes more power than TWR since DF uses 2 slots instead of 1 to broadcast information from the MR to end users. In this study we focus only on individual power consumption and power constraints and not on the global (network) power consumption.

As previously mentioned, with respect to the number of resource blocks (RBs) used at the same time, a user or a relay may transmit a certain transmission power which should not be above the maximum allowed transmission power. A few examples with a different RBs allocation schemes (represented in green) are given below in Figure 16 and Figure 17 for a user and a MR respectively. Each RB is represented as a 12 x 7 grid, and each RB is composed from 12 subcarriers (each with 15 kHz) and 7 symbols (when Normal Cyclic Prefix is being used) which are sent in a slot of 0.5 ms duration. Normally the resource allocation is performed on pairs of RBs (corresponding to a Time Transmission Interval of 1ms or a TTI). In Figure 16, the allocation scheme in the middle is not implementable in LTE, except in specific cases like in the PHY UL control channel, and it is given mainly for illustration purpose.

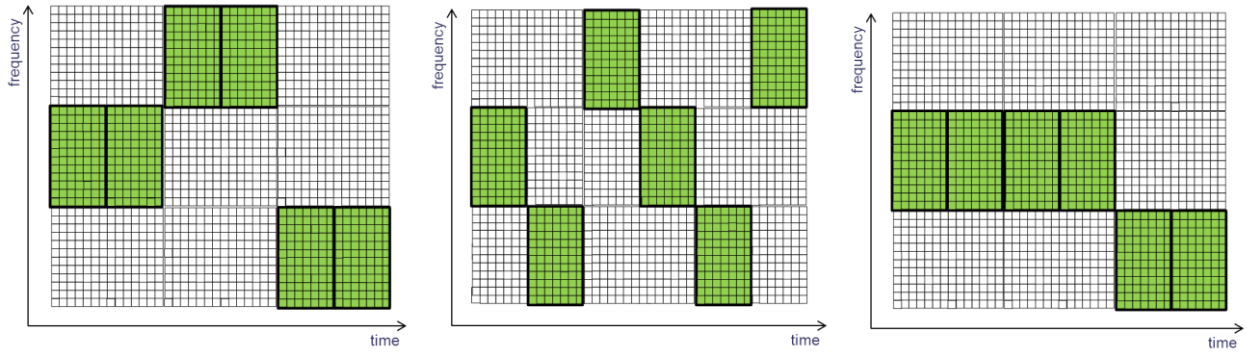

Figure 16: Example of Allocation Schemes for a User

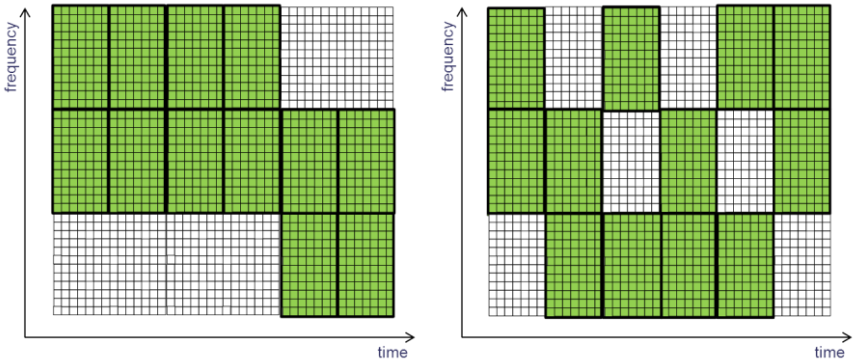

Figure 17: Example of an Allocation Scheme for a MR relaying 2 End-to-End links

The RB allocation can be continuous or discontinuous in time or in frequency domain. However, if the total number of RB transmitted at the same time on the frequency domain increases, the power allocated to each RB block will decrease as a result of the maximum power constraint on all the RB used at the same time. Suppose that the maximum transmission power constraint for a user is 1 W and for a MR is 10 W. As represented in Figure 16, if the user transmits on maximum 1 RB block at the time, then the maximum allowed power per 1 RB is 1 W. However, in the case of a MR represented in Figure 17, if the MR uses 2 RB instead of 1 RB (e.g. because it can simultaneously relay 2 End-to-End links as previously represented in Figure 15), the maximum allowed power per link will be 5 W, meaning that the MR cannot relay anymore at full power one single link. This would be a disadvantage for the MR in terms of transmission coverage:

1. if the goal is to extend coverage as far as possible, it is better if the MR is not relaying many users at the same time;
2. if the goal is to relay as many users as possible, it is better to use a MR in a scenario with shorter distances between relayed users.

2.4.2.2 Simulation Parameters

Physical and MAC layer simulation parameters have been represented in Table 4. The simulation considers a voice service and a SC-FDMA transmission scheme for its reduced PAPR characteristics. The rest of the parameters are LTE compliant.

Table 4: PHY & MAC Simulation Parameters

Parameter	Value
Frame Duration	10 ms

Slot Duration	0.5 ms
Voice Transmission Period	20 ms (vocoder parameter)
Coding Scheme	Convolutional coding with 1/3 coding rate
Subcarrier Spacing	15 kHz
Number of Subcarriers	72 (for 1.4 MHz) or 300 (for 5 MHz)
Number of Subcarriers per RB	12
Total # of Simultaneous Transmitted RBs per MR	6 (for 1.4 MHz) or 25 (for 5 MHz)
Total # of Simultaneous Transmitted RBs per UE	1
Number of Symbols per Slot	6 (Extended Cyclic Prefix)
Necessary transmitted information at PHY level (for e.g. voice service type PMR)	e.g. 1 packet of 480 bits each 20 ms
Number of Bits per Symbol	2 bits/symbol (QPSK modulation)
# of RBs necessary to transmit one packet	4 RBs each 20 ms
Total Throughput in Bits/Sec (including pilots)	1.728 Mb/sec or 7.2 Mb/sec
Transmission Scheme	SC-FDMA

Different scenarios have been evaluated as seen in Table 5 with the system parameters. For the simulations, an ITU channel model (ITU-R P.1411-4) designed for computing path loss between two terminals of low height (below roof-top) in urban environments has been used, combined with standard 3GPP Extended Typical Urban (ETU) and Extended Pedestrian A (EPA) channel models. It is also important to mention that the considered ITU model includes both Line-Of-Sight (LOS) and Non-Line-Of-Sight (NLOS) regions and models the rapid decrease in signal level noted at the corner between LOS and NLOS regions.

The used ITU model is based on measurements made in the UHF band with antenna heights between 1.9 and 3.0 m above ground, and transmitter-receiver distances up to 3 000 m. This model is also very well adapted to transmission ranges below 3000 m. The model includes the statistics of location variability in the LOS and NLOS regions, and provides a statistical model for the corner distance between the LOS and NLOS regions. For all these reasons, the ITU model is very well adapted to our scenarios where the terminals are located below roof-top height and in the Ultra High Frequency (UHF) range (from 300 MHz to 3 GHz). In our simulations results have been obtained for a location variability of 50% and 90% – however the model and the simulator provide different values which can be easily exploited for further work. We have also considered a Noise Figure of 7 dB and a Noise Density of -174 dBm/Hz. Different bandwidths and also different transmission powers have been further considered.

Table 5: System Parameters

System Parameter	**Values**
Inter-Site Distance, ISD (3GPP TR 36.814)	500 m (3GPP Urban) 1732 m (3GPP Rural)
Channel Type	ETU (Extended Typical Urban) EPA (Extended Pedestrian A)
Noise Figure	7 dB

Noise Density	-174 dBm/Hz
Location Variability for ITU Model (ITU-R P.1411-4)	1%, 10%, 50%, 90%, 99% (from LOS to NLOS)
Bandwidth	1.4 MHz or 5 MHz (in the 763-768 MHz band)
Carrier Frequency	763.7 MHz for 1.4 MHz bandwidth 765.5 MHz for 5 MHz bandwidth
# Antennas User	1 Tx, 1 Rx
# Antennas Mesh Relay	1 Tx, 2 Rx
Tx Power User	1 W
Tx Power Mesh Relay	1W - 10 W

2.4.2.3 Simulation Results

The choice of the simulation scenarios have been carefully taken into account. A first subsection "Multiple end-to-end transmissions (1.4 MHz and 5 MHz)" is dedicated to multiple end-to-end transmissions while the second subsection "Single end-to-end transmissions (best case)" supposes that the MR simultaneously relays only one transmission, which means that in the second subsection the MR can transmit with higher power than in the first subsection (see discussion from Section 2.4.2.1).

Multiple end-to-end transmissions (1.4 MHz and 5 MHz)

This subsection considers mainly two opposite simulation scenarios:

A scenario with a smaller frequency bandwidth for MR, a higher ISD and a lower location variability (corresponding to a smaller city for example, with lower number of users and lower roof-top height) – this scenario could be qualified as e.g. suburban or rural;

A scenario with a larger frequency bandwidth for MR, a lower ISD and a higher location variability (corresponding to a more populated city for example, with higher number of users and higher roof-top height – predominant NLOS scenario) – this scenario could be qualified as urban.

For the first scenario (i.e. scenario A) we have considered an EPA channel model, a 1.4 MHz MR bandwidth, 50% location variability for ITU model, a Noise Figure NF = 7 dB, a distance between users of 1732 m (ISD), multiple end-to-end transmissions through the relay (the maximum transmission power at MR level is shared between different end-to-end links), 1 W maximum transmission power for the user, 10 W maximum transmission power for the MR.

For the second scenario (i.e. scenario B) we have considered an EPA channel model, a 5 MHz MR bandwidth, 90% location variability for ITU model, a Noise Figure NF=7 dB, a distance between users of 500 m (ISD), multiple end-to-end transmissions through the relay (the maximum transmission power at MR level is shared between different end-to-end links), 1 W maximum transmission power for the user, 10 W maximum transmission power for the MR.

The End-to-End PER for DF schemes for scenario A and scenario B are shown respectively in Figure 18 and Figure 19. The abscissa represents the distance of the first link. In the first scenario, the MR transmission power of 10 W is divided between 6 simultaneous RBs occupying the 1.4 MHz frequency bandwidth (see Table 4). However, in the second scenario which uses a 5 MHz frequency bandwidth, the MR transmission power of 10 W is divided between 25 simultaneous RBs (see Table 4). In both scenarios we suppose that the frequency bandwidth is completely occupied by simultaneous links. This means that if the communication band is larger, the MR decreases the power allocated per user in order

to respect the power constraint. Moreover, the second scenario uses a higher location variability percentage (closer to NLOS model) but a much lower distance between users (only 500 m) and for these reasons the PER is much lower.

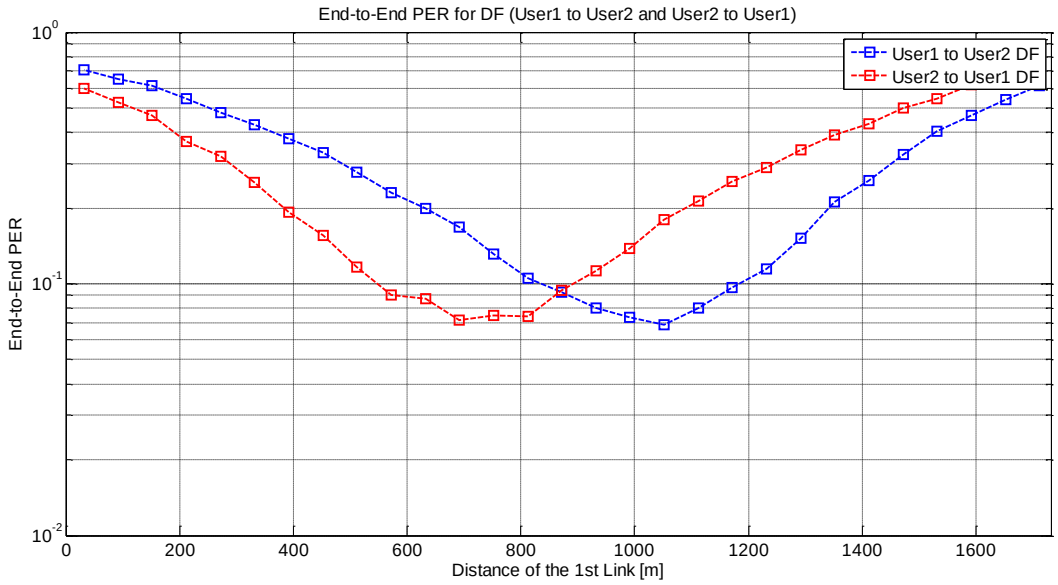

Figure 18: End-to-End PER for DF, Scenario A (EPA, 1.4 MHz, 50% location variability, NF=7 dB, 1732 m ISD, multiple end-to-end transmissions, 1 W maximum Tx power user, 10 W maximum Tx power for Mesh Relay)

It can be also noticed that the minimum PER for the DF scheme represented in Figure 18 is not for a MR located in the middle of the system. Surprisingly the best MR position is at 750 m (when transmitting from U2 to U1) and 1050 m (when transmitting from U1 to U2) for scenario A for 1732 m range between 2 users. This result can be explained because the MR uses two antennas in reception while the users U1 and U2 use only one. This fact creates and asymmetry in the link budgets.

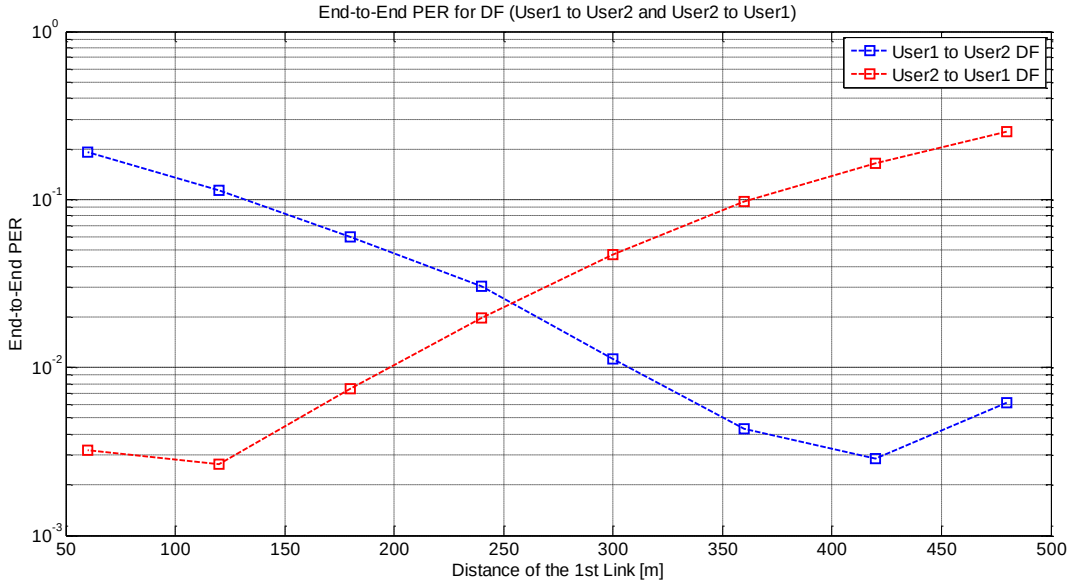

Figure 19: End-to-End PER for DF, scenario B (EPA, 5 MHz, 90% location variability, NF=7 dB, 500 m ISD, multiple end-to-end transmissions, 1 W maximum Tx power user, 10 W maximum Tx power for Mesh Relay)

A similar result as in Figure 18 can be obtained for Figure 19 as well: it can be again noticed that the minimum PER is not for a MR located in the middle of the system. For the scenario B represented in Figure 19, the best MR position is at around 100 m (when transmitting from U2 to U1) and at around 400 m (when transmitting from U1 to U2) – scenario B considers a maximum range between 2 users of

500 m. This result can be explained again because the MR uses two antennas in reception while the users U1 and U2 use only one. For the sake of comparison the algorithm used by MR for DF is a linear MMSE equalizer implemented in frequency domain. In the particular settings used here, each transmission is devoted to one specific user with one transmit antenna. Hence the MR receives with two antennas (standard SIMO system), the implemented equalizer yields a traditional MRC receiver in the frequency domain. For the TWR, a linear MMSE equalizer implemented in frequency domain was used too, but in the virtual MIMO case (multiple transmitters with one antenna) the linear MMSE equalizer is used both to separate the users (with residual interference depending on the specific channel realizations) and to recover spatial receive diversity through MRC.

Even so, in terms of mean PER (among the two end-to-end links), if only one MR is used for both directions (i.e. U1 to U2 and U2 to U1), later figures Figure 26 and Figure 27 show that the minimum mean PER is obtained in the middle of the ISD, i.e. at 866 m and 250 m respectively.

Further, Figure 20 and Figure 21 show a comparison in terms of End-to-End PER for different TWR schemes for scenario A and scenario B respectively. It is further showed that adaptive TWR is better (or equal) than simple TWR for different MR positions.

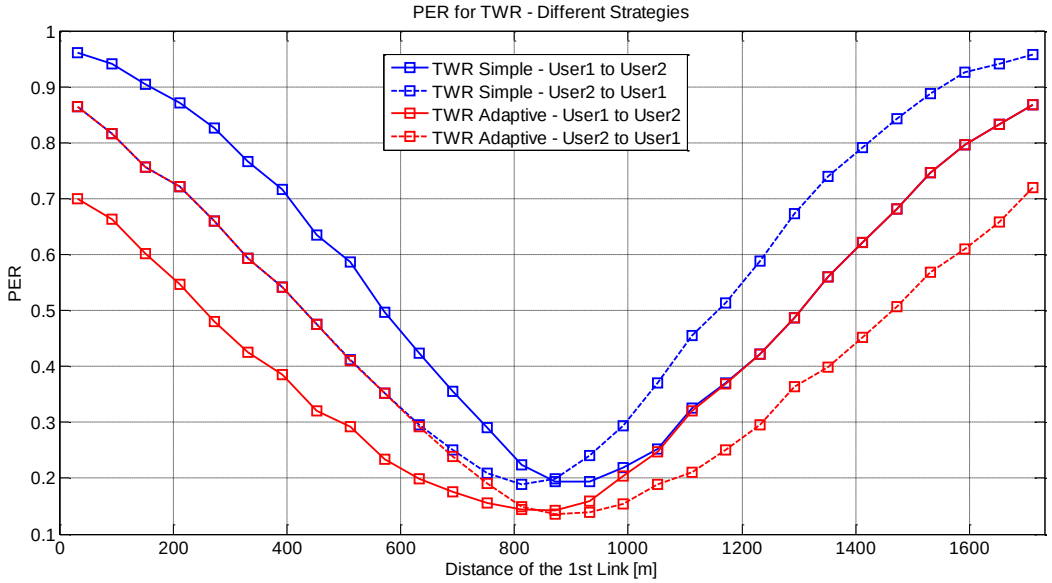

Figure 20: End-to-End PER for TWR, Scenario A

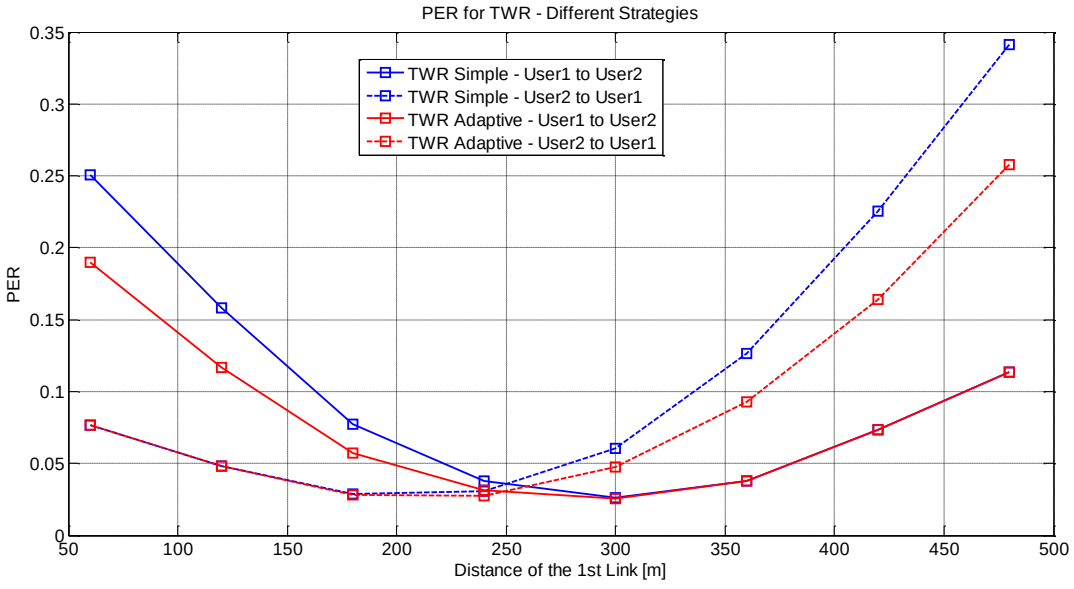

Figure 21: End-to-End PER for TWR, Scenario B

Figure 22 and Figure 23 show U1 to U2 End-to-End PER, as a comparison between TWR and DF schemes. It can be easily noticed that DF outperforms TWR in terms of PER. Moreover, in the case of Figure 23 the gap between TWR and DF is even higher and most probably because in the case of Figure 23 the MR transmits with lower power (since it relays more end-to-end links than in the case of Figure 22, but for the same maximum power of 10 W).

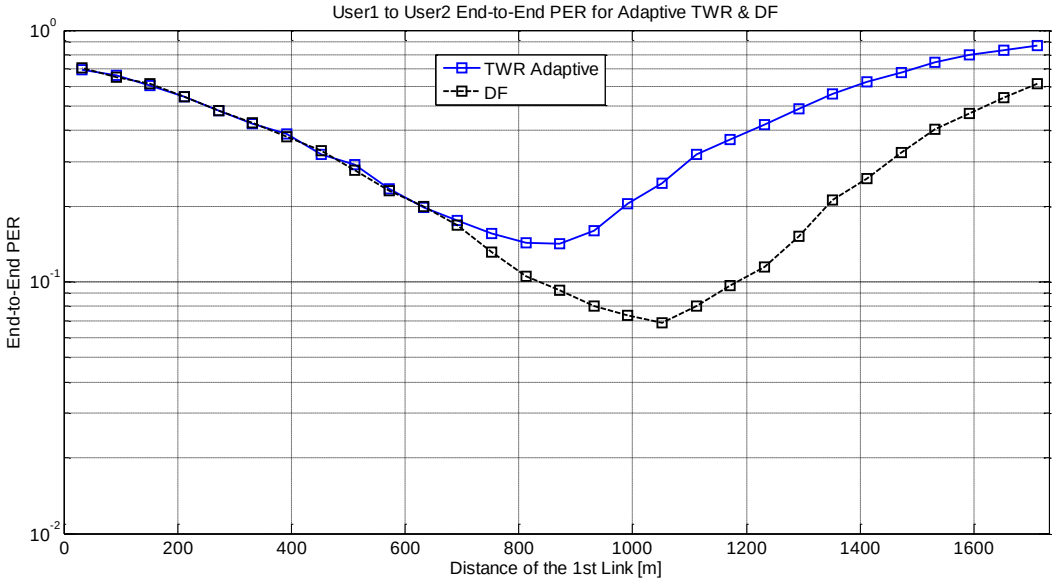

Figure 22: End-to-End PER U1 to U2, comparison between TWR and DF, Scenario A

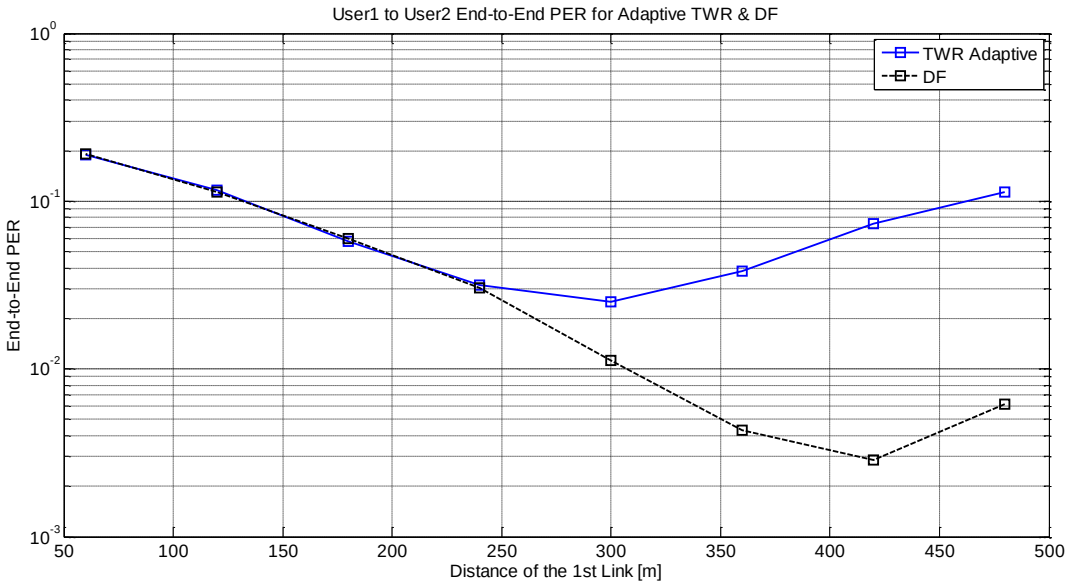

Figure 23: End-to-End PER U1 to U2, comparison between TWR and DF, Scenario B

Similar and symmetric results can be observed when we consider a U2 to U1 transmission represented in Figure 24 for scenario A and in Figure 25 for scenario B.

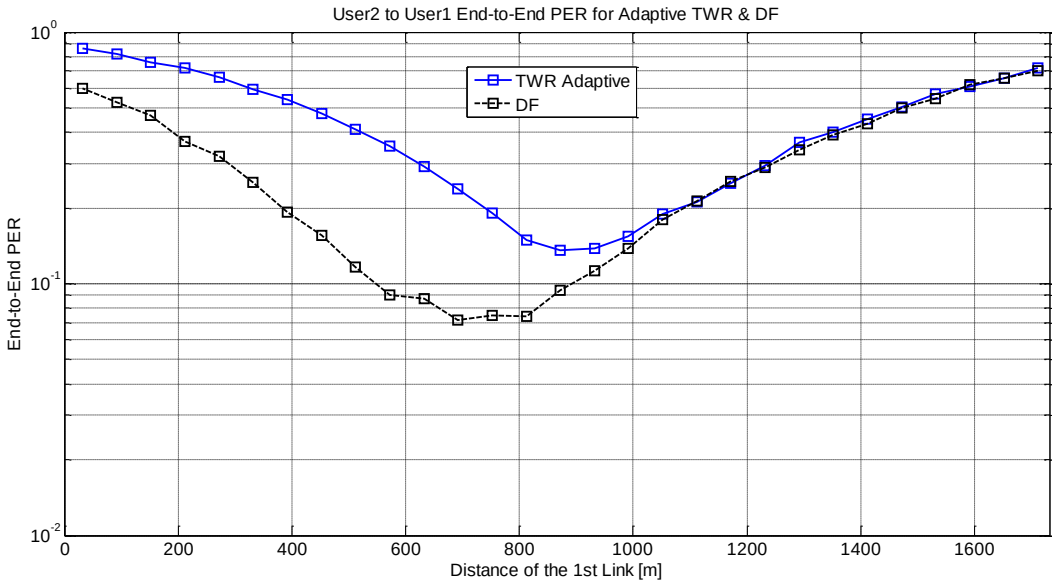

Figure 24: End-to-End PER U2 to U1, comparison between TWR and DF, Scenario A

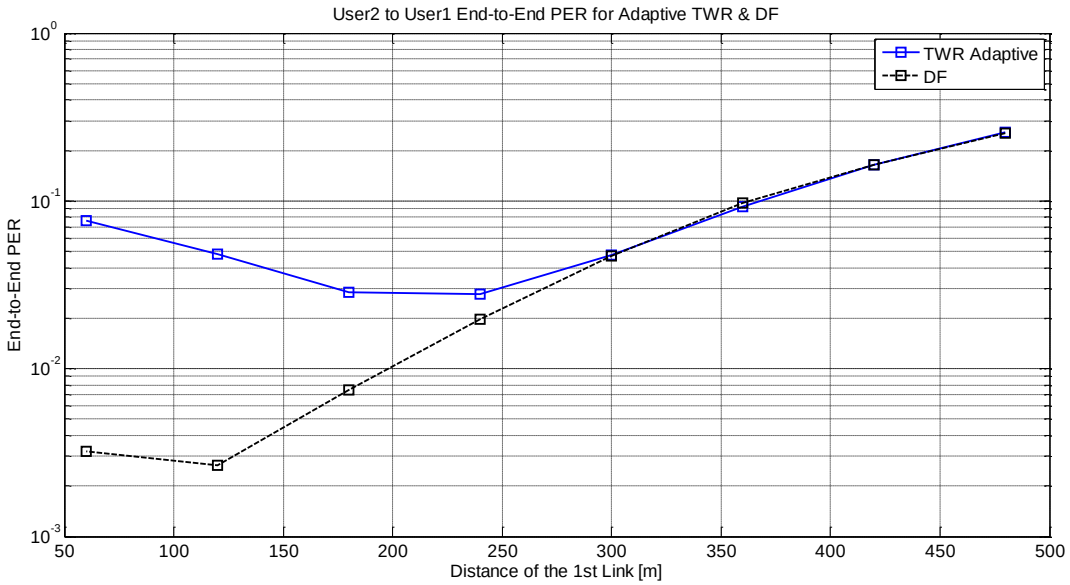

Figure 25: End-to-End PER U2 to U1, comparison between TWR and DF, Scenario B

Overall, as already previously mentioned, DF scheme is better than TWR scheme in terms of mean PER for both scenarios A and B represented in Figure 26 and Figure 27 respectively. As a matter of fact, the results can be explained because in the case of TWR the U1 and U2 are simultaneously transmitting in the first slot interfering with each other and thus increasing PER. However, in the case of DF scheme, U1 and U2 have dedicated transmission slots and therefore their interference at MR level is restricted.

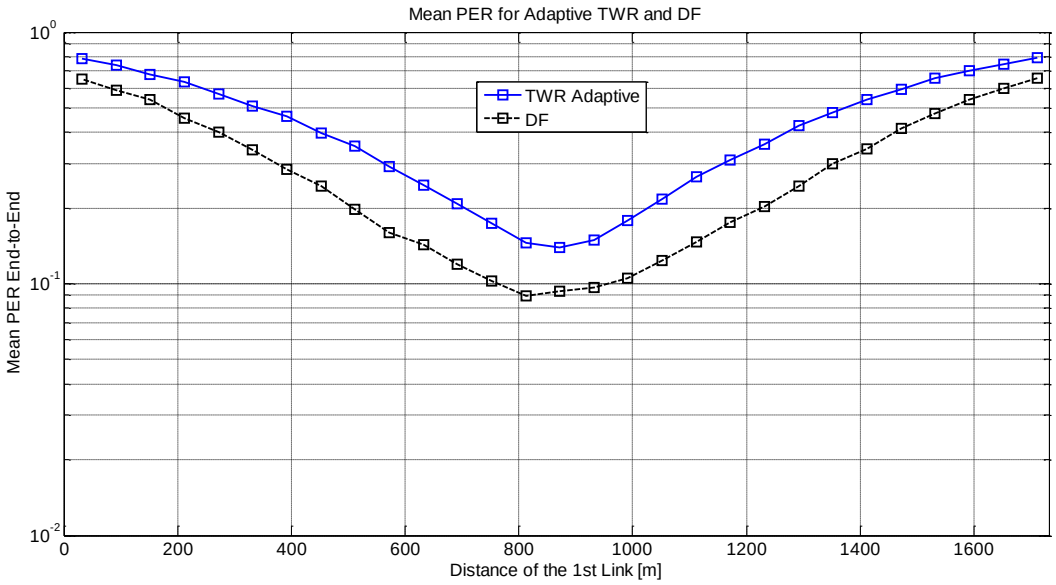

Figure 26: Mean End-to-End PER, comparison between TWR and DF, Scenario A

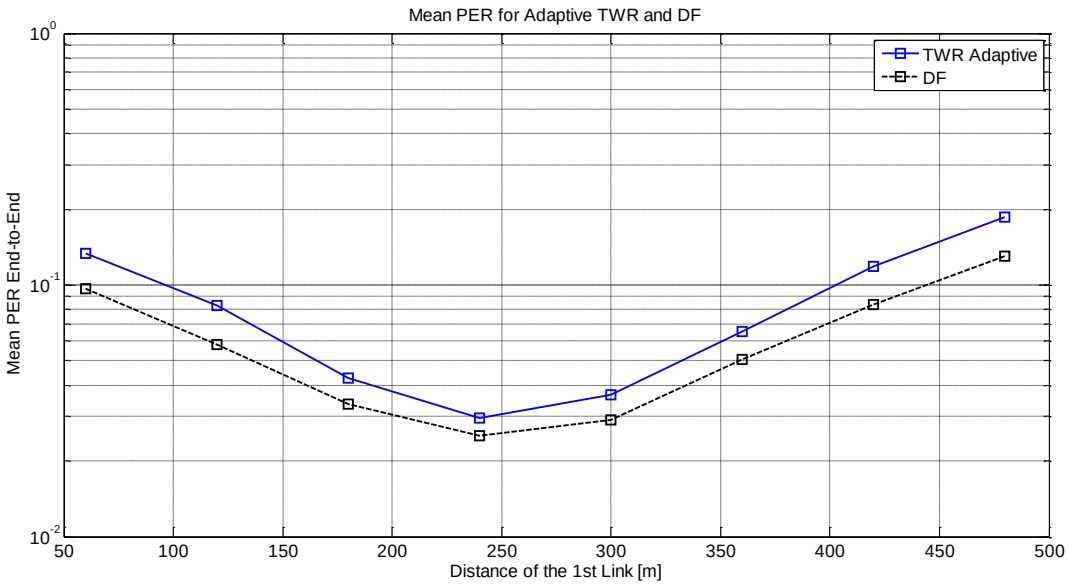

Figure 27: Mean End-to-End PER, comparison between TWR and DF, Scenario B

Another interesting result is in the case of Figure 27, where the PER gap between TWR and DF has been limited. This limitation can be explained because the ISD is much smaller compared to Figure 26, and despite of lower MR transmission power.

Figure 28 and Figure 29 present End-to-End throughput (from U1 to U2 and from U2 to U1) for adaptive TWR and simple TWR, for different MR positions between two users U1 and U2. The maximum throughput is achieved for Figure 28 (with a 1.4 MHz system bandwidth) at approximately 1300 packets/second for a MR located at half of the distance between the two users U1 and U2, and is achieved for Figure 29 (with a 5 MHz system bandwidth) at approximately 6100 packets/second for a MR located at one third of the distance between the two users U1 and U2.

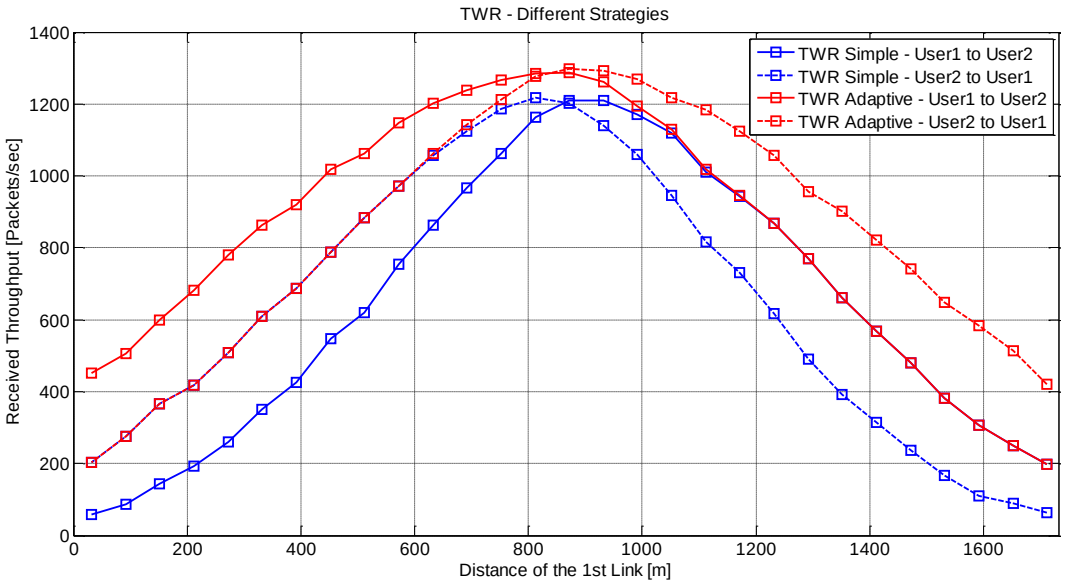

Figure 28. End-to-End Packet Throughput, comparison between Adaptive TWR and Simple TWR, Scenario A

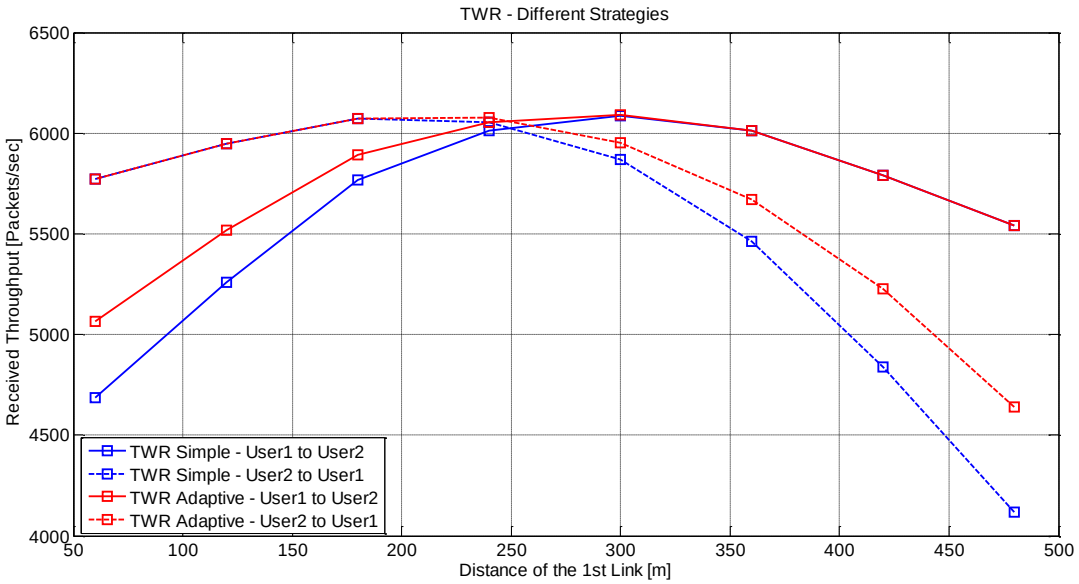

Figure 29: End-to-End Packet Throughput, comparison between Adaptive TWR and Simple TWR, Scenario B

In terms of U2 to U1 received total throughput (Figure 30 and Figure 31), adaptive TWR gives better results than DF in most of the simulation cases. Similar simulation results can be obtained when transmitting from U1 to U2 (as represented in Figure 32 and Figure 33). However, for scenario A, in the case of Figure 30 and Figure 32, when the MR is far away from the transmission source, it seems that DF has a small gain, which is somewhat expected. However, if the distance between U1 and U2 is very small - for scenario B in the case of Figure 31 and Figure 33, the total transmitted throughput is almost double for any MR position between the two users.

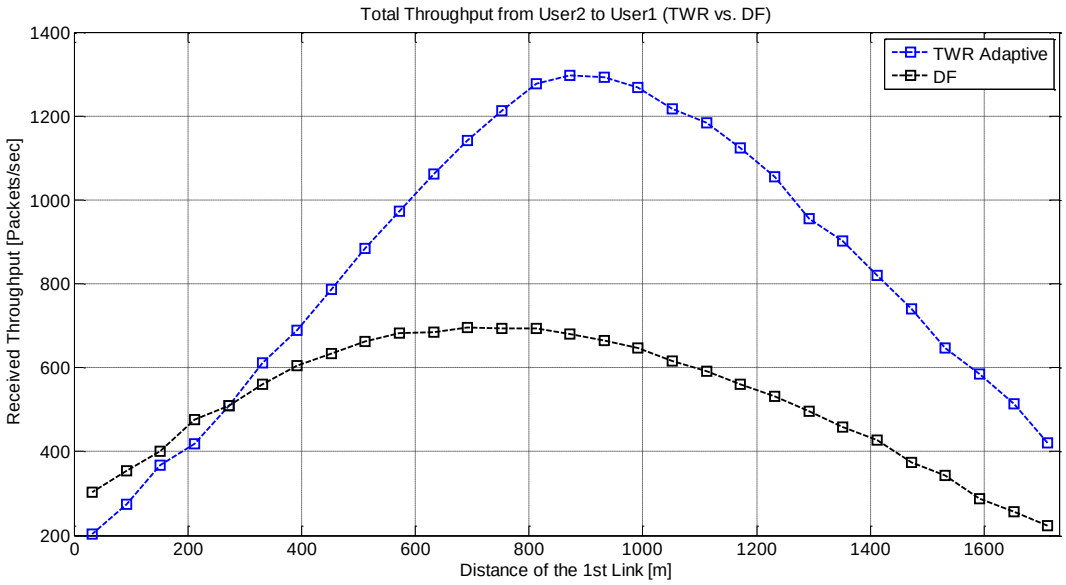

Figure 30: U2 to U1 Packet Throughput, comparison between Adaptive TWR and DF, Scenario A

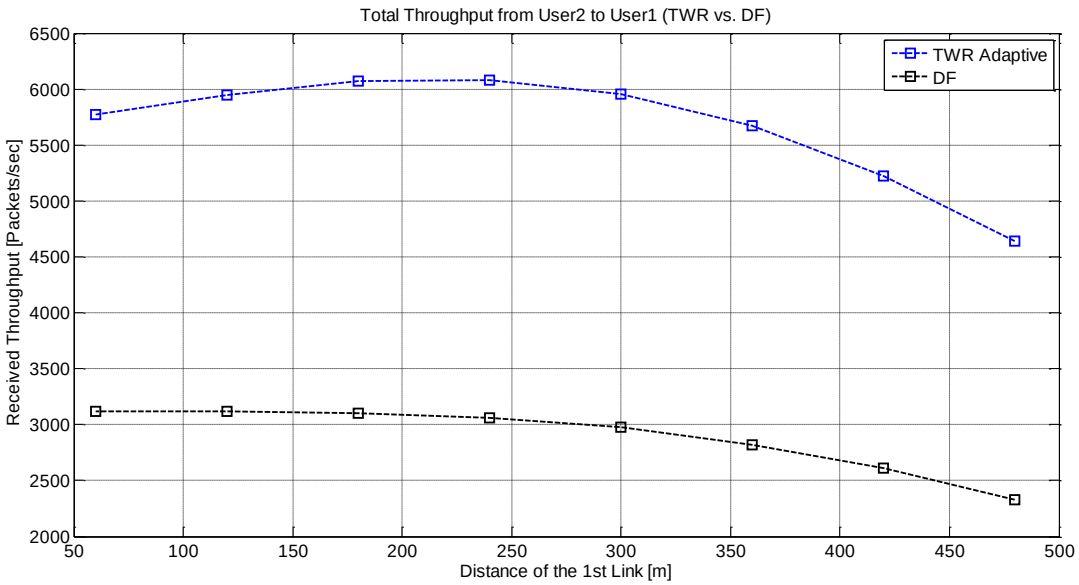

Figure 31: U2 to U1 Packet Throughput, comparison between Adaptive TWR and DF, Scenario B

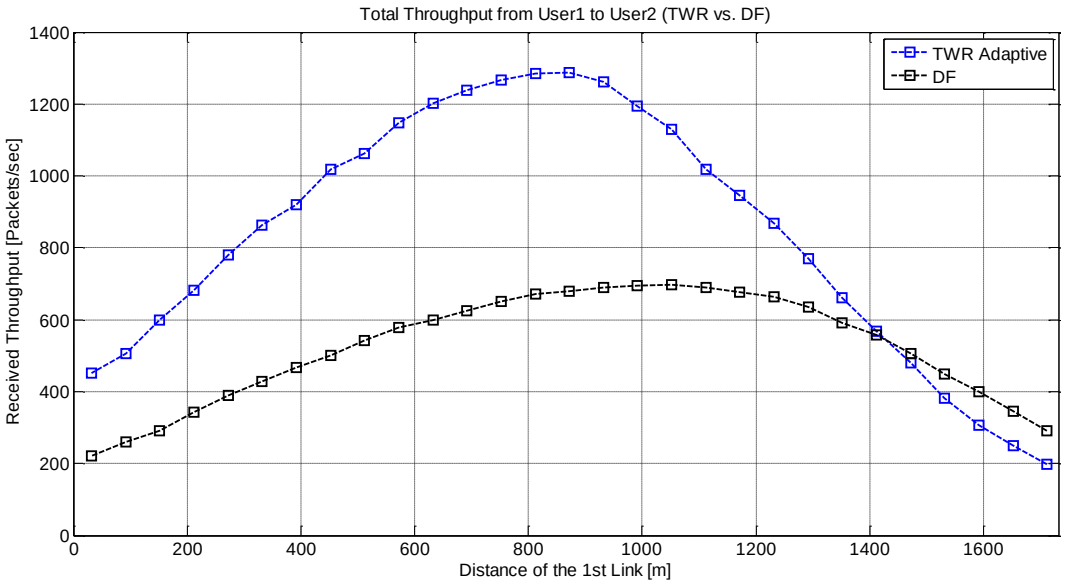

Figure 32: U1 to U2 Packet Throughput, comparison between Adaptive TWR and DF, Scenario A

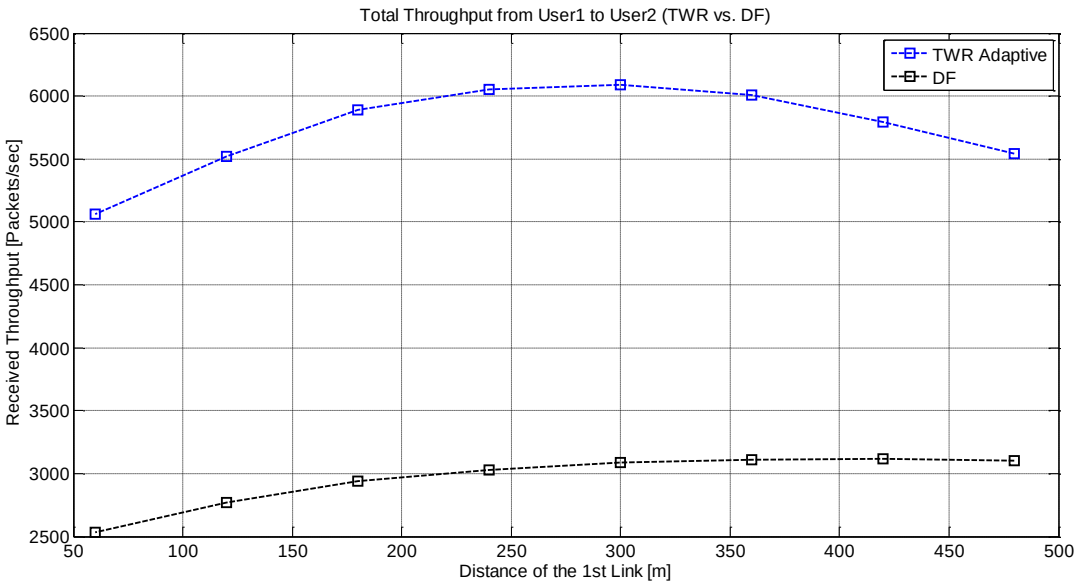

Figure 33: U1 to U2 Packet Throughput, comparison between Adaptive TWR and DF, Scenario B

Finally, if we compute the total transmission throughput (the sum of U1 to U2 throughput and of U2 to U1 throughput) we obtain that overall adaptive TWR gives better results in terms of achievable throughput for any of the scenarios A or B represented in Figure 34 and Figure 35.

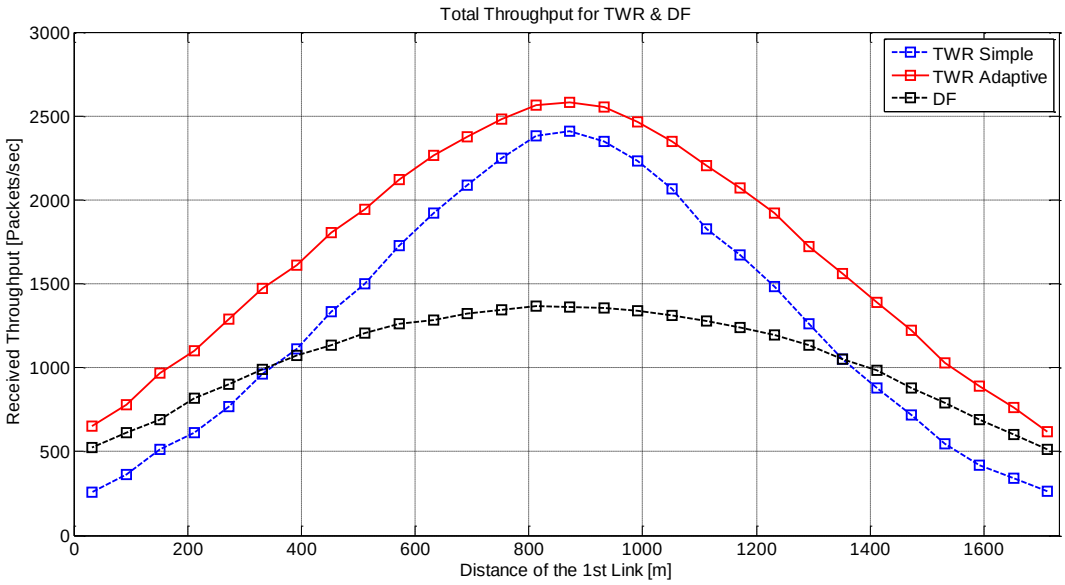

Figure 34: Total Packet Throughput, comparison between Adaptive TWR, Simple TWR & DF, Scenario A

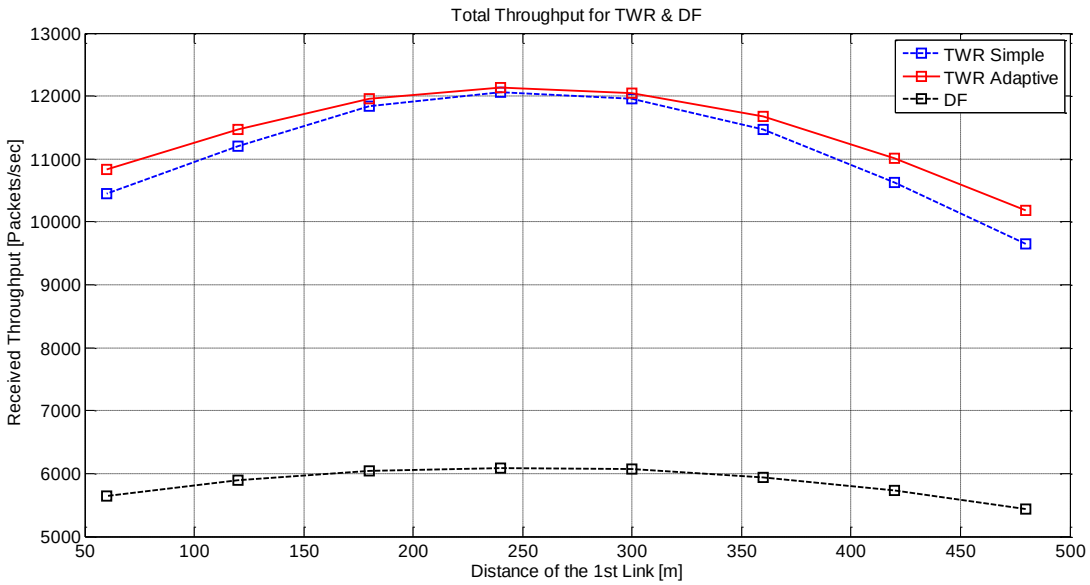

Figure 35: Total Packet Throughput, comparison between Adaptive TWR, Simple TWR & DF, Scenario B

Single end-to-end transmissions (best case)

For this scenario we have used an ETU channel model, 1.4 MHz (1.4 MHz or 5 MHz does not matter if there is only one user transmitting in frequency domain using only 1 RB), 1% location variability, a Noise Figure NF = 7 dB, 5000 m ISD - corresponding to a transmitting range larger than in the previous cases, since we want to check the performance in a best case scenario with a single end-to-end transmission relayed by the MR, 1 W maximum transmission power for the user, 10 W maximum transmission power for the MR.

The goal of this short section is to show that if the model is more likely to be LOS (i.e., 1% location variability), and the MR relays only one link at a time – which means that only one RB is actually used per slot and not 6 or 25 RBs, the total communication range can be increased.

End-to-End PER results from Figure 36 and Figure 37 show that adaptive TWR can still be used in the above scenario in the case of unidirectional end-to-end transmissions, but the position of the MR is essential. However, results from Figure 38 show that in terms of mean PER (over bi directional communications), it is no longer acceptable to use adaptive TWR schemes. In such situations - as in the

case of very long distances (e.g. up to 5000 m), DF scheme provides better results: DF is more robust to interference as opposed to TWR scheme. This aspect can be easily seen on both directions e.g. on Figure 36 and on Figure 37 respectively, but also on the results obtained in Figure 38 which represents the mean PER as a function of MR position between the 2 users.

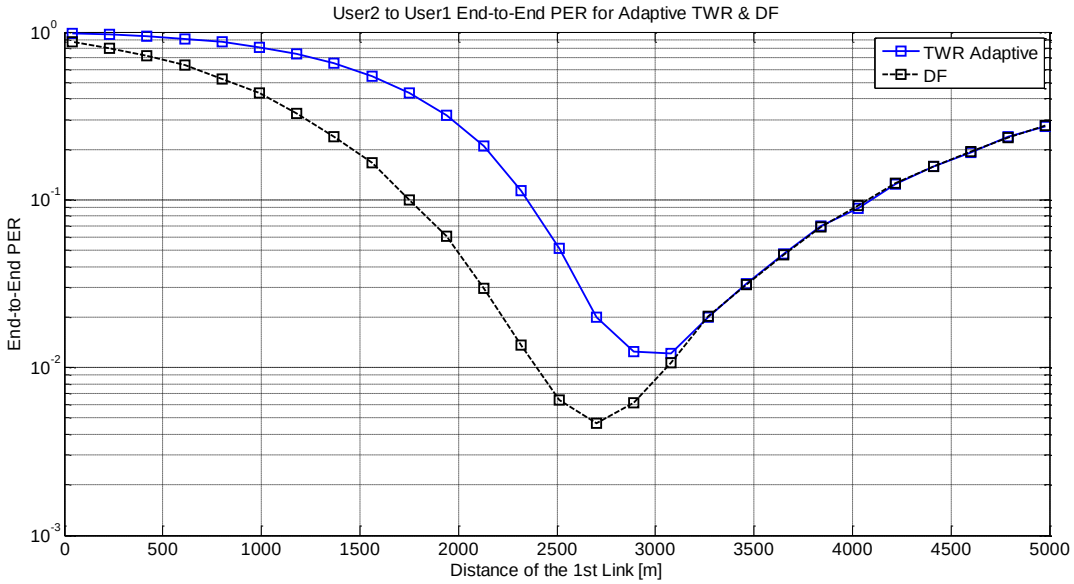

Figure 36: End-to-End PER U2 to U1, ETU, 1% location variability, NF=7 dB, 5000 m between users, single end-to-end transmissions, 1W maximum Tx power for user, 10W maximum Tx power for MR.

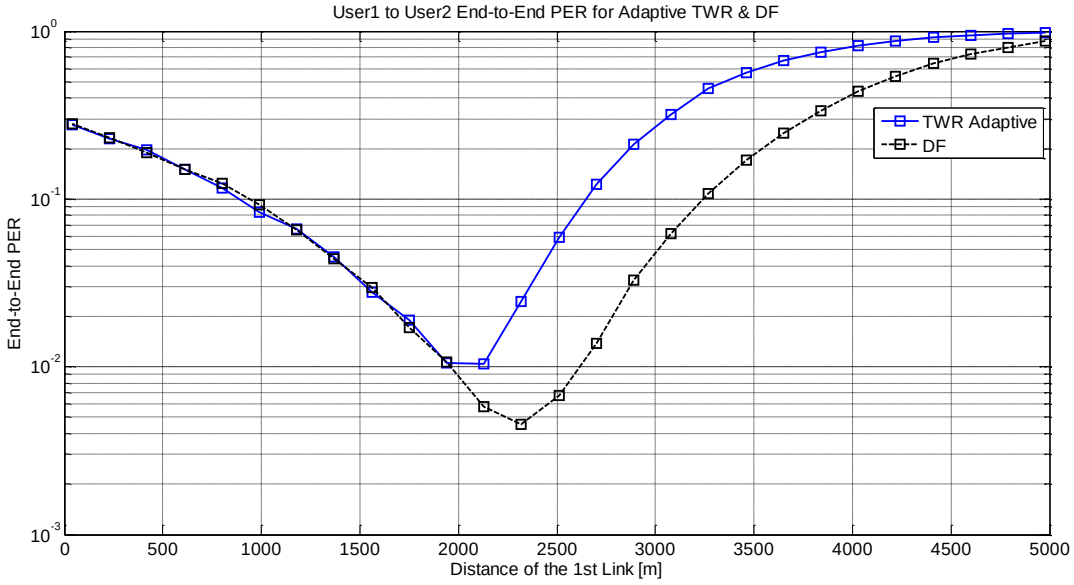

Figure 37: End-to-End PER U1 to U2, ETU, 1% location variability, NF=7 dB, 5000 m between users, single end-to-end transmissions, 1W maximum Tx power for user, 10W maximum Tx power for MR.

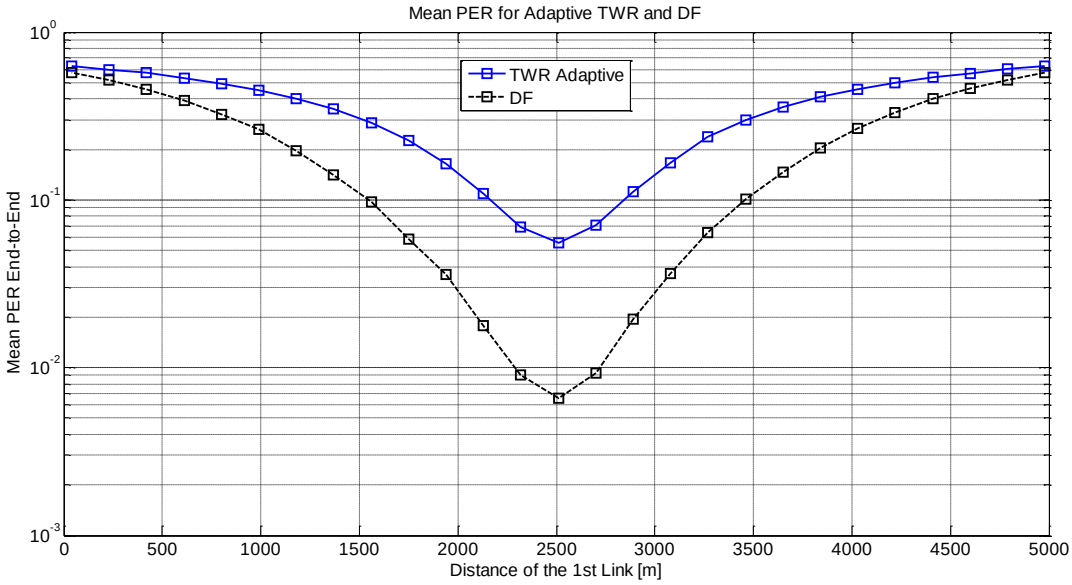

Figure 38: Mean PER, ETU, 1% location variability, NF=7 dB, 5000 m between users, single end-to-end transmissions, 1W maximum Tx power for user, 10W maximum Tx power for MR.

2.4.3 Discussion and conclusions

The focus of the work was at PHY / MAC layer on relaying strategies for inter-cluster communications, namely for the traffic going through bridging MRs. The bridging relay can be used between multiple users or between different base stations. In wireless mesh networks for fast deployable PMR systems, since the back-bone traffic is going through those MRs, and part of it may be bidirectional, we investigated a two-way relaying technique applied to the bridging MRs. Implementation of Two-Way Relaying (TWR) strategy needs the presence of a bi-directional flow between the CHs of the neighbouring clusters. LTE adaptation or design of new signalling and possibly protocols required to share the needed information between CHs will not be investigated in this deliverable.

Two-Way-Relaying has been compared with a traditional Decode-and-Forward strategy for two main deployment scenarios:

A) A scenario with a smaller frequency bandwidth for MR, a larger ISD and a lower location variability (corresponding to a smaller city for example, with lower number of users and lower roof-top height);

B) A scenario with a larger frequency bandwidth for MR, a smaller ISD and a higher location variability (corresponding to a more populated city for example, with higher number of users and higher roof-top height – predominant NLOS scenario).

These categories have been defined by taking into account architecture opportunities and real-deployment situations. Real 3GPP and ITU parameters and system constraints have been also considered: the 700 MHz band was considered for simulations since it is one of the main candidate bands for deployment of the future broadband PMR networks. Scenarios A and B show that TWR provides better throughput than DF, for any possible position of a MR. TWR typically doubles the throughput at the best MR position. In scenario A, TWR achieves significant throughput gains only for certain distances (typically the MR must be placed in between the served nodes). However, for more dense urban deployments like scenario B, throughput gains are weakly sensitive to the MR position, which is a desired feature in rapidly deployable PMR systems. It is also shown that DF is more robust than TWR in terms of end-to-end PER (e.g. DF has better or equal PER than TWR, depending on the MR position).

This section also investigated a best-case scenario for a PMR deployment in the case of voice services. In this case it is showed that for long-distance robust communications (e.g. up to 5 km) where

maximum limit for the achievable throughput is not of interest, the DF technique is an interesting approach.

2.5 Fair resource allocation for multi-hop communications

2.5.1 Scenario: Clustered wireless mesh networks based on LTE

The scenario focuses on rapidly deployable wireless mesh networks, to be used to cover an area which is not covered by fixed PMR infrastructure. It could be the case after a major natural disaster. Another possible use case is to deploy a wireless network in areas without any infrastructure, or where the main governmental or market actors do not want to invest on a wired infrastructure. A third use case, similar to coverage extension with relays, is when there is a specific and limited area which is not covered by the fixed network, then a wireless extension can be imagined with possibly multiple relays. Here we will focus on the first use case.

In order to reuse as much as possible the LTE structure and protocols, we propose a clustered wireless mesh network meaning that the network is divided in clusters, mapping (or equivalent) to LTE macro (or micro, depending on the available transmit power, type of equipment, etc.) cells. Each cell is controlled by a ClusterHead (CH) which is acting as a 3GPP eNodeB. Mesh Routers (MR) are acting as relays, and inherit relay and UE procedures from LTE. Some MRs, connected to 2 or 3 clusters, are called bridging MRs and allow communications between the clusters. Common bridging MRs between the clusters can cooperate for improving performance (robustness, throughput, latency). Edge MRs are possibly present, if the wireless mesh network is not independent but is linked to other networks via other technologies. A schematic representation of the clustered mesh network is given in the figure below.

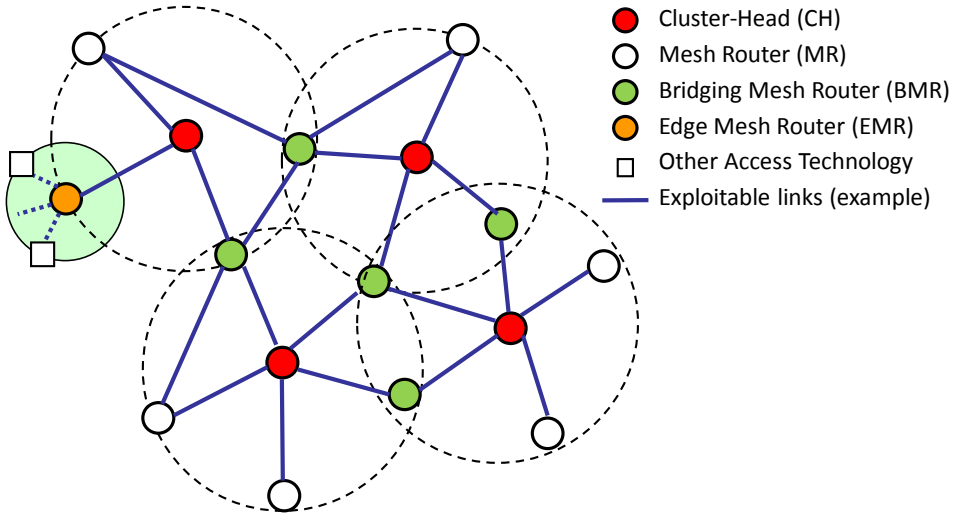

Figure 39: Clustered wireless mesh network

2.5.2 Fair joint scheduling/relaying schemes for multi-hop/mesh communications

A challenging aspect of this scenario is the design of adequate radio resource strategies that are able to efficiently exploit the benefit brought by the use of cooperative relaying techniques in this networking setting. Scheduling algorithms are of vital importance in today and future wireless communication systems. They are responsible for efficiently sharing scarce and expensive radio spectrum among different users while handling heterogeneous traffic demands and dealing with disparate radio conditions. Another challenge here is that we allow for direct communication inside a given cluster and, possibly, multiple hops inside the same cluster, always under the control of the CH. Please notice that the results described in the following subsections can also be applied to a cell in which direct communications are allowed.

We consider efficient and fair opportunistic scheduling of delay tolerant traffics in clustered/cellular environment with dynamic relaying. A wide range of nowadays applications generate this type of traffic, i.e. email, internet browsing, asynchronous file transfer, etc. They are generally classed as requiring a best effort service and give more flexibility to the system to handle them.

2.5.2.1 System setting

We consider a wireless communication system consisting in a single cluster having K users uniformly distributed around the CH in a circle of radius *R*. We consider a block fading channel of width W (one sub-channel in a multicarrier system) in a time-slotted manner (time division multiple access). We assume that the channel gains are independent but not necessarily identically distributed across the users. We further assume that the channel gains remain constant during each slot but change from one slot to another, and we assume that the scheduler has perfect information of the fading processes of each radio link in the cluster.

Let $h_{u,v}^n$ denotes the state of the radio channel between users u and v at slot n and $r_{u,v}^n = log_2(1 + \beta \frac{h_{u,v}^n}{N0})$ the transmission rate between users u and v at slot n, where N_0 is the thermal noise power and $0 < \beta < 1$ the SNR gap between the considered transmission system and its Shannon capacity limit.

In case where $h_{u,v}^n$ are Rayleigh distributed, the Probability Density Function (PDF) of $h_{u,v}^n$ is given as

$$P\left(h_{u,v}^n = x\right) = \frac{1}{Pr_{u,v}} e^{-\frac{x}{Pr_{u,v}}}$$

Where $Pr_{u,v}$ is the mean received power between u and v

$$Pr_{u,v} = Pt\left[\frac{d0}{d_{u,v}}\right]^{pl}$$

Pt is the transmit power, $d0$ is the minimum distance between any couple of users, and pl is the power loss factor.

We consider that each user has one delay tolerant traffic flow $f_{u,v}$ toward one of the $K-1$ other users. Traffic flows are in saturated traffic regime, i.e., each scheduled user has more data in its queue than the scheduled transmission rate.

2.5.3 Opportunistic schedulers

2.5.3.1 Maximum Multiuser Diversity Scheduling

The long-term average throughput of this system is maximized by scheduling on each slot the user with the best channel gain, exploiting hence fully the multiuser diversity of the system [20]. We call this scheme maximum multiuser diversity scheduling [20]. The winner user w is the one satisfying

$$w = argmax_{u=1,..K} r_{u,v}^n$$

2.5.3.2 Proportional Fair Scheduling

The Proportional Fair Scheduling was introduced in [21][22] in order to take advantage of multiuser diversity while providing good fairness level of channel access among users. The idea behind it is to normalize the score function of each user, i.e. user rate, by its average. Hence, the scheme schedules the user who is experiencing the best fading realization compared to its own past conditions, and not the user with the absolute best instantaneous rate.

The algorithm works as follows:

$$w = argmax_{u=1,..K} \frac{r_{u,v}^n}{RT_{u,v}^n}$$

$$Where\ RT_{u,v}^n = \begin{cases} \left(1 - \frac{1}{Tc}\right) RT_{u,v}^{n-1} + \frac{1}{Tc} r_{u,v}^n & if\ link\ (u,v)\ is\ scheduled \\ \left(1 - \frac{1}{Tc}\right) RT_{u,v}^{n-1} & otherwise \end{cases}$$

Tc (Tc > 1) is the length of the moving average window, in normalized units depending on the periodicity of scheduling.

2.5.3.3 Maximum Proportional Fair Scheduling

The maximal proportional fair scheduling was introduced in order to well benefit from multiuser diversity while still providing good level of fairness among users [23][22] .

Here, the users compete for the channel by normalizing their instantaneous achievable rate over their past maximal achievable rate.

Unlike the MUDS where the user with the best instantaneous rate is selected, in MPFS the winner is not necessarily the strongest one but the one who is likely experiencing its best radio conditions. And unlike CFS where the empirical distribution of rate is used to select the winner, in MPFS only the maximal value of past rates is used.

The algorithm is defined as follows:

$$w = argmax_{u=1,..K} \frac{r_{u,v}^n}{Rmax_{u,v}^n}$$

$$Where\ Rmax_{u,v}^n = max_{m=0...M-1}\ r_{u,v}^{n-m}$$

$Rmax_{u,v}^n$ is a dynamic threshold value around which the user's channel is considered as in its peak region, and M is the depth of moving average window.

2.5.3.4 Fair joint opportunistic scheduling and dynamic relaying

As opportunistic scheduling tries to exploit multiuser diversity to enhance the transmission efficiency, joint opportunistic scheduling and dynamic relaying is able to exploit also spatial diversity to enhance the overall network multiuser diversity.

In the context of clustered/cellular networks allowing Device to Device (D2D) communications, dynamic relaying will give the scheduler the choice between classical uplink/downlink through CH/BS transmission scheme, direct link transmission scheme, or dynamic one hop relay transmission scheme. Figure 40 describes the different relaying options offered to the scheduler.

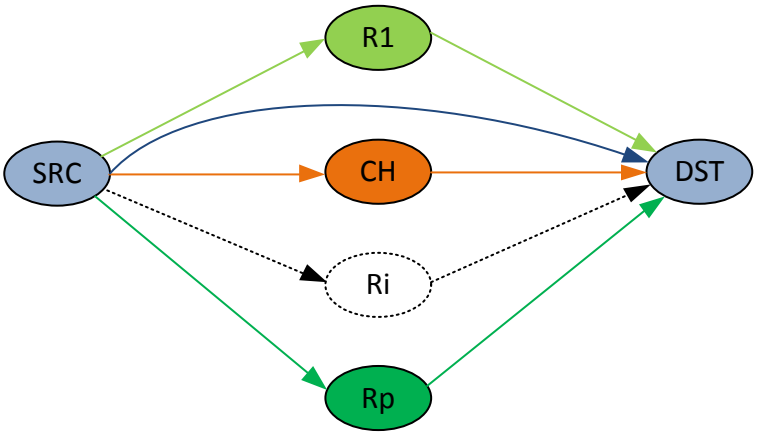

Figure 40: Dynamic relay selection

For each flow $f_{u,v}$ the scheduler compares the different relaying options using a max-min rule as follows

$$SF_{f_{u,v}}^n = max\left(Sc_{u,v}^{f_{u,v}n}, min(Sc_{u,R_{n,1}^{u,v}}^{f_{u,v}n}, Sc_{R_{n,1}^{u,v},v}^{f_{u,v}n}), \ldots, min(Sc_{u,R_{n,p}^{u,v}}^{f_{u,v}n}, Sc_{R_{n,p}^{u,v},v}^{f_{u,v}n})\right)$$

where

- $Sc_{a,b}^{f_{u,v}n}$ is the score function of the radio link between users a and b at slot n when transporting flow $f_{u,v}$

- $R_{n,i}^{u,v}$; $i = 1 \dots p$; are the available relays between users u and v at slot n (the CH is always a candidate relay for any flow).

The scheduler allocates then the channel to the flow achieving the best score

$$w = argmax_{u=1,..,K} SF_{f_{u,v}}^{n}$$

Depending on the relaying strategy of the winning flow $f_{u,v}$, the scheduler allocates the channel as follows:

- The channel is allocated during the whole slot to the link if the transmission is not relayed with rate $r_{u,v}^{n}$
- Otherwise, the first half of the slot is allocated to the link between the source and the selected relay and the second half to the link from the selected relay to the destination. We assume no queuing at the relays so the two links are allocated with rate $\min(r_{u,R}^{n} r_{R,v}^{n})$

The score functions of the different opportunistic scheduler are given in the following:

- MUDS

$$Sc_{a,b}^{f_{u,v},n} = r_{a,b}^{n}$$

- PFS

$$Sc_{a,b}^{f_{u,v},n} = \frac{r_{a,b}^{n}}{R_{f_{u,v}}^{n}}$$

$$RT_{f_{u,v}}^{n} = \begin{cases} (1 - 1/Tc) RT_{u,v}^{n-1} + rs_{f_{u,v}}^{n}/Tc\,, \; if \; f_{u,v} \; is \; scheduled \; at \; "n" \\ (1 - 1/Tc) RT_{u,v}^{n-1}, \; Otherwise \end{cases}$$

$$rs_{f_{u,v}}^{n} = \begin{cases} r_{u,v}^{n} \quad , \quad if \; direct \; transmission \\ \dfrac{r_{u,R}^{n} + r_{R,u}^{n}}{2} \quad , \quad if \; relayed \; through \; R \end{cases}$$

- MPFS

$$Sc_{a,b}^{f_{u,v},n} = \frac{r_{a,b}^{n}}{RM_{f_{u,v}}^{n}}$$

$$RM_{f_{u,v}}^{n} = max_{m=n,\dots,n-M+1} \, max\left(r_{u,v}^{m}, min(r_{u,R_{n,1}^{u,v}}^{m}, r_{R_{n,1}^{u,v},v}^{m}), \dots, min(r_{u,R_{n,p}^{u,v}}^{m}, r_{R_{n,p}^{u,v},v}^{m})\right)$$

2.5.4 Simulation Results

We consider users uniformly distributed around the CH within a range of $Dmax = d0.10^{-\frac{\Delta p}{10pl}}$, where Δp is the maximum SNR difference in dB between the strongest user and the weakest user in the network.

For our simulation we consider $\Delta p = 20dB,\ Pt = 10,\ Tc = 500$ and $M = 500$.

Figure 41 depicts the network's spectral efficiency achieved by MUDS, PFS, and MPFS for the 3 considered relaying schemes for different cluster size.

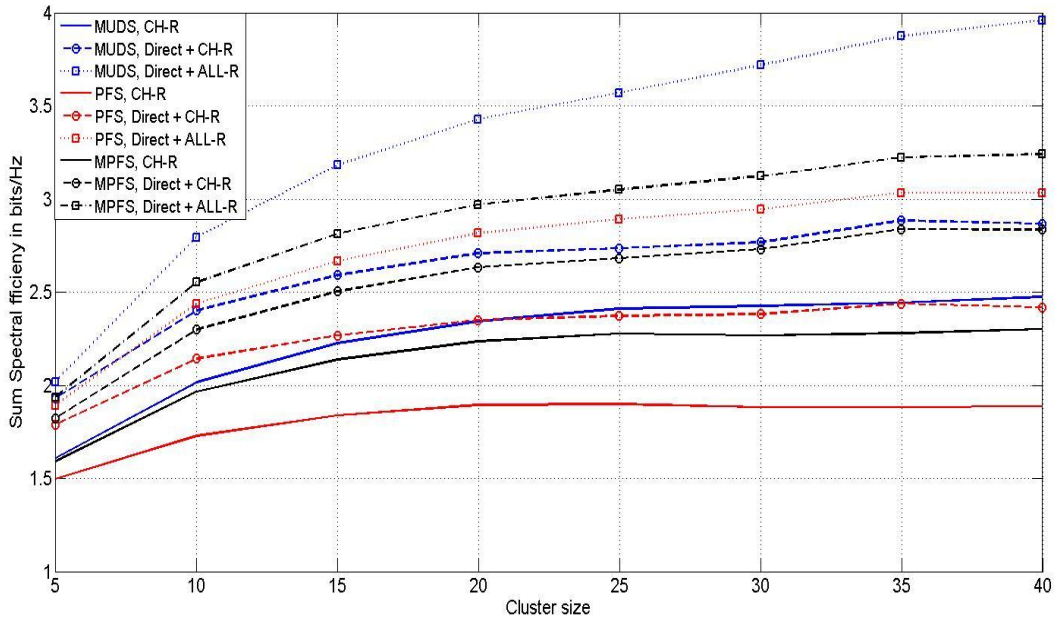

Figure 41: Spectral efficiency, i.e. the average of the network sum rate over simulation time, in saturated regime

We observe then that MUDS outperforms MPFS and largely outperforms PFS when only the CH is relaying ('CH-R' in the legend of the figure). Then we observe that allowing both direct transmission and relaying through the CH ('Direct + CH-R' in the legend of the figure) increases the spectral efficiency of all schemes and help MPFS to approach the performance of MUDS. Last, we observe that when allowing direct transmission and relaying through any node in the network ('Direct + All-R' in the legend of the figure) the performances of the three schemes are further improved and that MUDS largely outperforms MPFS as it is exploiting now much more multi-user diversity.

The second relaying scheme represents the best trade-off between performance and signalling overhead while the third relaying scheme, despite is very good performance, is much more unrealistic as it requires a huge amount of radio channels statistics feedback. As a matter of fact, when considering direct+CH scheme the source node feedbacks only information about its link to the destination node, assuming channel reciprocity. Only this information is needed by the CH which will then decide if the communication should be direct between the source and destination or should pass through itself. In direct+ALL-R scheme, all nodes needs to feedback information about all their links in order to select the best path.

The gain in throughput brought by efficient opportunistic schedulers comes obviously at the expense of fairness. To evaluate this fairness we use as measure the Jain Fairness Index (JFI)[24][24] .defined for a set '$x = \{x_1, .., x_k\}$' of 'N' elements as

$$JFI(x) = \frac{(\sum x_k)^2}{N \sum x_k^2}$$

The index varies between '1/N' in the worst fairness case and '1' in the perfect one. The x-axis is the access probability in saturated regime.

Figure 42 shows the JFI in term of channel's access probability of the three schedulers using the three relaying schemes.

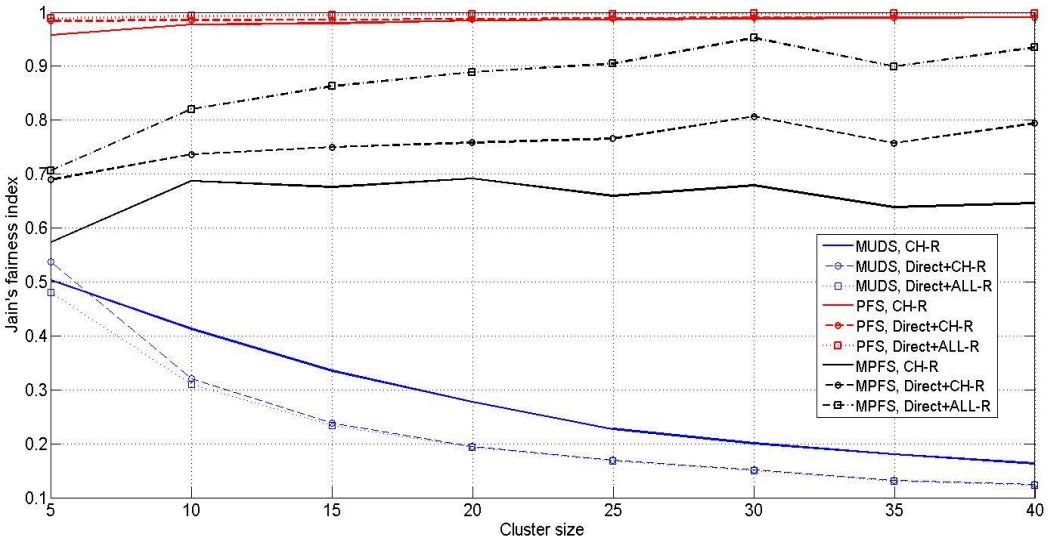

Figure 42: JFI on channel access probability in saturated regime

As expected, MUDS achieves the worst fairness and PFS the best possible one, while MPFS presents a good fairness above 70%. We observe also that increasing the number of possible relays help increasing the fairness of MPFS as pairs of source/destination radio links will share more relays.

2.5.5 Discussion and conclusion

In this section we provided a new class of joint scheduling/relaying algorithms for delay tolerant traffic. The joint scheduling and relaying is based on a dynamic max-min decision rule of the best relay for different opportunistic schedulers. The considered opportunistic schedulers are MUDS, PFS, and MPFS.

Simulation results showed that increasing the number of possible relays increases the spectral efficiency of the three schemes and help also enhancing the fairness of PFS and MPFS.

2.6 Impact of antenna position on performances in relay-assisted wireless network

2.6.1 Introduction

Enhanced capacity and extended coverage with increased cell edge bit rates are among the desired requirements of the beyond 4G wireless communication systems. Many solutions are being proposed in order to meet the above requirements. Among them, the relay technology appears to be a promising solution [28]. A basic relay network is composed of a Base Station (BS), Relay Station (RS) and Mobile Station (MS). The RS is an intermediate node which receives, processes and forwards the signal between BS and MS. By assuming that the backhaul link (BS-RS link) and the access link (RS-MS) attenuate less the signal that the direct link (BS-MS link), one can expect a throughput gain compared to the direct transmission when the signal is transferred via the relay.

Many studies have investigated the performance of the relaying technique either with a theoretical approach [29], or system-level simulations [30] or field measurements [31]. However, there are still lacks on understanding of the impact of the propagation conditions on the performance of the relaying technique. There is no clear answer if it makes sense from a strictly propagation point of view to transmit directly a signal from the source to the destination or to transmit the signal via a relay. Furthermore, impacts of key engineering parameters such as the relay antenna height or the relay position have not been considered yet.

This work aims to compare the relay-assisted communication throughput with the throughput provided by the direct link. Path loss models or measured values used for the analysis are extracted from a measurement campaign that was described in [32][33][34][35]. [32] is focused on the backhaul link whereas [6-8] are focused on the access link. All publications give many details about the measurement scenario and the BS, RS and MS locations. The comparison between relay-assisted and direct communication is performed for different relay antenna heights and positions. The work is divided in two main parts. We first describe the simulation setup and provides simulation results.

2.6.2 SIMULATION SETUP

2.6.2.1 Simulation parameters

We consider a base station BS which tries to communicate with the mobile by the assistance of a fixed relay. Both RS and MS are deployed in an outdoor environment and hence no penetration loss is taken into account. BS, RS and MS are alone in the cell and there is no interference from the other communicating nodes. These simulation assumptions would be oversimplified to estimate realistic throughputs but they are well-adapted in order to understand the impacts of the propagation channel or deployment parameters on the throughput. TABLE I. summarizes the simulation parameters adopted which are in agreement with [38].

TABLE I. SIMULATION PARAMETERS

BS transmit power	49 dBm
RS transmit power	33 dBm
Bandwidth, B	20 MHz
Carrier frequency	2.2 GHz
RS antenna height, h_{rs}	5-10 m
MS antenna height	2 m
Rooftop level, h_{roof}	15-25 m
Path loss, PL	Measured path loss or path loss models

Two scenarios are defined. The first one is illustrated by Figure 43. BS, RS and MS are collinear. This scenario is used to quantify the impact of the relay antenna or of the relaying protocol. A typical plot for this scenario is Figure 47 where the capacity is given as function of $d_{BS\text{-}MS}$.

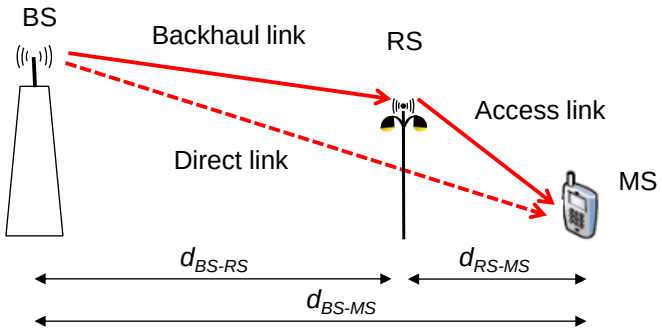

Figure 43: Relaying scenario

PL is calculated with models described in [32][33][34][35] and summarized by equations (1-6). Since RS and MS are often under the rooftops in an urban environment, the optical visibility between BS and RS or between BS and MS is unlikely. Therefore, we consider a NLOS single slope PL model for the direct and backhaul links. Regarding the access link, we consider a dual slope PL model which is a combination between the LOS and NLOS components since MS may have a LOS connection with RS when MS is close to RS. The LOS/NLOS distance dependent probability is defined in [35]. Received powers are processed by assuming isotropic antenna with 0 dBi gain at RS, BS and MS.

$$PL_{BS-MS} = 33.4\log_{10}(d_{BS-MS}) + 38.7 \quad (1)$$

$$PL_{BS-RS} = 33.4\log_{10}(d_{BS-MS}) + 38.7 - 20\log_{10}(h_{roof} - 2) + 20\log_{10}(h_{roof} - h_{RS}) \quad (2)$$

$$PL_{LOS}(dB) = 20\log_{10}(d_{RS-MS}) + 39 \quad (3)$$

$$PL_{NLOS}(dB) = 46\log_{10}(d_{RS-MS}) + 14.2 - 0.6h_{RS} \quad (4)$$

$$PL_{RS-MS} = prob_{LOS}PL_{LOS} + (1 - prob_{LOS})PL_{NLOS} \quad (5)$$

$$prob_{LOS}(d_{RS-MS}) = 0.5 - \min(0.5, 5\exp(-156/d_{RS-MS})) + \min(0.5, 5\exp(-d_{RS-MS}/30)) \quad (6)$$

with $d_{BS\text{-}MS}$, distance BS-MS and $d_{RS\text{-}MS}$, distance RS-MS

The second scenario is a measurement replay scenario when BS, RS, MS locations or path loss values are those from the measurement campaign. This scenario is used to illustrate the impact of the relay location. A typical plot is Figure 51where the capacity ratio is superimposed on an aerial view.

2.6.2.2 Capacity calculation and relaying scheme

We define $C_{BS\text{-}MS}$, $C_{BS\text{-}RS}$, $C_{RS\text{-}MS}$, capacities related to link BS-MS, BS-RS and RS-MS respectively. The capacity is calculated with the Shannon's equation:

$$C = B\log_2(1 + SNR) \quad (7)$$

with *SNR*, the signal to noise ratio

We consider three relaying protocol: half-duplex (HD), modified half duplex (mHD) and the full-duplex (FD). The decode-and-forward scheme was selected as it has be shown that amplify-and-forward outperforms decode-and-forward protocol especially for low SNR which is the case when the mobile is located at the cell edge [14]. The capacity in relay-assisted communication can be computed according to the relaying protocol.

HF relaying: In this relaying protocol, the resources are equally shared between the access and backhaul link in the time or frequency domain in order to avoid self-interferences. Figure 44 illustrates a HF relay with time sharing. The capacity experienced at the MS is given as follows:

$$C_{HD} = (1/2)\min(C_{BS-RS}, C_{RS-MS}) \quad (8)$$

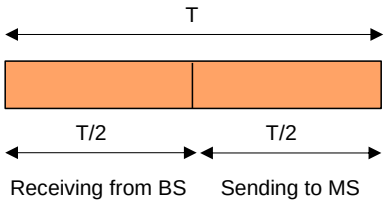

Figure 44: HD relay protocol

m-HD relaying: According to Equation (8), the capacity can be maximized if $C_{BS\text{-}RS}$ and $C_{RS\text{-}MS}$ are equal. The mHD relaying protocol allocates α and 1-α fraction of time or frequency band for the links BS-RS and RS-MS respectively as shown in Figure 45. Thus, the maximum capacity can be obtained when $\alpha C_{BS-RS} = (1-\alpha)C_{RS-MS}$ and C_{mHD} can be written as follows:

$$C_{mHD} = \frac{C_{BS-RS}C_{RS-MS}}{C_{BS-RS} + C_{RS-MS}} \quad (9)$$

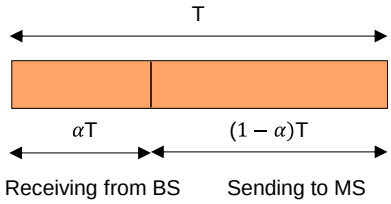

Figure 45: mHD relay protocol

FD relaying: RS simultaneously receives the signal from BS and forwards it to MS at the same time-frequency radio resource as shown in Figure 46 and the capacity can be calculated as follow :

$$C_{FD} = \min\left(C_{BS-RS}, C_{RS-MS}\right) \qquad (10)$$

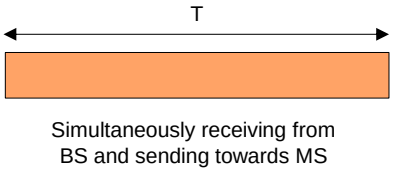

Figure 46: Full duplex protocol

This relaying protocol doubles the channel capacity compared to the HD protocol. However, this capacity can be achieved if self-interferences at RS can be completely canceled. Several methods have been proposed in order to mitigate the self-interference [15]. The FD protocol also assumes advanced receiver able to handle simultaneously the signal coming from BS and RS.

2.6.3 SIMULATION RESULTS

Here we describe and compare the simulation results of the various protocols using the channel measurement results.

2.6.3.1 Relaying protocol

The macrocell inter-site distance in urban environment ranged approximately between 500 m and 1500 m depending on the urban human density therefore the distance BS-RS may range between 250 m and 750 m assuming a BS-RS distance equal to the half of the inter-distance. Figure 47 and Figure 48 shows the relay capacity as a function of the different relaying protocol for a BS-RS distance equal to 300 m and 600 m.

The relay capacity achieves a maximum for all protocols when the mobile is close to RS and is symmetrical compared to a vertical axis set at a distance equal to the distance BS-RS. C_{FD} is constant for short $d_{RS\text{-}MS}$ due to the $C_{BS\text{-}RS}$ limitation. In the example given by Figure 47, this limitation occured for $d_{BS\text{-}MS}$ ranged from 200 m to 400 m. If RS was at street level, the threshold would be $C_{BS\text{-}MS}$ at $d_{BS\text{-}RS}$. As RS is located above the street level, the threshold is shifted upwards compared to the direct link capacity and the threshold level depends with the antenna height. When MS gets away from RS terminal, C_{FD} is no more limited by the backhaul link but by the access link and C_{FD} is equal to $C_{RS\text{-}MS.}$

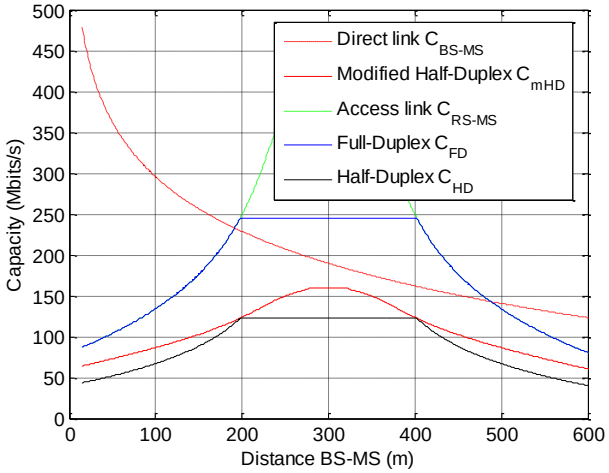

Figure 47: Capacity as function of relaying protocol, h_{roof}=15m, h_{rs}=10 m, $d_{BS\text{-}RS}$= 300 m

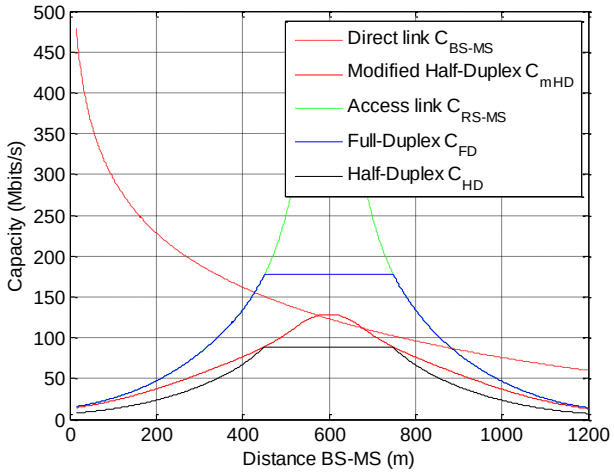

Figure 48: Capacity as function of relaying protocol, h_{roof}=15m, h_{rs}=10 m, $d_{BS\text{-}RS}$= 600 m

The capacity difference between the macrolink and the relay link depends with $d_{BS\text{-}RS}$, but HD and m-HD capacities are almost systematically lower than the direct link capacity. The bad performance of these relaying protocols is due to the time-frequency resource sharing between the access and backhaul links. Practically, carrier aggregation techniques or specific scheduling algorithm favoring cell edge users would give higher performances than HD and m-HD relay and would not require any additional equipment deployment. Hence, HD or m-HD relay is not an efficient solution to diminish the cell edge problem. The FD relay gives a substantial gain compared to the HD or m-HD relay. In the example given in Figure 47, the FD relay outperforms the direct link for $d_{BS\text{-}MS}$ ranged from 200 m to 500.

The full-duplex capacity is strongly limited by the backhaul capacity limitation and would not be an efficient solution compared to a microcell with a fiber optics backhaul. However, fiber optics may be not accessible in an entire city and $C_{BS\text{-}RS}$ may be increased by increasing the antenna height, by optimizing the relay location or by using directive antenna with higher gain at RS. Hence, the full duplex relay is a potential solution for enhancing the channel capacity. In the following section, we consider only the FD protocol and define a new metric to compare simply the relay-assisted communication throughput with the direct throughput as defined in the following equation:

$$C_{ratio} = 100 \times \frac{C_{FD} - C_{BS-MS}}{C_{BS-MS}} \qquad (11)$$

For C_{Ratio} < 0, the direct link is better than the relay-assisted one. When C_{Ratio} > 0, the relaying solution increases the capacity compare the direct link. The relay coverage refers to the geographical area where C_{ratio} is positive.

2.6.3.2 Relay antenna height

Figure 49 and Figure 50 show C_{FD} and C_{Ratio} for 2 different relay antenna heights (5 and 10 meters) and 2 rooftop level (15 and 25 meters). We observe that C_{Ratio} ranges from 0% and 40 % depending on d_{RS-MS}, h_{roof} and h_{rs}. The higher the antenna height, the higher the capacity ratio. However, this relation is not linear especially when the relay capacity is limited by the backhaul capacity. As indicated by eq. 2, the backhaul PL is not a linear function of the relay distance to the ground but an exponential function of the relay distance to the building rooftop level. With h_{roof} = 25 m, C_{Ratio} increases by about 20 % between the lowest and highest antenna height. With h_{roof} = 15 m, C_{Ratio} increases by about 20 % between the lowest and highest antenna height. This result suggests that the relay antenna height would have a significant impact in suburban environment or moderate urban environment when buildings have 3 or 4 floors, but will have a limited impact in dense urban environment when buildings have more than 5 floors.

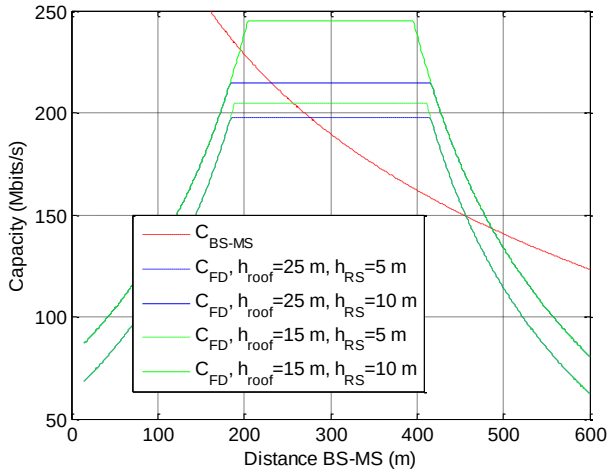

Figure 49: Impact on antenna height on relay capacity

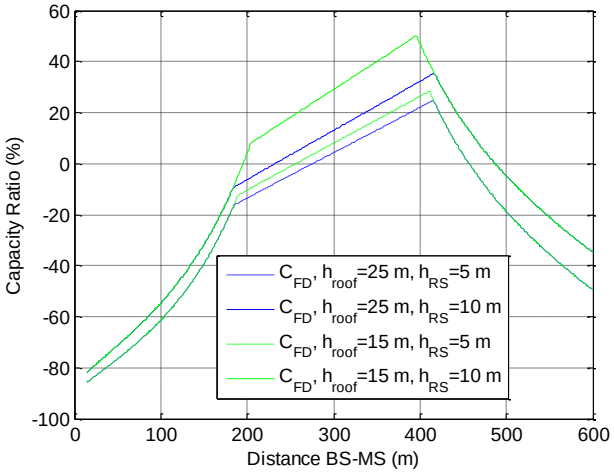

Figure 50: Capacity ratio as function of the antenna height

2.6.3.3 Relay location

The performance of the relaying technique is also affected by the relay position, i.e. by the environment around the relay as illustrated by Figure 51, Figure 52, Figure 53 and Figure 54. In order to highlight areas where the relay provides gain compared to the macrocell, 3 C_{Ratio} levels are arbitrary defined: C_{Ratio} < 0%, 0% < C_{Ratio} < 30% and C_{Ratio} > 30%.

Figure 51 and Figure 52 show C_{Ratio} of RS7 and RS9 respectively. RS7 is located in a street canyon perpendicular to the BS-RS axis and RS9 is beside a park with moderate vegetation. We observe clearly that the RS9 coverage is better than that of RS7 although RS7 and RS9 are very close to each other. Different distances between BS and RS, or between RS and MS cannot explain this difference. Therefore the environment around the relay may change significantly C_{FD}. We also observe that RS7 and RS9 coverage are complimentary. An optimal relay location would be somewhere between RS7 and RS9, probably at the nearest street intersection. Figure 53 and Figure 54 give two other examples illustrating the impact of the relay position. RS1 and RS2 are still close to each other, but RS1 is located at a street intersection and RS2 is located in a small square surrounded by buildings. The RS2 coverage is limited to the square where RS2 is located and to a small segment of the main road, whereas RS1 coverage includes most the RS2 coverage and includes many streets with a ratio capacity higher than 30 % and higher than 50 % in limited segments. Both examples demonstrate that relay performances can be enhanced by an optimized relay location. Practically, an efficient relay deployment would require powerful planning tool software including consistent and comprehensive propagation channel models for macrocell and microcell environments.

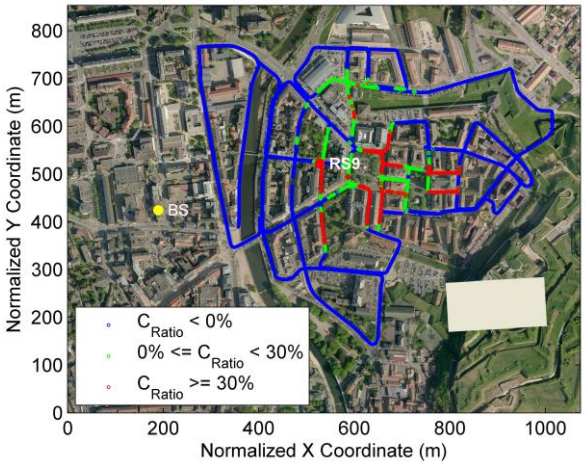

Figure 51: Capacity ratio RS 9, h_{rs}=8.8 m

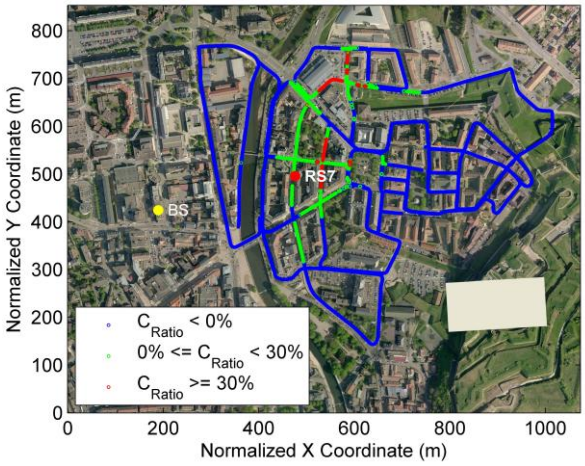

Figure 52: Capacity ratio RS7, h_{rs}=8.8 m

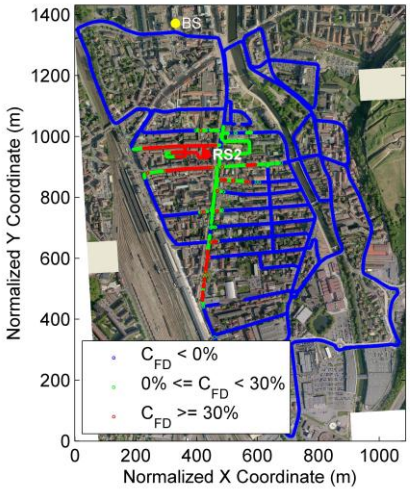

Figure 53: Capacity ratio RS2, h_{rs}=8.8 m

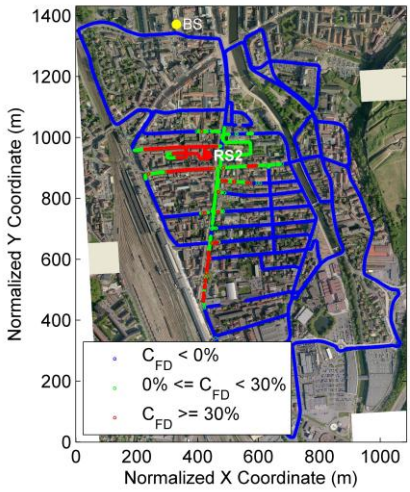

/

Figure 54: Capacity ratio RS1, h_{rs}=8.8 m

2.6.4 Conclusion

We showed that the direct link capacity can be over performed by a relay-assisted communication when a full-duplex relay technology is used. The capacity gain provided by the relay reaches more than 30 % depending on the antenna relay height and location. The analysis assumed omnidirectional antenna at RS and was performed at 2.2 GHz. Future work will analyze the frequency dependency of relay performances. Higher frequencies would allow the use of antenna array with a limited physical size but able to generate high gain directional beam enhancing the backhaul and access link capacities. But the actual benefits of directional antennas depend on the received signal spatial distribution. Consequently, future work will also investigate the directions of arrival at RS.

3 DEVICE-TO-DEVICE COMMUNICATION

In this section we recall two of the resource allocation strategies described in D5.2. Firstly, we describe general framework for sharing the uplink resource of a cellular network with D2D communications and provide a set of optimal resource allocation strategies under the assumption of receivers which treat interference a noise (D5.2 Section 4). Secondly we extend the feasibility study from D5.2 (Section 5) where we described the system architecture and protocol. We now review the results of simulations based on real constraints from recent 3GPP standardization activities. The reader is referred to D5.2 for details on the system architecture and we focus our investigation here on the conditions for such an allocation scheme to serve the expected Quality of Service (QoS) on both cellular and D2D links. Interference constraints have to be identified and new interference control techniques have to be implemented along with a possible associated LTE system design.

3.1 Resource allocation and interference management for off-loading scenario

In this work, we consider the resource allocation for *device-to device* (D2D) communications underlaying cellular networks to maximize the overall network throughput while guaranteeing the *quality of service* (QoS) of both regular *cellular users* (CUs) and D2D users. Firstly, we develop a three-step optimal resource allocation framework when considering *base station* (BS) has perfect *channel state information* (CSI) of all links in the network. Then, we investigate the resource allocation for D2D communications with only partial CSI available at BS. Probability based strategy by utilizing channel statistical characteristics and user selection based limited feedback strategy are proposed, respectively, to deal with the channel uncertainty. Simulation results have demonstrated that the proposed algorithms are promising and there are substantial benefits by D2D communication.

3.1.1 Introduction

Recently, the tremendous popularity of smart phones and electronic tablets has spurred the explosive growth of high-rate multimedia wireless services. According to a recent report by Bell Labs [36], global mobile traffic is increasing by 25 times from 2011 to 2016. To alleviate the huge infrastructure investment for the exponential growth of mobile traffic and improve local service flexibility, *device-to-device* (D2D) communications have been considered one of the key techniques in the *Third Generation Partnership Project* (3GPP) *Long Term Evolution Advanced* (LTE-Advanced)[37].

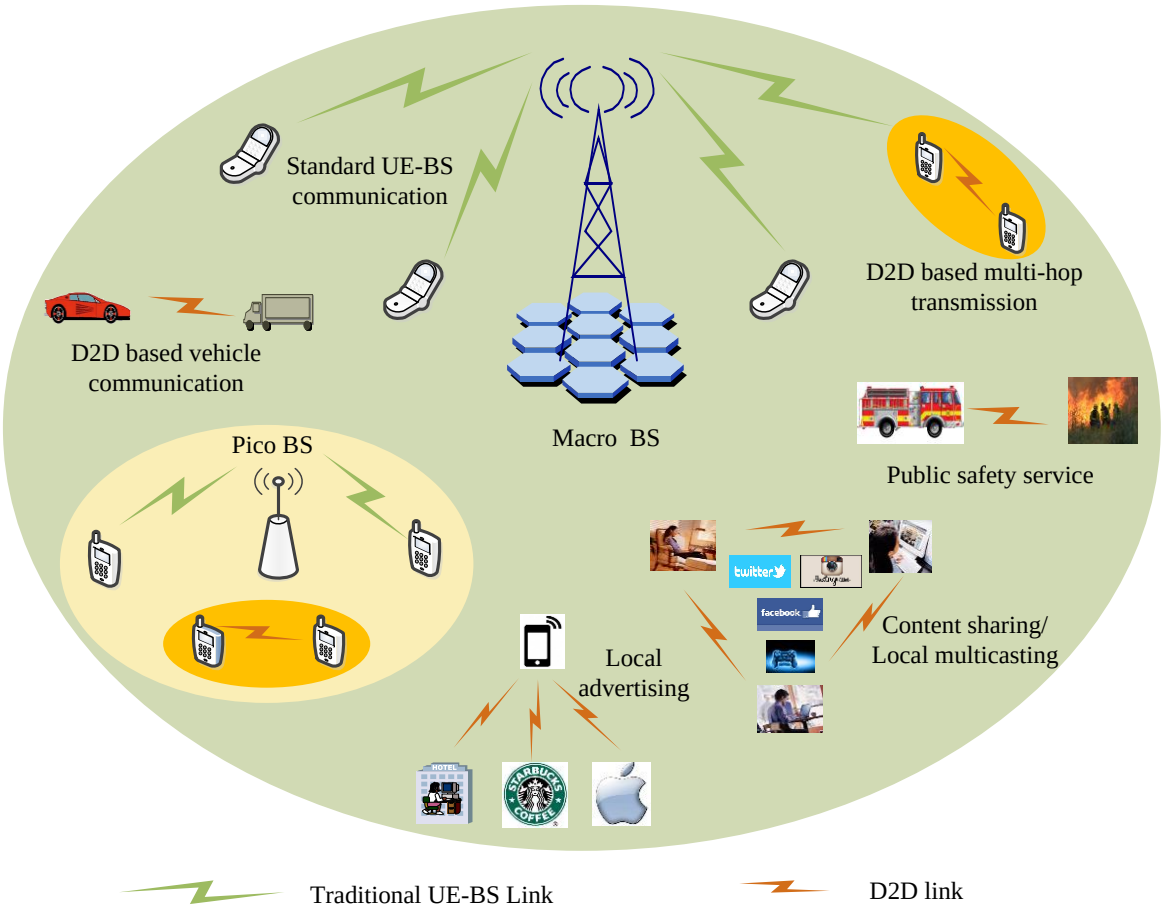

Figure 55: D2D communications in HetNets and its applications

Figure 55 from [38] illustrates the concept of D2D communications in heterogeneous networks (HetNets) and its applications. From the figure, apart from the standard base station (BS) relaying communications, user equipment (UE) in close proximity can also communicate directly through D2D communications. Due to the physical proximity and the potential reuse gain and hop gain [39], D2D communications can significant increase network spectral-efficiency (SE) and energy-efficiency (EE) [39],[40],[38]. Similar to the existing short range wireless transmission techniques (e.g., Wi-Fi Direct, Bluetooth, and UWB), D2D communications can also bring low transmission delay. Furthermore, D2D communications utilize the licensed spectrum bands and thus can guarantee uniform of service provision and quality of service (QoS). Moreover, by using the licensed bands, the operators can easily design the charge mechanism to get new revenue opportunities and encourage users to offload their traffic by D2D connections to avoid congestion in the core network. In addition, as the reliable feature, D2D communications has also been considered as cost effective solution for public safety service in case of lack of network coverage [37]. To better understand the differences between D2D communications and the existing short range transmission techniques, their main features are compared and outlined in Table 6.

Table 6: Comparison of Short Range Wireless Transmission Techniques

Feature Name	D2D	Wi-Fi Direct	NFC	ZigBee	Bluetooth	UWB
Standardization	3GPP LTE-Advanced	802.11	ISO 13157	802.15.4	802.15.1	802.15.3a
Frequency band	Licensed band for LTE-A	2.4 GHz, 5GHz	13.56 MHz	868/915MHz, 2.4GHz	2.4GHz	3.1-10.6 GHz
Max transmit distance	10-1000m	200m	0.2m	10-100m	10-100m	10m
Max data	1Gbps	250Mbps	424kbps	250kbps	24Mbps	480Mbps
Device discovery	BS coordination	ID broadcast and embed soft access point	Radio-frequency identification	ID broadcast or coordinator assistant	Manual paring	Manual paring
Uniformity of service provision	Yes	No	No	No	No	No
Application	Smart metering, Content sharing, Local advertising, Cellular relay	Content sharing, Group gaming, Device connection	Contactless payment systems, Bluetooth and Wi-Fi connections	Home Entertainment and Control, Environmental monitoring	Object Exchange, Peripherals connection	Wireless USB, High-definition video, Precision location and tracking systems, Auto Radar

3.1.2 Literature Review

D2D communications can bring great potential benefits to the cellular system in terms of SE and EE. However, it also leads to more complex interference situations and may interfere the existing cellular networks if not designed properly [38],[41]. Thus, efficient resource allocation and QoS guaranteeing are the most challenging but also importance issue in D2D communications. Many works have been done to deal with this issue.

Power control is a direct way to limit interference. In [40], restricting the transmit power of D2D users is suggested. Optimal power control along with mode switching with respect to the overall network throughput is investigated in [43]. In [44], fixed power margin scheme is proposed to coordinate interference among D2D pairs and RCUs for the scenarios with multiple D2D pairs and multiple RCUs. For the scheme in [44], it is supposed that there exists a power margin in the transmit power of regular RCUs to counteract the interference from D2D pairs and D2D pairs are aware of the power margin and can adjust their transmit power to satisfy the minimum SINR requirements. This scheme is simple but not necessarily optimal since it is hard to find a suitable power margin. A higher margin will reduce the number of RCUs those are capable to share resources with D2D users while a lower one will decrease the probability that the minimum SINR of D2D users can be satisfied.

Efficient scheduling is also an effective way to mitigate interference. In [45], a time hopping based method is used to randomize the interference generated by D2D pairs while a *successive interference canceling* (SIC) based receive mode selection scheme is introduced in [46] to assist the reliable demodulation at the D2D receivers. In [26], a heuristic scheduling algorithm is proposed to pair D2D users and RCUs while guaranteeing the QoS for both types of users, where the BS marks the CU with highest channel power gain of the CU-BS link a high priority to share resource with the D2D pair with the lowest interference channel power gain of the RCU-D2D receiver link. These schemes are easy to be implemented, however, the power cooperation among D2D pairs and RCUs, which may further improve the network performance, has not been considered.

3.1.3 System Model

We investigate spectrum sharing for D2D communications underlaying cellular networks, where *M* D2D pairs coexist with *N* CUs. In particular, uplink (UL) resource sharing is considered since UL spectrum is under-utilized comparing to that of downlink (DL) in the frequency division duplexing (FDD) based cellular systems [47], [48]. Furthermore, UL resource sharing in D2D communications only affects the BS and incurred interference can be mitigated by BS coordination. We also assume a fully loaded cellular network scenario similar to [43]. That is, N active cellular users occupy the N orthogonal channels in the cell and there is no spare spectrum. In the following, we use $C = \{1, \ldots, N\}$ and $D = \{1, \ldots, M\}$ to denote the index sets of active cellular users and D2D pairs, respectively. In addition, we assume both CUs and D2D pairs have their minimum QoS requirements.

We consider independent block fading for all links in the network. Thus, the instantaneous channel gain between CU *i* and the BS can be expressed as

$$g_{i,B} = C \cdot \beta_{i,B} d_{i,B}^{-\alpha}, \quad (1)$$

where C is a constant determined by system parameters, $\beta_{i,B}$ is the channel fading component, α is the pathloss exponent, and $d_{i,B}$ is the distance between CU *i* and the BS. Similarly, we can express the channel gain of D2D pair *j* when reuse the channel of CU *i*, $g_{dj,i}$, and the channel gains of the interference links, from the transmitter of D2D pair *j* to the BS, $h_{d\,j,i}$, and that from CU *i* to the receiver of D2D pair *j*, $h_{i,j}$. The power of additive white Gaussian noise on each channel is assumed to be σ^2 .

Optimal Resource Allocation with Perfect CSI

D2D communications can be used to improve the performance of fully loaded cellular networks. When BS has the perfect CSI of all links in the system, the QoS of both D2D pairs and CUs can be guaranteed in terms of the minimum SINR requirement. A D2D pair is set up only when the minimum SINR requirement can be guaranteed and incurred interference to the CUs is below a threshold. In this case, we call it the admissible pair and the CU to be shared resource as reuse partner. The overall throughput optimization problem can be formulated as follows

$$\max_{\rho_{i,j},P_{ci},P_{dj}} \{\sum_{i\in \mathrm{C}} \log_2(1+\xi_{ci}) + \sum_{j\in S} \log_2(1+\xi_{dj})\} \quad (2a)$$

$$s.t.\ \ \xi_{ci} = \frac{P_{ci} g_{i,B}}{\sigma^2 + \rho_{i,j} P_{dj} h_{dj,i}} \geq \xi_{ci,\min}, \forall i \in \mathrm{C}, \quad (2b)$$

$$\xi_{dj} = \frac{P_{dj} g_{dj,i}}{\sigma^2 + \rho_{i,j} P_{ci} h_{i,j}} \geq \xi_{dj,\min}, \ \forall j \in \mathrm{S}, \quad (2c)$$

$$\rho_{i,j} \in \{0,1\}, \ \ \sum_j \rho_{i,j} \leq 1, \ \forall i \in \mathrm{C}, \quad (2d)$$

$$\rho_{i,j} \in \{0,1\}, \ \ \sum_i \rho_{i,j} \leq 1, \ \forall j \in \mathrm{S}, \quad (2e)$$

$$P_{ci} \leq P_{c,\max}, \forall i \in \mathrm{C}, \quad (2f)$$

$$P_{dj} \leq P_{d,\max}, \forall j \in \mathrm{S}, \quad (2g)$$

where $\mathrm{S}\ (\mathrm{S} \subseteq \mathrm{D})$ denotes the set of admissible D2D pairs, $\rho_{i,j}$ is the resource reuse indicator for CU *i* and D2D pair *j*, $\rho_{i,j} = 1$when D2D pair *j* reuses the resource of cellular user *i*; otherwise, $\rho_{i,j} = 0$. $\xi_{ci,\min}$ and $\xi_{dj,\min}$ denote the minimum SINR requirements of CU *i* and D2D pair *j*, respectively, and $P_{ci,\max}$ and $P_{dj,\max}$ denotes the maximum transit power of CU and D2D pair, respectively. Constraints (2b) and (2c) represent the QoS requirements of cellular users and D2D pairs, respectively. Constraint (2d) ensures that the resource of an existing cellular user can be shared at most by one D2D pair. While constraint (2e) indicates that a D2D pair shares at most one existing cellular user's resource. Constraints (2f) and (2g) guarantee that the transmit powers of cellular users and D2D pairs are within the maximum limit.

The problem in (2) is a nonlinear constraint optimization problem. It is difficult to obtain the solution directly. In the following, we will divide the problem into three sub-problems and solve them one by one.

QoS-Aware Admission Control

If D2D pair *j* can share the spectrum with CU *i*, these constraints in (2b), (2c), (2f), and (2g) are satisfied, that is,

$$\begin{cases} \xi_{ci} = \dfrac{P_{ci} g_{i,B}}{\sigma^2 + P_{dj} h_{dj,i}} \geq \xi_{ci,\min}, & (3a) \\ \xi_{dj} = \dfrac{P_{dj} g_{dj,i}}{\sigma^2 + P_{ci} h_{i,j}} \geq \xi_{dj,\min} & (3b) \\ P_{ci} \leq P_{c,\max}, \ \ P_{dj} \leq P_{d,\max}, & (3c) \end{cases}$$

It means that a D2D pair can share resource with an existing user only when both their SINR requirements are satisfied. Let R_j denote the set of reuse candidates for D2D pair *j*. D2D pair *j* is

admissible ($j \in \mathrm{S}$) if and only if $\mathrm{R}_j \neq \varnothing$. In the following, we will demonstrate how to find the reuse candidates.

Without D2D user sharing resource with CU *i* $(P_{dj} = 0)$, the SINR of CU *i* can be guaranteed by transmitting a signal at the power,

$$P_{ci,\min} = \frac{\xi_{ci,\min}\sigma^2}{g_{i,B}}. \tag{4}$$

Similarly, without CU *i*, the minimum SINR of D2D user *j* can be reached by transmitting a signal at the power,

$$P_{dj,\min} = \frac{\xi_{dj,\min}\sigma^2}{g_{dj,i}}. \tag{5}$$

The admission constraints in (3) can be shown as in Figure 56, where lines l_c and l_d represent constraints (3a) and (3b) with equality, respectively. The area on the right of line l_d is where the minimum SINR for D2D pair *j* is satisfied. The area above line l_c is where the minimum SINR of CU *i* is satisfied. The square area denotes the maximum power constraints for CU *i* and D2D pair *j*.

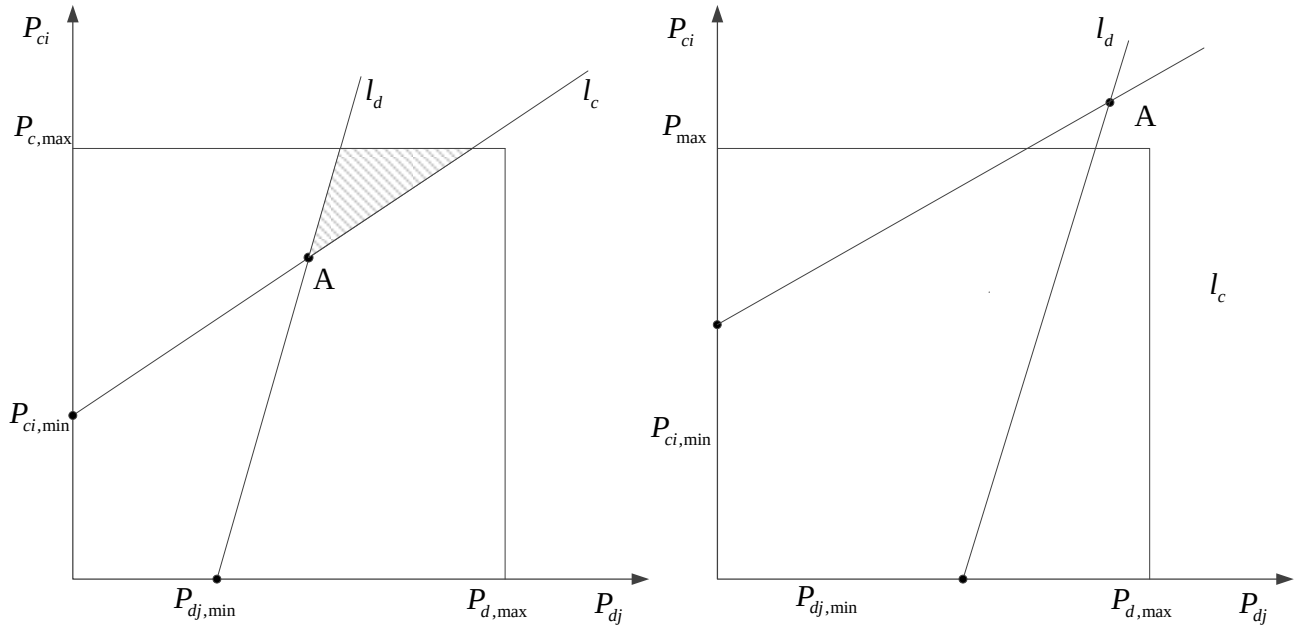

(a) with admissible area (b) without admissible area

Figure 56: D2D Communication Admissible Area.

Denote point A to be the intersection of l_c and l_d. To ensure l_c and l_d to have an intersection point in the first quarter, the slope of l_d must be larger than that of l_c, that is

$$\frac{\xi_{ci,\min}h_{dj,i}}{g_{i,B}} < \frac{g_{dj,i}}{\xi_{dj,\min}h_{i,j}} \tag{6}$$

which is the condition for CU *i* and D2D pair *j* to be possible to share resource without transmission power constraints. The coordinates of A, $(P_{dj,A}, P_{ci,A})$ can be found by

$$\begin{cases} \dfrac{P_{ci} g_{i,B}}{\sigma^2 + P_{dj} h_{dj,i}} = \xi_{ci,\min}, \\ \dfrac{P_{dj} g_{dj,i}}{\sigma^2 + P_{ci} h_{i,j}} = \xi_{dj,\min}. \end{cases} \tag{7}$$

Therefore,

$$\begin{cases} P_{ci,A} = \dfrac{(g_{dj,i}\xi_{ci,\min} + h_{dj,i}\xi_{ci,\min}\xi_{dj,\min})\sigma^2}{g_{dj,i}g_{i,B} - \xi_{ci,\min}\xi_{dj,\min}h_{i,j}h_{dj,i}}, \\ P_{dj,A} = \dfrac{(h_{i,j}\xi_{ci,\min}\xi_{dj,\min} + g_{i,B}\xi_{dj,\min})\sigma^2}{g_{dj,i}g_{i,B} - \xi_{ci,\min}\xi_{dj,\min}h_{i,j}h_{dj,i}}, \end{cases} \tag{8}$$

which are the minimum transmission powers for CU *i* and D2D pair *j* to satisfy the minimum SNIR requirements if the maximum transmission power constraints are not considered.

If point A is within the square area as in Fig. 4.2a, then it is possible to find transmit powers for CU *i* and D2D pair *j* to satisfy all constraints in (3). In that case, any point in the shaded area will satisfy (3), if point A is beyond the square area as in Fig. 4.2b, D2D pair *j* is not admissible to share the spectrum with CU *i* due to the maximum power limit.

In summary, the admissible conditions will be

$$\begin{cases} 0 \le \dfrac{(g_{dj,i}\xi_{ci,\min} + h_{dj,i}\xi_{ci,\min}\xi_{dj,\min})\sigma^2}{g_{dj,i}g_{i,B} - \xi_{ci,\min}\xi_{dj,\min}h_{i,j}h_{dj,i}} \le P_{c,\max}, \\ 0 \le \dfrac{(h_{i,j}\xi_{ci,\min}\xi_{dj,\min} + g_{i,B}\xi_{dj,\min})\sigma^2}{g_{dj,i}g_{i,B} - \xi_{ci,\min}\xi_{dj,\min}h_{i,j}h_{dj,i}} \le P_{d,\max}. \end{cases} \tag{9}$$

Then, simplifying the two inequalities in (9), we can get following minimum distance requirement for D2D pair *j* to select reuse candidates.

$$d_{i,j}^{\min} = \begin{cases} \left[\dfrac{C\beta_{i,j}\xi_{ci,\min}\xi_{dj,\min}P_{c,\max}h_{dj,i}}{(P_{\max}g_{i,B} - \xi_{ci,\min}\sigma^2)g_{dj,i} - \xi_{ci,\min}\xi_{dj,\min}\sigma^2 h_{dj,i}}\right]^{\frac{1}{\alpha}} & \text{if} \quad \dfrac{P_{c,\max}g_{i,B}}{\sigma^2 + P_{d,\max}h_{dj,i}} \le \xi_{ci,\min}, \\ \left[\dfrac{C\beta_{i,j}\xi_{ci,\min}\xi_{dj,\min}(\sigma^2 + P_{c,\max}h_{dj,i})}{g_{i,B}(P_{d,\max}h_{dj,i} - \xi_{dj,\min}\sigma^2)}\right]^{\frac{1}{\alpha}} & \text{if} \quad \dfrac{P_{c,\max}g_{i,B}}{\sigma^2 + P_{d,\max}h_{dj,i}} > \xi_{ci,\min}, \end{cases} \tag{10}$$

Let $d_{i,j}$ denote the distance between CU *i* and the reviver of D2D pair *j*. When $d_{i,j} \ge d_{i,j}^{\min}$, D2D pair *j* can be accessed by reusing the channel of CU *i* while both the minimum SINR can be satisfied.

Optimal Power Allocation

In the last subsection, we have addressed admission control for a D2D pair. Here, we investigate how to allocate power for the D2D transmitter and the corresponding reuse partner to maximize the overall throughput. Mathematically, the problem can be expressed as,

$$(P_{ci}^{*}, P_{dj}^{*}) = \arg\max_{P_{ci},P_{dj}} \{\log_2(1+\xi_{ci}) + \log_2(1+\xi_{dj})\}, \quad (11)$$

$$s.t. \quad \xi_{ci} = \frac{P_{ci} g_{i,B}}{\sigma^2 + P_{dj} h_{dj,i}} \geq \xi_{ci,\min}, \quad (11a)$$

$$\xi_{dj} = \frac{P_{dj} g_{dj,i}}{\sigma^2 + P_{ci} h_{i,j}} \geq \xi_{dj,\min} \quad (11b)$$

$$P_{ci} \leq P_{c,\max}, \quad P_{dj} \leq P_{d,\max}, \quad (11c)$$

In the previous subsection, we have addressed admission control for CU *i* and D2D pair *j*, from the discussion there, three possible shapes of admissible area are shown as in Figure 57 a-c. Note that all power pairs within the admissible area satisfy constraints (11a)-(11c). Therefore, the optimization problem in (11) is to find the power pair in the admissible area.

Figure 57

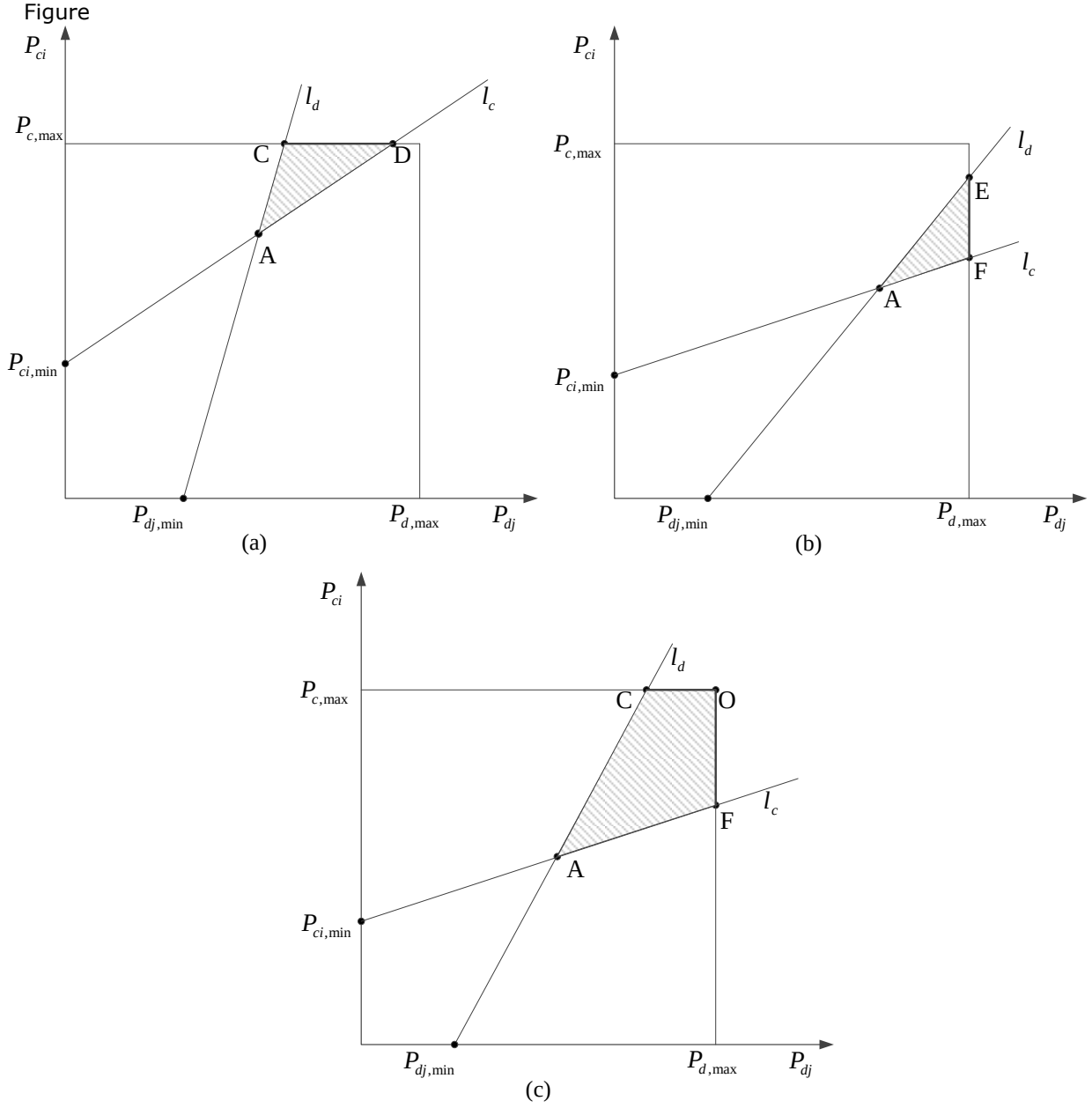

Figure 57: Optimal Power Allocation for Cellular User D2D User.

Denoting $f(P_{ci}, P_{dj}) \triangleq \log_2(1+\xi_{ci}) + \log_2(1+\xi_{dj})$, the optimal power vector (P_i^{c*}, P_j^{d*}) in (11) is derived as follows,

$$(P_{ci}^*, P_{dj}^*) = \begin{cases} \arg\max\limits_{(P_{ci}, P_{dj}) \in \mathrm{P}_1} f(P_{ci}, P_{dj}) & \text{if} \quad \dfrac{P_{c,\max} g_{i,B}}{\sigma^2 + P_{d,\max} h_{dj,i}} \le \xi_{ci,\min}, \\ \arg\max\limits_{(P_{ci}, P_{dj}) \in \mathrm{P}_2} f(P_{ci}, P_{dj}) & \text{if} \quad \dfrac{P_{c,\max} g_{i,B}}{\sigma^2 + P_{d,\max} h_{dj,i}} > \xi_{ci,\min} \text{ and } \dfrac{P_{c,\max} g_{gj,i}}{\sigma^2 + P_{d,\max} h_{dj,i}} < \xi_{dj,\min}, \\ \arg\max\limits_{(P_{ci}, P_{dj}) \in \mathrm{P}_3} f(P_{ci}, P_{dj}) & \text{if} \quad \dfrac{P_{c,\max} g_{i,B}}{\sigma^2 + P_{d,\max} h_{dj,i}} > \xi_{ci,\min} \text{ and } \dfrac{P_{c,\max} g_{gj,i}}{\sigma^2 + P_{d,\max} h_{dj,i}} < \xi_{dj,\min}, \end{cases} \tag{12}$$

where

$$\mathrm{P}_1 = \{(P_{c,\max},\ P_1),\ (P_{c,\max},\ P_2)\}, \quad \mathrm{P}_2 = \{(P_3,\ P_{d,\max}),\ (P_4,\ P_{d,\max})\},$$
$$\mathrm{P}_3 = \{(P_{c,\max},\ P_1),\ (P_{c,\max},\ P_{d,\max}),\ (P_4,\ P_{d,\max})\},$$
$$P_1 = \frac{(\sigma^2 + P_{c,\max} h_{i,j}) \xi_{j,\min}^d}{g_{dj,i}}, \qquad P_2 = \frac{P_{c,\max} g_{i,B} - \xi_{ci,\min} \sigma^2}{\xi_{ci,\min} h_{dj,i}},$$
$$P_3 = \frac{P_{d,\max} g_{dj,i} - \xi_{dj,\min} \sigma^2}{\xi_{dj,\min} h_{i,j}}, \qquad P_4 = \frac{(\sigma^2 + P_{d,\max} h_{dj,i}) \xi_{ci,\min}}{g_{i,B}},$$

From the above proposition, the optimal power pair for CU *i* and D2D pair *j* resides on one of the corner points of the admissible area as points C, D, O, E, and F in Figure 57. Besides, at least one user is transmitting at the peak power for maximizing the overall throughput.

Maximum D2E Pairs and CUs Match

For a CU *i* ($i \in \mathrm{R}_j$), when there is no D2D, the maximum throughput on the used spectrum is

$$T_{i,\max} = \log_2 (1 + \frac{P_{c,\max} g_{i,B}}{\sigma^2}). \tag{13}$$

When it shares resource with D2D pair *j*, the maximum achievable sum throughput, $T_{i,j}^{sum}$, can be expressed as

$$T_{i,j}^{sum} = \log_2 (1 + \frac{P_{ci}^* g_{i,B}}{P_{dj}^* h_{dj,i} + \sigma^2}) + \log_2 (1 + \frac{P_{dj}^* g_{dj,i}}{P_{ci}^* h_{i,j} + \sigma^2}), \tag{14}$$

where (P_{ci}^*, P_{dj}^*) is given by the equation (12). Thus, the D2D throughput gain can be expressed as

$$T_{i,j}^G = T_{i,j}^{sum} - T_{i,\max}. \tag{15}$$

Hence, we can find the optimal reuse partner of D2D pair *j*,

$$i^* = \arg\max_{i \in \mathrm{R}_j} T_{i,j}^G. \tag{16}$$

By now, we can get the optimal solutions of (2) for a single D2D scenario. If there are multiple D2D pairs in the system, the optimal resource allocation problem turns to be a maximum weight bipartite matching problem. It can be formulated as

$$\begin{aligned} &\max_{i\in\mathrm{C}^{'},j\in\mathrm{S}} \rho_{i,j}T_{i,j}^{G}, \\ &s.t. \quad \sum_{j}\rho_{i,j}\le 1,\ \rho_{i,j}\in\{0,1\},\ \forall i\in\mathrm{C}^{'}, \\ &\qquad \sum_{i}\rho_{i,j}\le 1,\ \rho_{i,j}\in\{0,1\},\ \forall j\in\mathrm{S}, \end{aligned} \tag{17}$$

where $\mathrm{C}^{'}$ is the union of all the reuse candidate sets of D2D pairs. Fig. 4.4 explains the maximum weight bipartite matching problem in (17), where the set of D2D pairs and the union of all the reuse candidate of D2D pairs are assumed as the two groups of vertices in the bipartite graph. Vertex *i* is joined with vertex *j* by an edge *ij*, when the user *i* is a reuse candidate of D2D pair *j*. D2D throughput gain $T_{i,j}^{G}$ is considered as the weight of edge *ij*. We can use the classic Kuhn-Munkres algorithm [49] to solve (17). Thus, the solution of the optimal resource allocation problem for multiple D2D pairs with targeted QoS requirements can be derived and illustrated by the algorithm 3.1.1 below

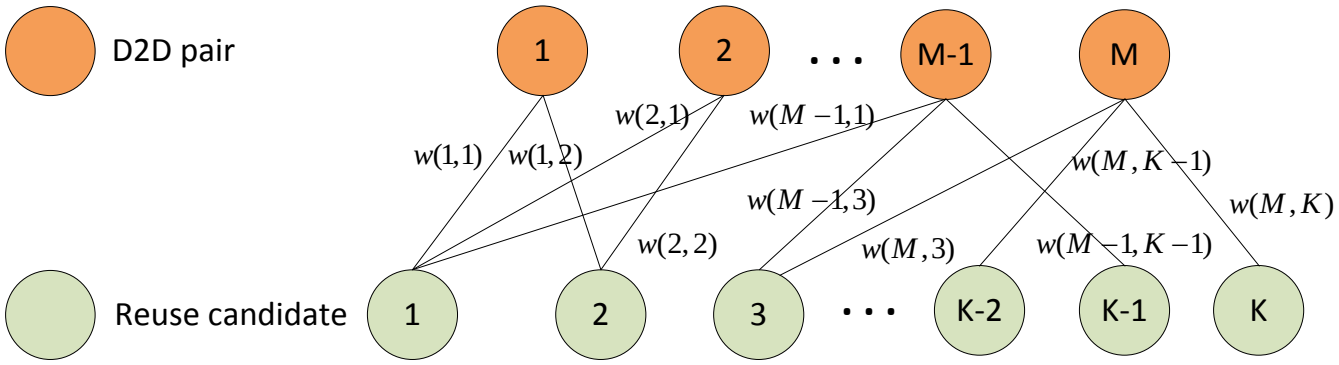

Figure 58: Bipartite graph for D2D pairs and the reuse candidates matching problem.

Algorithm 3.1.1 Optimal Resource Allocation Algorithm

1 : C : The set of existing cellular users

2 : D : The set of D2D pairs

3 : R_j : The set of reuse candidates of D2D pair *j*

4 : $\mathrm{C}^{'}$: The set of reuse candidates of D2D pair *j*

5 : Step 1

6 : **for all** $j\in\mathrm{D}$ and $i\in\mathrm{C}$ **do**

7 : calculate $d_{i,j}^{\min}$ ⟵ **Proposition 1**

8 : **if** $d_{i,j}<d_{i,j}^{\min}$ **then**

9 : $i\in\mathrm{R}_j$ (Find reuse candidates)

10 : **end if**

11 : **end for**

12 : **if** $\mathrm{R}_j \neq \varnothing$ **then**

13 : $\mathrm{D} = \mathrm{D} - j$ (Delete not accessible candidates)

14 : **end if**

15 : Step 2

16 : **for all** $j \in \mathrm{D}$ and $i \in \mathrm{R}_j$ **do**

17 : calculate (P_{ci}^{*}, P_{dj}^{*}) $\leftarrow$ **Proposition 2**

18 : **end for**

19 : Step 3

20 : **if** $|\mathrm{D}| = 1$ **then**

21 : $i^{*} = \arg\max_{i \in \mathrm{R}_j} T_{i,j}^{G}$ (For only one D2D pair)

22 : **else**

23 : get i^{*} from (17) (Kuhn-Munkres algorithm)

24 : **end if**

3.1.4 Resource Allocation with Partial CSI

For the optimal resource allocation strategy in [42], the accurate CSI information of all links is imperative. In general, BS can collect the CSI of users by the classic channel training and estimation. Nevertheless, for the interference links between CUs and D2D pairs that are not connected to the BS the traditional methods are not applicable and obtaining the instantaneous CSI is difficult and causes high overhead [50], especially when the number of CUs and D2D pairs are large. Thus, it is more reasonable to assume the BS only have partial CSI, including distance based pathloss and shadowing, which can be obtained by empirical measurements. In the following, we will investigate the resource allocation strategies for the BS only knows partial CSI of links between the regular CUs to D2D receivers that are not connected to the BS [51].

User Selection Based Limited Feedback

To solve the problem in (2), the interference channel gain of $h_{i,j}$ is indispensable; however, this will need lots of feedback and cause high overhead. Note that the CSI of each CU-D link within the same D2D pair is not equally important. For example, the CUs that are far away from the D2D receivers are more likely to be the reuse partners, and thus the CSI of CU-D links belong to these faraway CUs may be more important. Thus, to reduce the feedback overhead, the key is to find the best potential partner CUs for each D2D pair and then to feed the corresponding CSI back. To choose the most potential partner CUs, one intuitive method is to choose the CUs farthest away from the D2D receiver and we call this method, KFAR. However, other factors, such as the QoS requirements of CUs and the channel power gain of CU-BS link, will also affect the access of the D2D pair. In (10), we have derived a minimum distance metric to evaluate the access ability for a D2D pair *j* sharing resource with a regular CU *i*. This metric has comprehensively considered all the factors that may affect access of the D2D pair.

With the minimum distance metric in (10), the BS can easily decide whether D2D pair *j* can share the resource with CU *i* or not. However, this metric depends on the fading components , $\beta_{i,j}$ which are not known at the BS. Therefore, we derive a modified distance metric $D_{i,j}^{\min}$, which is the required minimum distance between CU *i* and the receiver of D2D pair *j* to satisfy all the access constraints in (2) without considering the fading effect of CU-D link by setting $\beta_{i,j}=1$. The modified metric can be expressed as,

$$D_{i,j}^{\min}=\begin{cases}\left[\dfrac{C\xi_{ci,\min}\xi_{dj,\min}P_{c,\max}h_{dj,i}}{(P_{\max}g_{i,B}-\xi_{ci,\min}\sigma^2)g_{dj,i}-\xi_{ci,\min}\xi_{dj,\min}\sigma^2h_{dj,i}}\right]^{\frac{1}{\alpha}} & \text{if} \quad \dfrac{P_{c,\max}g_{i,B}}{\sigma^2+P_{d,\max}h_{dj,i}}\le\xi_{ci,\min}, \\ \left[\dfrac{C\xi_{ci,\min}\xi_{dj,\min}(\sigma^2+P_{c,\max}h_{dj,i})}{g_{i,B}(P_{d,\max}h_{dj,i}-\xi_{dj,\min}\sigma^2)}\right]^{\frac{1}{\alpha}} & \text{if} \quad \dfrac{P_{c,\max}g_{i,B}}{\sigma^2+P_{d,\max}h_{dj,i}}>\xi_{ci,\min}, \end{cases} \tag{18}$$

When the $D_{i,j}^{\min}$ is calculated, the BS can select the K CUs with the largest maximum distance ratio (MDR) between the actual distance and the required minimum distance without considering fading, $d_{i,j}\big/D_{i,j}^{\min}$, as the best potential partner CUs for each D2D pair. We use MDR as the user selecting metric is for the following two reasons:

1) As $D_{i,j}^{\min}$ is required minimum distance to satisfy all the access constraints without considering the fading effect, thus the bigger the ratio, the more ability shows to counteract the fading;

2) A lower $D_{i,j}^{\min}$ implies that the CU can tolerant more D2D interference, and can get higher D2D throughput gain if the CU is selected.

After the user selection procedure is finished, each D2D pair can trace and report the CSI of the respective *K* selected CUs. When the CSI is available at BS, the optimal power allocation and CU and D2D pair match algorithms can be used. Thus, the problem in (2) can be solved by the selected-*K* feedback with MDR metric (KMDR) scheme, and the whole procedure is illustrated as in Algorithm 3.1.2 below.

Algorithm 4.2 Optimal Resource Allocation with KMDR

1 : C : The set of existing cellular users

2 : D : The set of D2D pairs

3 : MDR : The maximum distance ratio ($d_{i,j}\big/D_{i,j}^{\min}$)

4 : C_j : The selected K CU set for D2D pair j

5 : R_j : The set of reuse candidates of D2D pair j

6 : Step 1 *K CU Selection*

7 : **for all** $j\in\mathrm{D}$ and $i\in\mathrm{C}$ **do**

8 : calculate $D_{i,j}^{\min}$ and MDR;

9 : **sort** (MDR, column, 'descend') ;

10 : $C_j \leftarrow$ the first K sorted list in jth column of MDR

11 : **end for**

12 : Step 2 *Optimal Power Allocation*

13 : **for all** $j \in D$ and $i \in C_j$ **do**

14 : calculate $d_{i,j}^{\min}$;

15 : **if** $d_{i,j} \geq D_{i,j}^{\min}$ **then**

16 : calculate (P_{ci}^{*}, P_{dj}^{*})

17 : **end if**

18 : **if** $R_j \neq \varnothing$ **then**

19 : $D = D - j$

20 : **end if**

21 : **end for**

22 : Step 3 Optimal Match for Regular CU and D2D Pair

23 : **if** $|D| = 1$ **then**

24 : $i^{*} = \arg\max_{i \in R_j} T_{i,j}^{G}$

25 : **else**

26 : get i^{*} from Kuhn-Munkres algorithm

27 : **end if**

Probability-based Resource Allocation

In this subsection, we consider to utilize channel statistical characteristics as an alternative to deal with channel uncertainty.

We assume that BS provides guaranteed QoS for each CU and D2D pair. For CUs, since all the related channel power gains, $g_{i,B}$ and $h_{dj,i}$, are known at the BS, minimum SINR, $\xi_{c,\min}$, can be guaranteed. For D2D pairs, the channel fading component, $\beta_{i,j}$, is unavailable at the BS and therefore the exact SINR cannot be determined. Thus, outage probability is used to provide QoS for D2D users. When D2D pair *j* use the channel *i* ($\rho_{i,j} = 1$), the outage probability can be expressed as, $\Pr\{\xi_{dj} < \xi_{\text{th}}\} \leq \psi$.

where ψ denotes the maximum acceptable outage probability for D2D users.

When an admissible D2D pair *j* is accessed on channel *i*, eliminating the throughput in outage state, the ergodic (expected) throughput of D2D pair *j* can be expressed as,

$$\mathrm{E}\left\{[\log(1+\xi_j^d)]\middle|\xi_j^d \geq \xi_{\mathrm{th}}\right\}$$

where $\mathrm{E}\{\bullet|\bullet\}$ denotes conditional expectation.

Therefore, the optimal resource allocation problem for maximizing the overall network throughput of regular CUs and the admissible D2D pairs with guaranteed QoS in fading channels can be expressed as

$$\max_{\rho_{i,j},P_i^c,P_j^d}\left\{\sum_{i\in C}\log(1+\xi_i^c)+\rho_{i,j}\sum_{j\in S}\mathrm{E}\left\{[\log(1+\xi_j^d)]\middle|\xi_j^d\geq\xi_{\mathrm{th}}\right\}\right\}, \tag{19}$$

$$\text{s.t.}\quad \xi_i^c=\frac{P_i^c g_i}{\sigma^2+\rho_{i,j}P_j^d h_{j,i}^d}\geq\xi_{i,\min}^c,\forall i\in C,$$

$$\Pr\left\{\xi_j^d \square \frac{P_j^d g_{j,i}^d}{\sigma^2+\rho_{i,j}P_i^c h_{i,j}}<\xi_{\mathrm{th}}\right\}\leq\psi,\ \forall j\in S,$$

$$\rho_{i,j}\in\{0,1\},\ \sum_j\rho_{i,j}\leq 1,\ \forall i\in C,$$

$$\rho_{i,j}\in\{0,1\},\ \sum_i\rho_{i,j}\leq 1,\ \forall j\in S,$$

$$P_i^c\leq P_{\max}^c,\forall i\in C,\quad P_j^d\leq P_{\max}^d,\forall j\in S$$

Without considering the channel fading component of the CU-D link, ($\beta_{i,j}=1$), the admissible D2D pairs can be found by the minimum distance metric derived in the previous subsection.

Obviously, when channel fading, $\beta_{i,j}$, is considered, the minimum distance, $D_{i,j}^{\min}$, should be changed by a distance factor, γ , that is $d_{i,j}=\gamma D_{i,j}^{\min}$ to counteract the fading effect and thus to satisfy the access constraints in (19). In this case, the corresponding channel gain will be $\bar{h}_{i,j}=C\beta_{i,j}(\gamma L_{i,j}^{\min})^{-\alpha}$. The distance factor can be determined by

$$\Pr\left\{\frac{P_{dj}g_{dj,i}}{\sigma^2+P_{ci}\bar{h}_{i,j}}<\xi_{\mathrm{th}}\right\}=\Pr\left\{\frac{P_{dj}g_{dj,i}}{\sigma^2+P_{ci}\bar{h}_{i,j}}<\frac{P_{dj}g_{dj,i}}{\sigma^2+P_{ci}C(D_{i,j}^{\min})^{-\alpha}}\right\}$$

$$=\Pr\left\{\bar{h}_{i,j}>C(D_{i,j}^{\min})^{-\alpha}\right\}=\Pr\left\{C\beta_{i,j}(\gamma D_{i,j}^{\min})^{-\alpha}>C(D_{i,j}^{\min})^{\alpha}\right\}$$

$$=\Pr\left\{\beta_{i,j}>\gamma^{\alpha}\right\}\leq\psi \tag{20}$$

Denote $\gamma_{\min}$ to be the minimum distance factor satisfying the outage probability. Then, it can be found by $\Pr\left\{\beta_{i,j}>{\gamma_{\min}}^{\alpha}\right\}=\psi$ .From the above, the distance factor depends on the pdf of fading. For Rayleigh fading channel, $\beta_{i,j}$ is exponentially distributed. Here, assuming it is with unite mean, thus the cdf can be expressed as

$$F_R(\beta_{i,j})=1-e^{-\beta_{i,j}},\beta_{i,j}>0. \tag{21}$$

Substituting it into (20), the minimum distance factor in Rayleigh fading can be expressed as

$\gamma_R = (-\ln \psi)^{1/\alpha}$.

When the minimum distance factor is obtained, we can express the modified minimum distance metric for D2D access in fading channels as follows

$$d_{i,j}^{\min} = \gamma D_{i,j}^{\min}. \qquad (22)$$

Then, we can determine whether a D2D pair can be accessible or not and also find all the potential partner CUs for the D2D pair if it is accessible by this metric. Figure 59 illustrated the modified admissible area in the heavy shaded pattern.

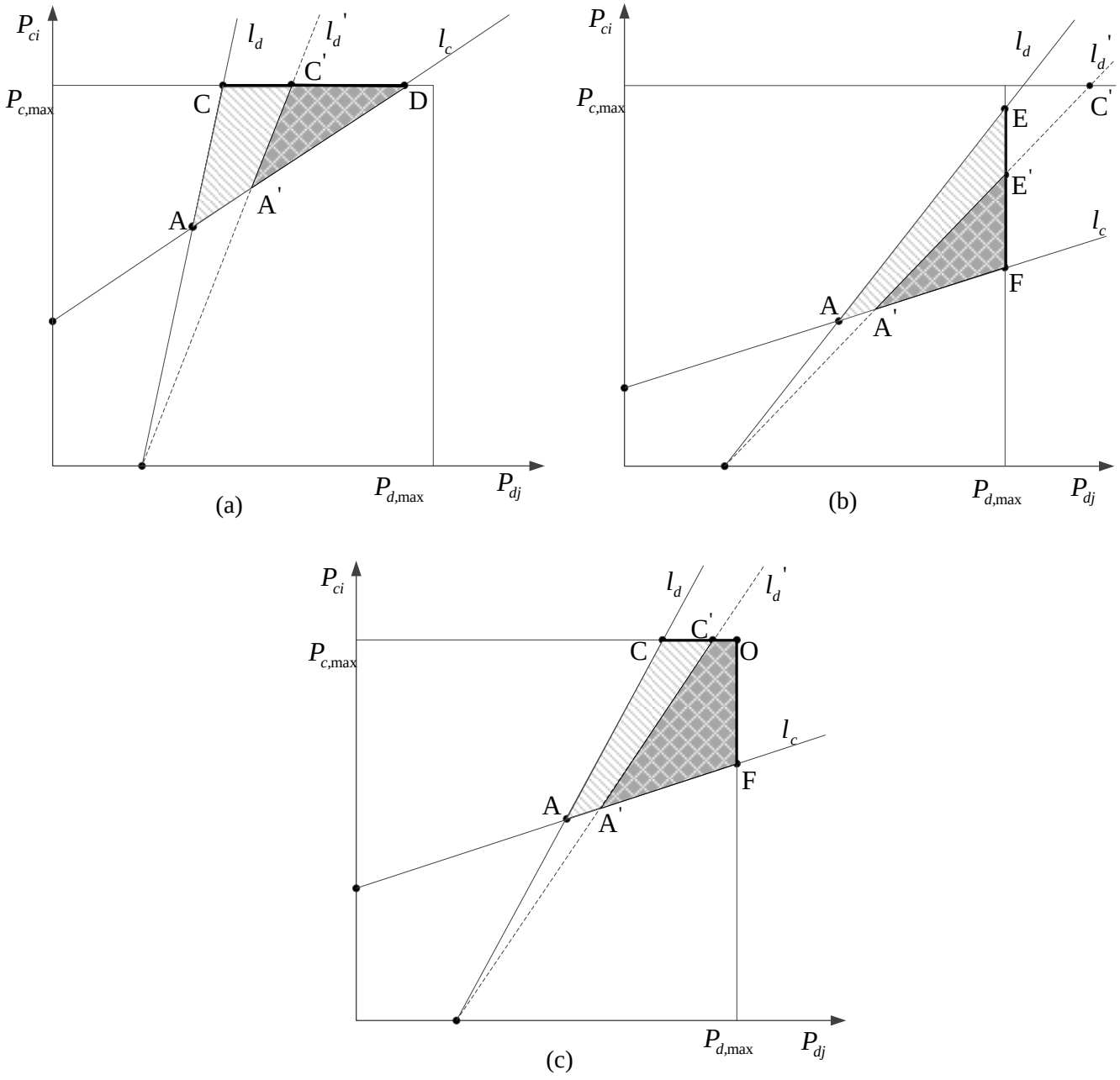

Figure 59: D2D admissible area. Light- and heavy- shaded patterns represent the admissible area without and with fading, respectively.

Similar to the power allocation with perfect CSI, denoting $g(P_{ci}, P_{dj}) \triangleq \log_2(1+\xi_{ci}) + \mathrm{E}\{[\log(1+\xi_{dj})] \mid \xi_{dj} \geq \xi_{\mathrm{th}}\}$, the maximum of this function g is achieved by the optimal power vector (P_i^{c*}, P_j^{d*}) which can be derived as follows,

$$(P_{ci}^*, P_{dj}^*) = \begin{cases} \arg\max_{(P_{ci}, P_{dj}) \in \mathrm{P}_1} f(P_{ci}, P_{dj}) & \text{if} \quad \dfrac{P_{c,\max} g_{i,B}}{\sigma^2 + P_{d,\max} h_{dj,i}} \leq \xi_{ci,\min}, \\ \arg\max_{(P_{ci}, P_{dj}) \in \mathrm{P}_2} f(P_{ci}, P_{dj}) & \text{if} \quad \dfrac{P_{c,\max} g_{i,B}}{\sigma^2 + P_{d,\max} h_{dj,i}} > \xi_{ci,\min} \text{ and } P_{dj,C'} \geq P_{d,\max}, \\ \arg\max_{(P_{ci}, P_{dj}) \in \mathrm{P}_3} f(P_{ci}, P_{dj}) & \text{if} \quad \dfrac{P_{c,\max} g_{i,B}}{\sigma^2 + P_{d,\max} h_{dj,i}} > \xi_{ci,\min} \text{ and } P_{dj,C'} < P_{d,\max}, \end{cases}$$

where

$$\mathrm{P}_1 = \{(P_{c,\max}, P_{dj,C'}), (P_{c,\max}, P_{dj,D})\}, \quad \mathrm{P}_2 = \{(P_{dj,E'}, P_{d,\max}), (P_{dj,F}, P_{d,\max})\},$$

$$\mathrm{P}_3 = \{(P_{c,\max}, P_{dj,C'}), (P_{c,\max}, P_{d,\max}), (P_{dj,F}, P_{d,\max})\},$$

$$P_{dj,C'} = \frac{[P_{c,\max} \bar{h}_{i,j} F^{-1}(1-\psi) + \sigma^2]\xi_{\mathrm{th}}}{g_{dj,i}}, \qquad P_{dj,D} = \frac{P_{c,\max} g_{i,B} - \xi_{ci,\min}\sigma^2}{\xi_{ci,\min} h_{dj,i}},$$

$$P_{dj,E'} = \frac{P_{d,\max}(P_{d,\max} g_{dj,i} - \xi_{\mathrm{th}}\sigma^2)}{\xi_{dj,\min} \bar{h}_{i,j} F^{-1}(1-\psi)}, \qquad P_{dj,F} = \frac{(\sigma^2 + P_{d,\max} h_{dj,i})\xi_{ci,\min}}{g_{i,B}}.$$

After obtaining the power allocations for a D2D pair and its corresponding partner CUs, we can estimate the D2D throughput gain brought by the D2D pair. However, in this report, we cannot obtain the exact throughput gain since the channel gain of CU-D link is unknown. Instead, we estimate the expected D2D throughput gain, defined as the difference between the maximum expected sum throughput and the maximum throughput of the partner CU without D2D, that is

$$T_{i,j}^G = g(P_{ci}^*, P_{dj}^*) - \log_2(1 + \frac{P_{c,\max} g_{i,B}}{\sigma^2}).$$

Finally, we can obtain the optimal D2D pair and CU match by the classic Kuhn-Munkres algorithm. The whole procedure of the probabilistic strategy can be illustrated as in Algorithm 3.1.

Algorithm 3.1.3 Probabilistic Resource Allocation Scheme

1 : C : The set of existing cellular users

2 : D : The set of D2D pairs

3 : γ : Accepted maximum outage probability for D2D pairs

4 : Step 1 *D2D Admission control*

5 : **for all** $j \in \mathrm{D}$ and $i \in \mathrm{C}$ **do**

6 : calculate $d_{i,j}^{\min}$ with given γ ;

7 : **if** $d_{i,j} \geq d_{i,j}^{\min}$ **then**

8 : $i \in \mathrm{R}_j$;

9 : **end if**

10 : **if** $\mathrm{R}_j \neq \varnothing$ **then**

11 : $\mathrm{D} = \mathrm{D} - j$

12 : **end if**

13 : **end for**

14 : Step 2 *Power control*

15 : **for all** $j \in \mathrm{D}$ and $i \in \mathrm{R}_j$ **do**

16 : calculate (P_{ci}^*, P_{dj}^*)

17 : **end for**

18 : Step 3 *Optimal Match for Regular CU and D2D Pair:* Kuhn-Munkres algorithm)

3.1.5 Numerical Results

Figure 60 shows the access rate and the throughput improvement of D2D communications with the simulation parameters of [51]. From the figure, in a fully loaded cellular network, the number of D2D pairs that can access the network based on our proposed optimal resource allocation algorithm with perfect CSI is up to 70% of the number of existing non-D2D UEs and the *quality-of-service* (QoS) requirements of all the users can be guaranteed. Compared to the fixed margin scheme in [44] and heuristic scheme in [47], the proposed scheme brings significantly performance gains. It is also seen that for a fixed number of active CUs, N, when the number of D2D pairs, M, increases to a certain amount, the network will be saturated, no more D2D pairs can be accessed and the multi-D2D pair diversity can only provide some secondary increase on the throughput gain. In addition, for any proportion of D2D pairs, the performance slightly increases with the increase of the number of the active CUs due to the increase of the potential multiuser diversity gain.

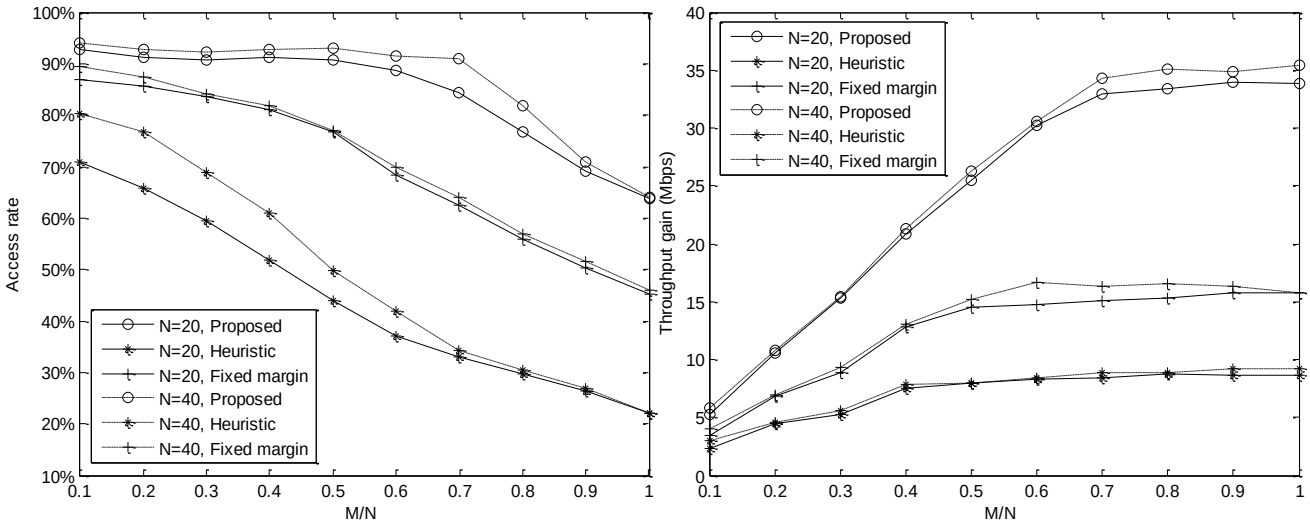

Figure 60: D2D access rate and throughput gain for different number

Figure 61 compares the performance of the proposed KMDR scheme with the optimal resource allocation and also an intuitive method, KFAR scheme under different channel fading models. In the figure, since the optimal scheme has the full CSI and the KFAR scheme only relates to the distance between users,

their performance does not change with channel models. As the more fading are brought from Rayleigh fading, lognormal fading, and Rayleigh-lognormal channels models, the performance of the probabilistic scheme also decreases in turn. Note that when K=6, for all the channel models, the performance of the KMDR scheme is almost the same as that of the optimal algorithm. That implies KMDR scheme can reduce significant feedback information, around 70% of total feedback information at the D2D receivers, while providing a near optimal performance. It is also seen that the performance of KMDR scheme is much better than that of KFAR scheme.

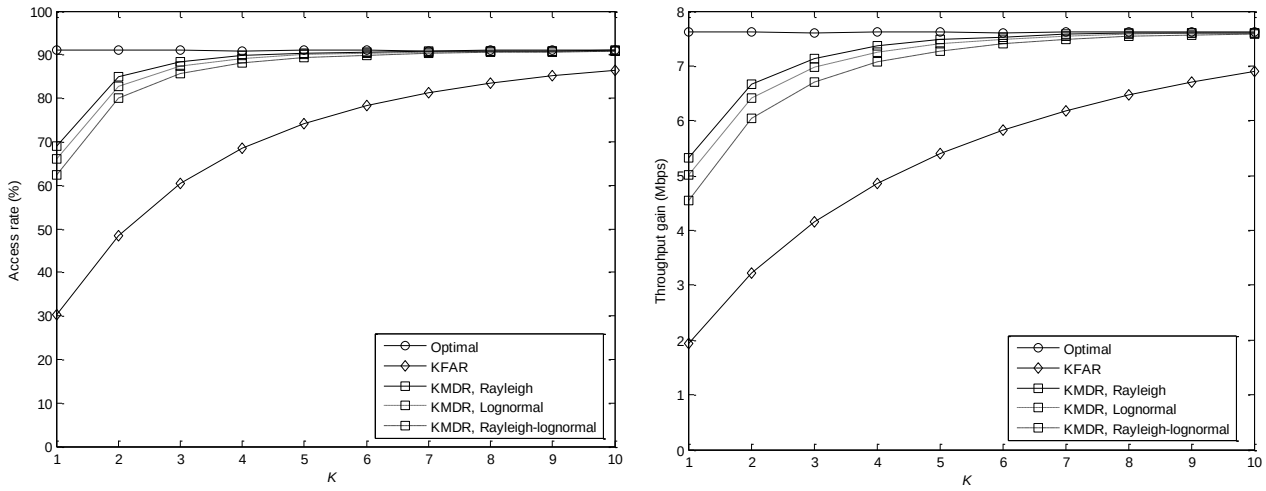

Figure 61: D2D access rate and throughput gain versus the number of feedback CUs under different channel models for the limited feedback schemes.

Figure 62 compares the performance of the proposed probabilistic resource allocation scheme under different channel fading models with the optimal scheme. From the figure, both access rate and D2D throughput gain for the probabilistic scheme increase with outage probability threshold at first, and then decrease after the maximum values. As a result, there exists an optimal threshold of the outage probability.

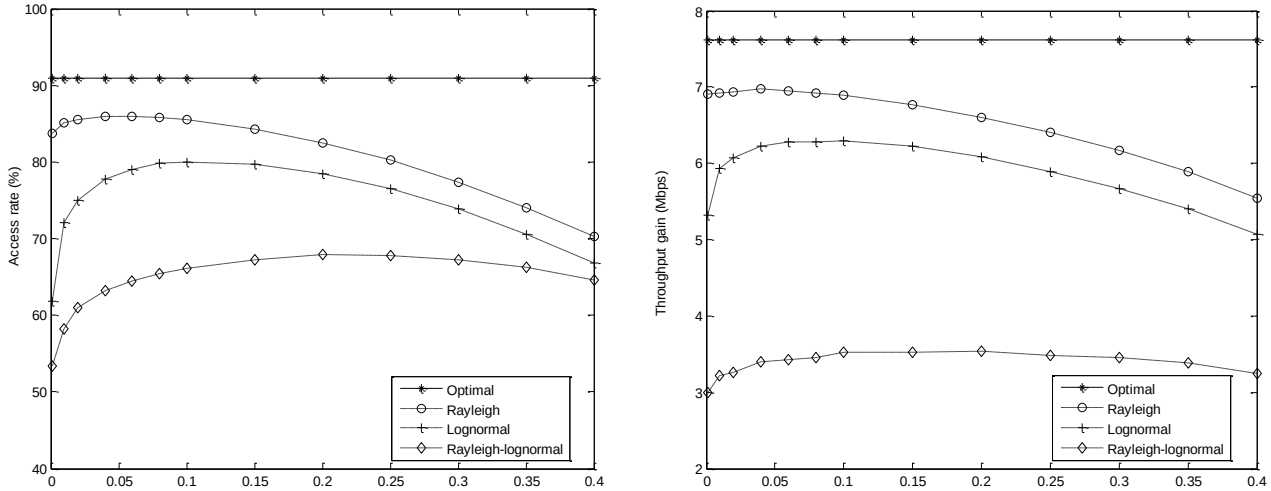

Figure 62: D2D access rate and throughput gain versus outage threshold under different channel models for the probabilistic algorithm.

Figure 63 illustrates the actual D2D outage rates under different channel models and different outage threshold. From the figure, in all the channel models, the actual D2D outage rate increases with the outage threshold. This is because that as the outage threshold increase , the required minimum distance between CU and the D2D receiver for the D2D to access decreases, thus increasing the outage probability.

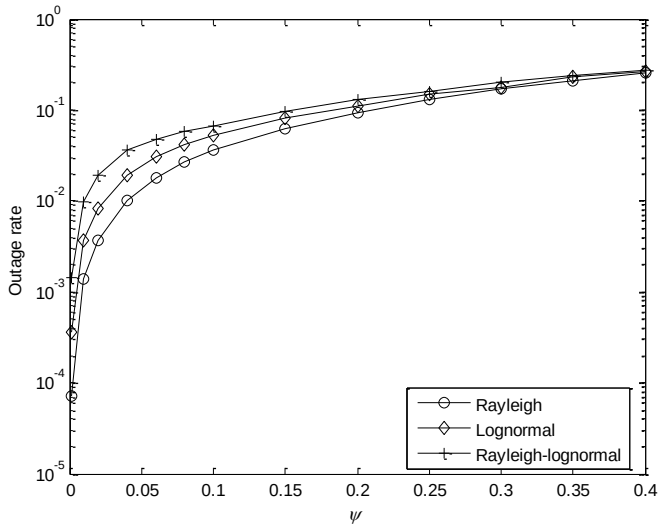

Figure 63: D2D actual outage rate versus outage threshold under different channel models for the probabilistic algorithm.

3.1.6 Conclusions

In this work, we have discussed the resource allocation strategies for D2D communications underlaying cellular networks to optimize the overall network performance. The results of our preliminary research are promising and have shown that there are substantial benefits by D2D communications.

3.2 Resource Allocation under 3GPP System Constraints

As previously described in D5.2, this work considers two main constraints:

1. symmetrical QoS protection (for both D2D link and cellular link) and
2. latest 3GPP system constraints.

Also, as many parameters such as distance, communication channel, maximum allowed power and interference control play important roles in D2D communication, it is difficult to conclude which is the best KPI to use as it depends on the situation and the goal of the proposed algorithm, e.g. sum rate throughput maximization, cellular QoS, or fairness of use between cellular and D2D users.

The approach of this work is different from previous works as it considers both the QoS of the cellular communication and the QoS of the D2D communication at the same time. D2D communication should be used only if there are clear benefits for both operator and D2D user and therefore the work investigates the conditions for D2D communication to offer this double benefit.

Moreover, the use cases considered by this work are a subset of those covered by 3GPP ProSe: both 1:1 and 1:many features are supported, with D2D peers under coverage of the same cell.

We further define the involved channels UE-C-to-UE-D as h_{cd}, UE-S-to-eNodeB as h_{sb}, UE-C-to-eNodeB as h_{cb}, and UE-S-to-UE-D as h_{sd}. Without any further loss of generalization, in the case when UE-S is broadcasting to multiple UE-D, for each UE-D_i receiving from UE-S we can further define the channel between UE-C and UE-D_i as $h_{cd,i}$, and each of the channels between UE-S and UE-D_i as $h_{sd,i}$. Figure 64 describes a use case where a cellular user equipment UE-C is connected to eNodeB and two user equipments (i.e. UE-S and UE-D) are involved in D2D communication, while camped on the same cell as UE-C. UE-C is transmitting using cellular uplink allocated resources by the eNodeB, and UE-S is reusing

those resources for transmitting towards UE-D. This reuse, as represented in Figure 64, will create additional interference at eNodeB side (i.e. from UE-S) but also at UE-D side (i.e. from UE-C): our solution is looking at selecting a relevant UE-C so that both interferences are kept under the limits fixed by the QoS requirements for both cellular and D2D links.

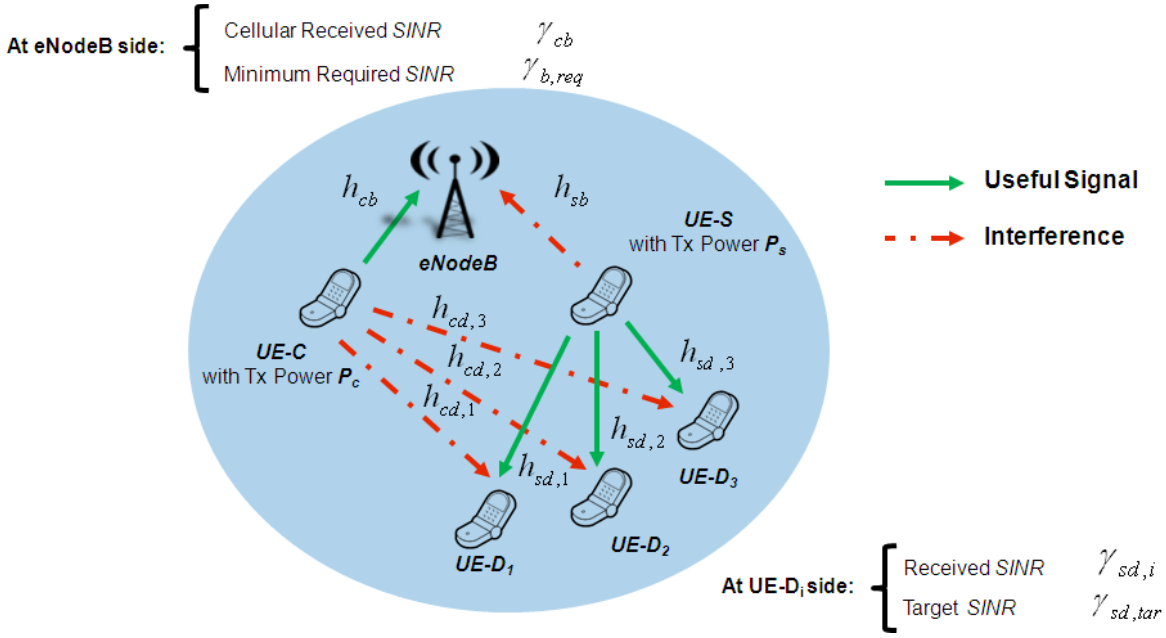

Figure 64. System Model

As described in Figure 64 and as presented further, h_{cb} and h_{sd} are the channel gains of the useful signal (for cellular and D2D users respectively) while h_{sb} and h_{cd} are the channel gains of the interference signal (for cellular and D2D users respectively).

Moreover, at eNodeB side and per each given UE-C, there is a minimum required Signal to Noise plus Interference Ratio (SINR) $\gamma_{b,req}$ to be respected, and at UE-D side there is a target SINR $\gamma_{sd,tar}$ to be considered, where the target is per each given UE-S reusing UE-C resources to transmit towards each UE-D.

The system model of the solution is further as follows:

- Prior to any sharing, the eNodeB configures a candidate UE-C to broadcast Sounding Reference Signals (i.e. SRS, as defined for legacy LTE in uplink) and UE-S/UE-D to listen to these SRS;
- UE-S/UE-D report SRS measurements to eNodeB;
- Based on measurements, eNodeB estimates potential mutual interferences to determine the relevance of the sharing with regard to QoS requirements;
- If check is positive, eNodeB allocates same resource to both UE-C and UE-S.

This contribution investigates the conditions to be fulfilled for successful D2D communication reusing resource primarily allocated for legacy cellular communication. We assume that the SINR γ_{cb} of a cellular UE to the eNodeB is expressed as

$$\gamma_{cb} = \frac{P_c h_{cb}}{N_0 + P_s h_{sb}},$$

where P_c is the transmit power of the cellular UE (UE-C), P_s is the transmit power of the D2D transmission source (UE-S) and N_0 is the power of the background noise. Moreover, as already represented in Figure 64, it is assumed that the interference consists only of the interference from D2D communication that is reusing the cellular resource. The SINR of a UE-C experienced at eNodeB side must be higher than a required threshold $\gamma_{b,req}$, to guarantee a minimum QoS for cellular legacy

communications, which yields to $\gamma_{cb} \geq \gamma_{b,req}$ or $P_c h_{cb} \geq \gamma_{b,req}\left(N_0 + P_s h_{sb}\right)$. This latest inequality gives us a condition with respect to the D2D transmission power

$$P_s \leq \frac{1}{h_{sb}}\left(\frac{P_c h_{cb}}{\gamma_{b,req}} - N_0\right) = P'_{s,\max}, \qquad \text{(a)}$$

where $P'_{s,\max}$ is the maximum transmission power that the network should impose on D2D communication. Moreover, the transmission power of a (D2D) LTE device is constrained anyway to be lower than a maximum available power $P_{s,\max}$ and therefore $P_s \leq \min\left(P'_{s,\max}, P_{s,\max}\right)$. Following the same reasoning for the QoS of a D2D communication, we consider the SINR experienced at a given D2D user equipment UE-D_i as

$$\gamma_{sd,i} = \frac{P_s h_{sd,i}}{N_0 + P_c h_{cd,i}} \geq \gamma_{sd,tar},$$

where $\gamma_{sd,i}$ is the SINR experienced at UE-D_i D2D receiver side. If N is the maximum number of users UE-D_i receiving the broadcasted information from UE-S, then the condition for at least one UE-D user to receive from UE-S is

$$\max_{1 \leq i \leq N}\left(\frac{P_s h_{sd,i}}{N_0 + P_c h_{cd,i}}\right) \geq \gamma_{sd,tar},$$

And the condition for all UE-D user to receive from UE-S is

$$\min_{1 \leq i \leq N}\left(\frac{P_s h_{sd,i}}{N_0 + P_c h_{cd,i}}\right) \geq \gamma_{sd,tar}.$$

Following the above mentioned reasoning, we obtain the constraint on the transmission power of the UE-S D2D transmission such as:

- at least one UE-D user is able to receive the broadcasted information from UE-S under network imposed target QoS:

$$P_s \geq \gamma_{sd,tar} \cdot \min_{1 \leq i \leq N}\left(\frac{N_0 + P_c h_{cd,i}}{h_{sd,i}}\right); \qquad \text{(b1)}$$

- all the UE-D users are able to receive the broadcasted information from UE-S under network imposed target QoS:

$$P_s \geq \gamma_{sd,tar} \cdot \max_{1 \leq i \leq N}\left(\frac{N_0 + P_c h_{cd,i}}{h_{sd,i}}\right). \qquad \text{(b2)}$$

The two conditions (b) and (a) should be fulfilled in order to ensure a given QoS for D2D communication and to protect the legacy cellular communication at the same time. If, generally speaking, the conditions (b) and (a) are not fulfilled, reusing the UE-C resource is not profitable because it would either cause harmful interference to UE-C, or to D2D communication resulting in a poor D2D QoS. We therefore obtain the following resource reuse strategy:

$$
(S)\begin{cases}
P_s = \min\left(\frac{1}{h_{sb}}\left(\frac{P_c h_{cb}}{\gamma_{b,req}} - N_0\right), P_{s,\max}\right) & \\
if \quad P_s \geq \gamma_{sd,tar} \cdot \max\limits_{1\leq i\leq N}\left(\frac{N_0 + P_c h_{cd,i}}{h_{sd,i}}\right), & then \quad useful \quad reuse \\
if \quad P_s < \gamma_{sd,tar} \cdot \min\limits_{1\leq i\leq N}\left(\frac{N_0 + P_c h_{cd,i}}{h_{sd,i}}\right), & then \quad harmful \quad reuse \\
if \quad \gamma_{sd,tar} \cdot \min\limits_{1\leq i\leq N}\left(\frac{N_0 + P_c h_{cd,i}}{h_{sd,i}}\right) \leq P_s < \gamma_{sd,tar} \cdot \max\limits_{1\leq i\leq N}\left(\frac{N_0 + P_c h_{cd,i}}{h_{sd,i}}\right), & then \quad partial \quad reuse
\end{cases}
$$

The proposed algorithm is practical and can be used without any difficulties, without significant change of 3GPP specifications. Moreover, SRS configuration and measurement can be performed by using current 3GPP RRC messages. The contribution presents a situation where a UE-S possibly transmits towards multiple UE-D_i (and therefore a broadcast D2D transmission), but the use case can be restricted to only one UE-D (and therefore a unicast D2D transmission).

The proposed algorithm can be performed as follows:

1. We assume that UE-S is connected to the eNodeB which knows the channel gain hsb from UE-S to the eNodeB, and we assume that UE-S knows the SINR thresholds $\gamma_{sd,tar}$ for successful D2D communication, and the eNodeB knows the required minimum SINR $\gamma_{b,req}$ for cellular uplink QoS. The channel gains hsd,i are assumed to be known by UE-S.
2. UE-S intends to send information to one or more UE-Ds within a certain range (e.g. UE-D located in the proximity of UE-S). We consider three classes of D2D communication ranges: short range (around 100 meters), medium range (around 500 meters) and long range (around 1000 meters). The transmit power of UE-S depends on the intended communication range, for long range communication the transmit power should be high while for short range communication the transmit power should be low.
3. The eNodeB (once notified about the intention of UE-S) will estimate the transmit power Ps of UE-S to achieve the intended range communication, and the eNodeB will search for a UE-C with low probability of interference to UE-S. A successful UE-C should verify the inequality $P_s \leq P'_{s,\max}$. Once the eNodeB finds a successful UE-C, it configures that UE-C to transmit SRS.
4. The eNodeB sends to UE-S information about the SRS parameters used by UE-C. The interference from cellular communication which is perceived at the D2D receiver can be estimated if the channel condition from UE-C to the D2D receiver is known. Therefore, UE-S will send to each UE-Di the SRS parameters of UE-C, so each UE-Di can decode the SRS and report to UE-S. Thanks to SRS measurements reporting, UE-S estimates the channel gains hcd,i from the cellular UE-C to the D2D receiver UE-Di.
5. Thanks to the estimation of hcd,i, UE-S can perform the reuse test (S) and decide whether or not to perform D2D communication reusing the resource of the cellular UE-C.

The following assumptions are considered:

1) It is assumed that D2D communication takes place on the same resources used for UL communication. The reasons behind this consideration are:
   a. normally DL bandwidth is overused;
   b. is easier to perform interference management at eNB side (since eNB normally allocates resources).

2) It is assumed that D2D resource reuse with cellular communications is related to scenarios where there are not sufficiently available resources. It is therefore reasonable to consider the reuse of cellular resources only in urban scenarios (and not in rural scenarios).

3) A standard cell size with 1000 m radius has been considered, and a D2D range of 100 m and 500 m have been considered (the later corresponds to a situation where if the D2D transmitter is located at the edge of the cell it should be able to communicate with a D2D receiver located near the base station).
4) It is assumed that D2D communication propagation environment is different from the cellular environment:
    a. For cellular environment the propagation is considered to be Urban Macro UMa (due to longer involved distance from cellular UE to eNB) and LOS (if the eNB cannot directly "see" the cellular user) or NLOS (if the eNB can directly "see" the cellular user);
    b. For D2D communication environment it is considered that the propagation is Urban Micro UMi like (due to shorter involved distance from source UE to destination UE). The environment is likely to be LOS for shorter-range D2D communication scenarios (e.g. below 100 m) and NLOS for higher-range D2D communication scenarios (e.g. for 500 m). In order to cope with all situations we have considered for D2D an ITU-R propagation model (ITU-R P.1411-4) for communications under the roof top, which is valid for distances up to 3000 m, in the range 300-3000 MHz and for antenna heights of maximum 3 m above ground. This model includes a location variability parameter with values between 1% and 99% which defines the percentage of NLOS. For example, 1% location variability corresponds to model LOS-predominant and 99% location variability corresponds to a model NLOS-predominant.

There are two kinds of Key Performance Indicators (KPIs) being tested:

1) The probability of resource reuse for a given UE-C, which is computed as the ratio between A) the number of users for which reuse conditions are met (all the remaining users may potentially be UE-S) and B) the total number of users. For example, if all the users (except UE-C) are possible candidates the probability of reuse is 1. We further denote this probability as PUEC, and we can refer to this probability as the probability, for given UE-C, to be a successful candidate.
2) The probability of resource reuse for a given UE-S, which is computed as the ratio between A) the number of users for which reuse conditions are met (all the remaining users may potentially be UE-C) and B) the total number of users. For example, if all the users (except UE-S) are possible candidates, then the probability of reuse is 1. We further denote this probability as PUES, and we can refer to this probability as the probability, for given UE-S, to find a candidate UE-C.

The experiments further performed consider the following simulation parameters:

Simulation Parameter	Value(s)
UE-C maximum transmission power	24 dBm
UE-S (D2D) maximum transmission power (linearly scaled with maximum Tx distance, cf. RAN1 agreement & TR 36.843)	21 dBm for 100 m range; 28 dBm for 500 m range
Background noise level	-174 dBm/Hz
Transmission frequency	0.7 GHz or 2.6 GHz
Cell radius	1000 m
eNB antenna height	10 m
UE-C, UE-S and UE-D antenna heights	1.5 m
Cellular environment channel model	3GPP Urban Macro (UMa)
D2D environment channel model	ITU-R P.1411-4
Cellular propagation conditions	LOS & NLOS
D2D propagation conditions	Location variability parameter 1% & 10%
UE-C required SINR $\gamma_{b,req}$	5 dB, 0 dB & -10 dB
UE-D target SINR $\gamma_{sd,tar}$	0 dB, -10 dB

In all figures presented in the sections dedicated to simulation results we have considered that the base station is placed in the center of the figure, with the coordinates (0, 0). Moreover, a 3-sector cell model is used, and the eNB antenna radiation pattern to be used for each sector in a 3-sector cell scenario is

given by 3GPP Technical Report 36.942. For these simulations the UEs have been pseudo uniformly distributed within the cell (both X-coordinates and Y-coordinates are distributed following a uniform distribution). Two different ranges for D2D communication have been considered: a maximum distance between UE-S and UE-D of 100 m (corresponding to a short range scenario), a maximum distance between UE-S and UE-D is set to 500 m (corresponding to a medium up to long range scenario).

3.2.1 PUEC comparison in terms of transmitted frequency and D2D transmission ranges

Figure 65 and Figure 66 present two-dimensional P_{UEC} probability evaluation for $\gamma_{b,req}=5$ dB, $\gamma_{sd,tar}=0$ dB, NLOS cellular environment of type UMa, D2D ITU environment with location variability of 10%, for two carrier frequencies of 2.6 GHz and of 0.7 GHz, and for 2 different transmission ranges: 100 m range for Figure 65 and 500 m range for Figure 66.

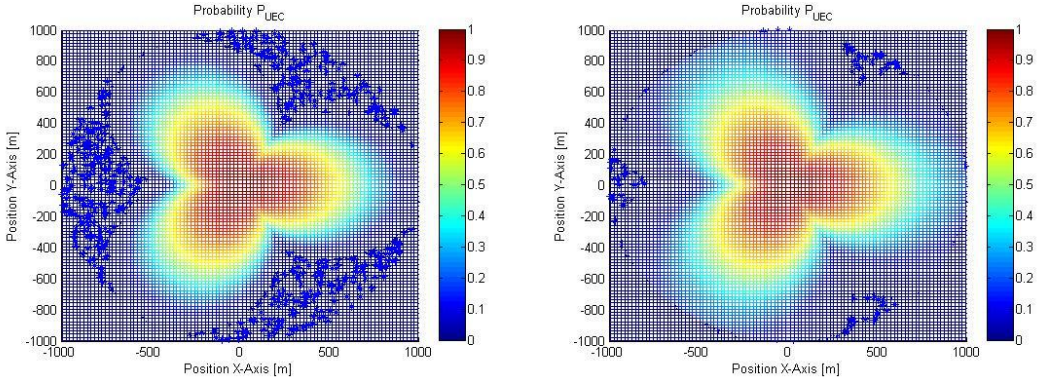

Figure 65. P_{UEC} evaluation for $\gamma_{b,req}=5$ dB; $\gamma_{sd,tar}=0$ dB, cellular UMa, NLOS; D2D ITU 10%, 100 m range, a) 2.6 GHz (left hand side); b) 0.7 GHz (right hand side).

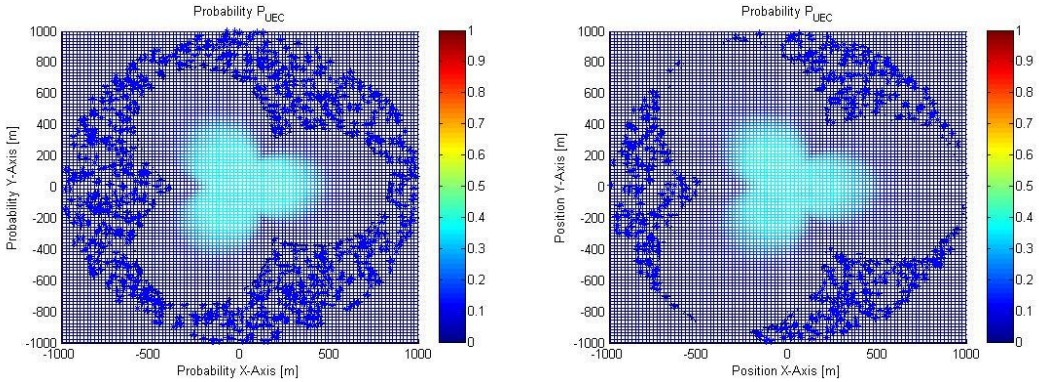

Figure 66. P_{UEC} evaluation for $\gamma_{b,req}=5$ dB; $\gamma_{sd,tar}=0$ dB, cellular UMa, NLOS; D2D ITU 10%, 500 m range, a) 2.6 GHz (left hand side); b) 0.7 GHz (right hand side).

In both Figure 65 and Figure 66 it seems clear that when using a lower carrier frequency, for a given UE-C, we can easily find a D2D pair (with 100 m transmission range and 500 m transmission range respectively) to reuse the same resource, compared with the situation when using a higher carrier frequency. Potential cellular UE-C for cellular resource reuse can be found easier in the direction of the antenna lobes, for a lower D2D transmission range, and when a lower frequency carrier is used. The probability P_{UEC} is therefore higher for a lower D2D transmission range, for a lower frequency carrier used, and in the direction of the base station antenna lobes.

Another important conclusion is that for a UE-C located near the base station we can always find a D2D pair communicating in a 100 m range and which can reuse the same resource as the one used for legacy cellular communication. However, when the D2D communication range increases and becomes comparable with the cell radius, the probability to find a convenient D2D pair considerably decreases.

3.2.2 PUEC comparison in terms of cellular propagation models, frequency and D2D transmission ranges

Another important conclusion can be extracted with respect to Figure 67 and Figure 68, where QoS parameters, D2D channel models and carrier frequencies and transmission ranges are kept constant, but the cellular propagation environment is varied from NLOS to LOS.

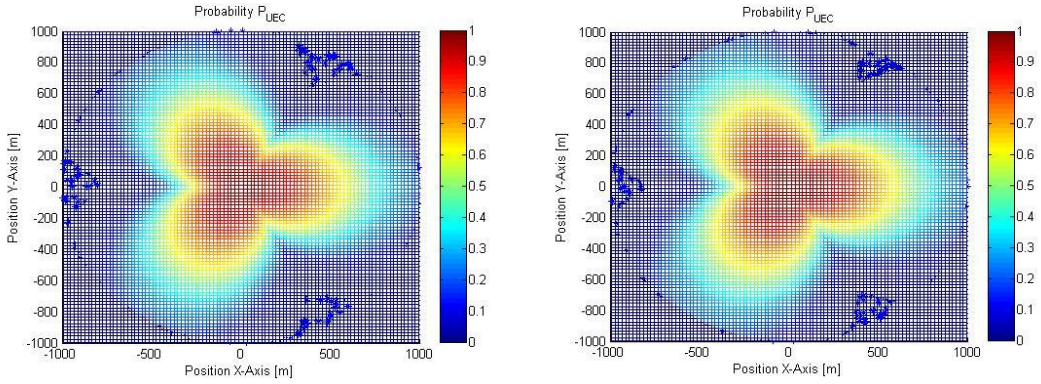

Figure 67. P_{UEC} evaluation for $\gamma_{b,req}$=5 dB; $\gamma_{sd,tar}$=0 dB, cellular UMa, D2D ITU 10%, 0.7 GHz, 100 m range, a) NLOS (left hand side); b) LOS (right hand side).

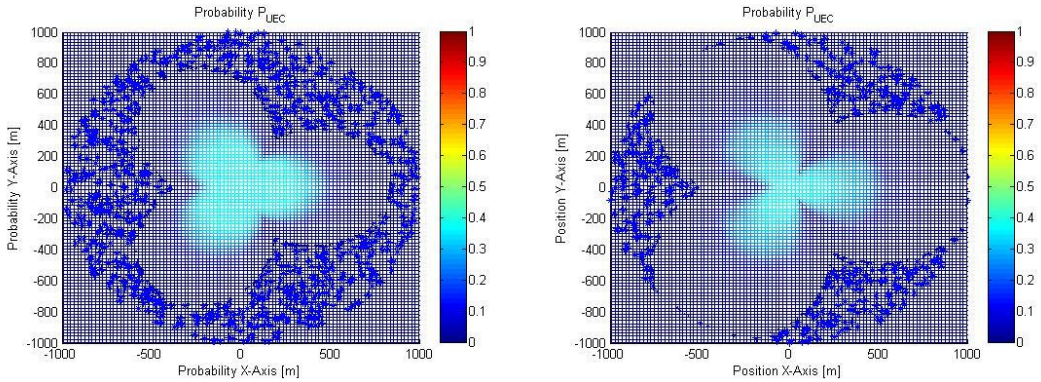

Figure 68. P_{UEC} evaluation for $\gamma_{b,req}$=5 dB; $\gamma_{sd,tar}$=0 dB, cellular UMa, D2D ITU 10%, 2.6 GHz, 500 m range, a) NLOS (left hand side); b) LOS (right hand side).

Results from Figure 67 and Figure 68 show that generally a better cellular propagation, for a given UE-C, may help to find a suitable D2D pair for the reuse. As obtained in previous figures, a decrease in P_{UEC} probability might be expected when D2D communication range is higher and when communication frequency is higher.

Moreover, Figure 68 showed that at higher frequency it can be better noticed the impact of LOS channel. Further, Figure 69 evaluates P_{UEC} at higher frequency but at lower D2D ranges. Compared with Figure 68 it can be seen an improvement in terms of probability of reuse, which shows once more the impact of the D2D communication range. Furthermore, on the right hand side of both Figure 68 and Figure 69 it can be seen that at higher frequency ranges cellular LOS propagation affects the reuse: the reuse decreases between the antenna lobes but it increases in the direction of the lobes.

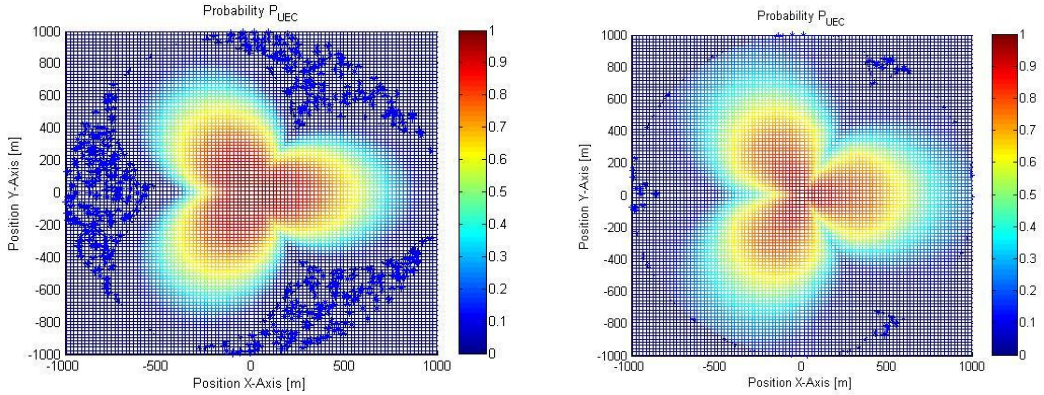

Figure 69. P_{UEC} evaluation for $\gamma_{b,req}$=5 dB; $\gamma_{sd,tar}$=0 dB, cellular UMa, D2D ITU 10%, 2.6 GHz, 100 m range, a) NLOS (left hand side); b) LOS (right hand side).

3.2.3 PUEC comparison in terms of D2D propagation models and transmitted frequency

In previous sections it has been studied the impact of cellular communications propagation environment on the reuse probability. In this section we present a selected comparison between different D2D channel models. It is further showed in Figure 70 and Figure 71 that the impact of D2D channel model (LOS or NLOS) is minimal when communication is performed in a LOS cellular environment, at 2.6 GHz or 0.7 GHz frequency, at 100 m range. A small improvement on reuse probability can be noticed at low frequency ranges for NLOS D2D channels in Figure 71 (see right hand side of the figure for ITU propagation model with 90% location variability), but once more, it is showed that the parameters with highest impact are the cellular model (please recall the discussion on cellular LOS model from the previous section) and to some extent the carrier frequencies. If the cellular communication channel would have been NLOS, the performance obtained in Figure 70 compared to Figure 71 would have been similar.

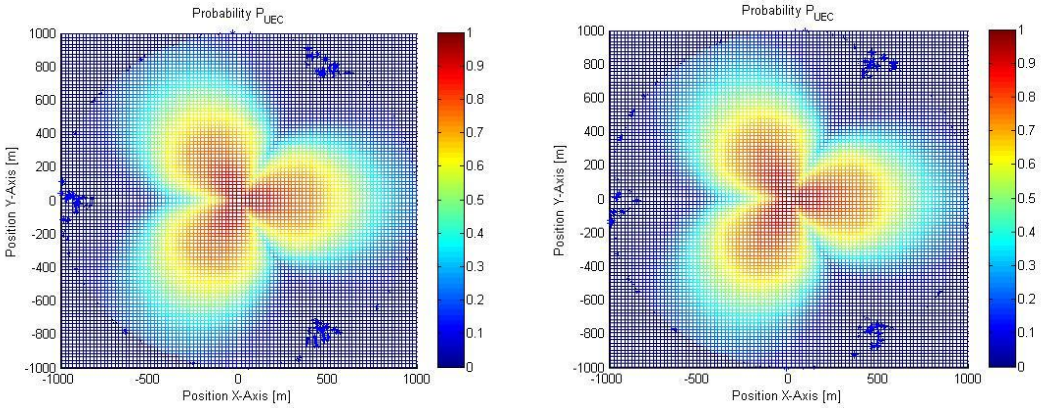

Figure 70. P_{UEC} evaluation for $\gamma_{b,req}$=5 dB; $\gamma_{sd,tar}$=0 dB, cellular UMa, LOS; 2.6 GHz, 100 m range, a) D2D ITU 1% (left hand side); b) D2D ITU 90% (right hand side).

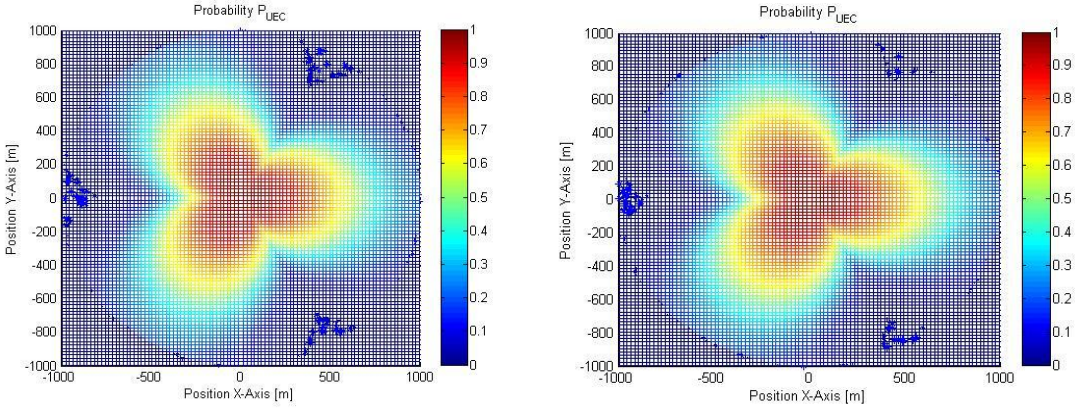

Figure 71. P_{UEC} evaluation for $\gamma_{b,req}$=5 dB; $\gamma_{sd,tar}$=0 dB, cellular UMa, LOS; 0.7 GHz, 100 m range, a) D2D ITU 1% (left hand side); b) D2D ITU 90% (right hand side).

3.2.4 PUES comparison in terms of transmitted frequency

Similar to Figure 65 and Figure 66, Figure 72 and Figure 73 present two-dimensional P_{UES} probability evaluation for two carrier frequencies: 2.6 GHz (left hand side) and 0.7 GHz (right hand side). A cellular LOS environment for an UMa scenario with 100 m D2D communication range and an ITU location variability parameter of 1% have been considered. Moreover, Figure 72 considers a less constraited QoS ($\gamma_{b,req}$=0 dB; $\gamma_{sd,tar}$=0 dB) while Figure 73 considers a more conservative QoS ($\gamma_{b,req}$=5 dB; $\gamma_{sd,tar}$=0 dB) where the cellular users are better protected.

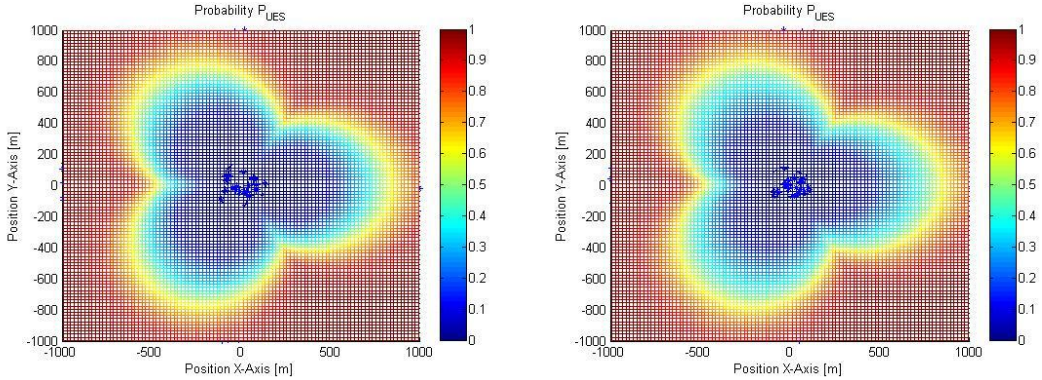

Figure 72. P_{UES} evaluation for $\gamma_{b,req}$=0 dB; $\gamma_{sd,tar}$=0 dB, cellular UMa, LOS; D2D ITU 1%, 100 m range, a) 2.6 GHz (left hand side); b) 0.7 GHz (right hand side).

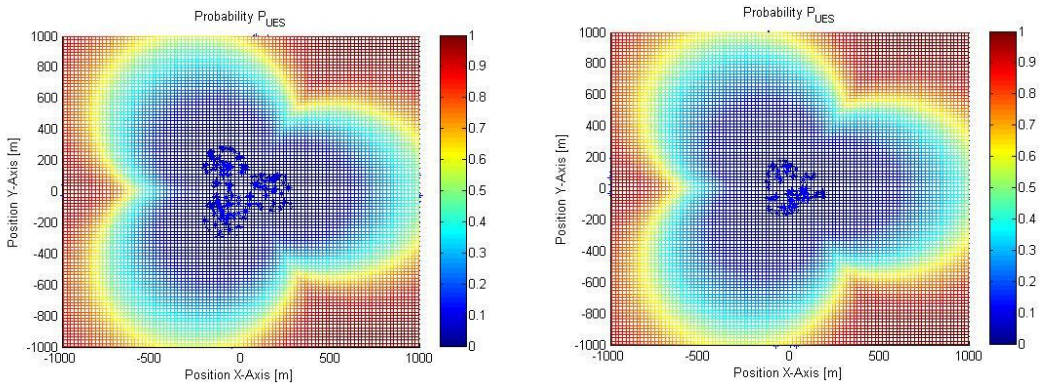

Figure 73. P_{UES} evaluation for $\gamma_{b,req}$=5 dB; $\gamma_{sd,tar}$=0 dB, cellular UMa, LOS; D2D ITU 1%, 100 m range, a) 2.6 GHz (left hand side); b) 0.7 GHz (right hand side).

Conclusions are not obvious, but it seems that at 100 m D2D range, for a given UE-S, the probability to find a D2D pair that can reuse the same resource as the cellular user is higher when lower carrier frequency is used, and at lower cellular QoS requirements.

An explanation for the general shape of the P_{UES} function can be the following: 1) if UE-S is located near eNB in the direction of the antenna lobe, it is very difficult to find candidate UE-C, and similarly, 2) if UE-S is located at eNB coverage edge, at the limit between two antenna sectors, it is easier to find candidate UE-C. There is therefore a UE-S predominant direction, a direction that provides increased probability of reuse. Moreover, it seems that the frequency of use is not very important at fixed range; what it really counts are the target/expected QoS.

3.2.5 PUES comparison in terms of QoS requirements

This section compares P_{UES} reuse probabilities for fixed carrier frequencies (2.6 GHz), fixed cellular UMa LOS model, fixed D2D transmission ranges (100 m) and fixed D2D channel models (D2D ITU with 1% location variability), with variable QoS requirements on both cellular communication and D2D communication side. In Figure 74 it is required a "standard" QoS parameterization for cellular and D2D ($\gamma_{b,req}$*=5 dB,* $\gamma_{sd,tar}$*=0 dB)*. We call this parameterization as "standard" because it has been also used in previous sections, but it also implies realistic QoS cellular requirements.

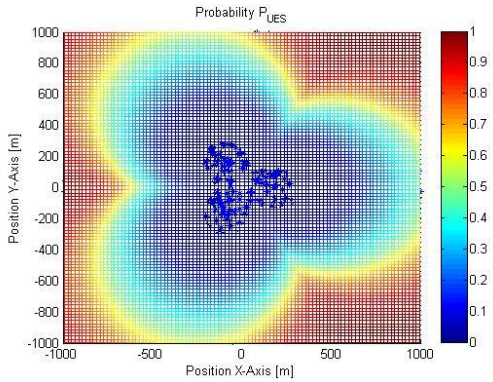

Figure 74. P_{UES} evaluation for cellular UMa, LOS; D2D ITU 1%, 2.6 GHz, 100 m range, $\gamma_{b,req}$=5 dB, $\gamma_{sd,tar}$=0 dB.

On the other hand, Figure 75 and Figure 76 both present results for cellular required performance threshold of *0 dB* and *-10 dB* respectively ($\gamma_{b,req}$*=0 dB* for Figure 75, and $\gamma_{b,req}$*=-10 dB* for Figure 76), for different D2D communication targeted QoS parameters. The reason for this study was therefore to check out which QoS parameters are more important in the evaluation of P_{UES} reuse probabilities. It has been therefore found that the parameter with highest importance is not the QoS D2D parameter but the QoS cellular parameter.

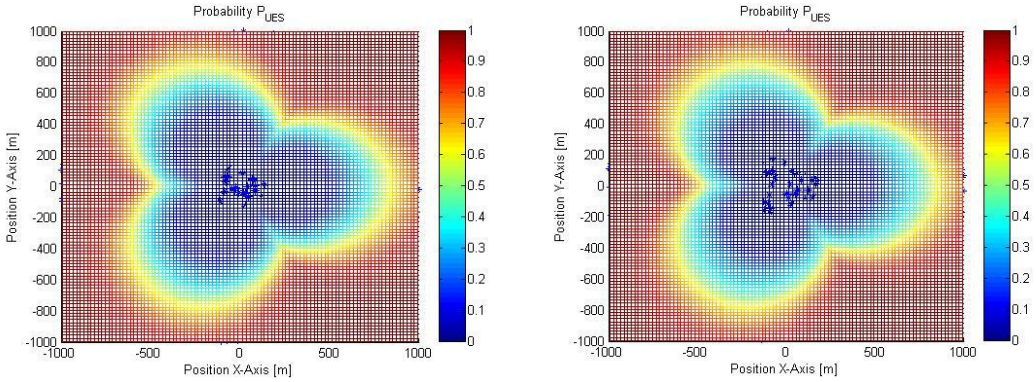

Figure 75. P_{UES} evaluation for cellular UMa, LOS; D2D ITU 1%, 2.6 GHz, 100 m range, a) $\gamma_{b,req}$=0 dB, $\gamma_{sd,tar}$=0 dB (left hand side), b) $\gamma_{b,req}$=0 dB, $\gamma_{sd,tar}$=-10 dB (right hand side).

At 100 m D2D range with D2D LOS channels (ITU D2D channel location variability is 1%) it can be seen that the variation of D2D QoS parameter has lower impact (if we compare for example Figure 75 left hand side a) with Figure 75 right hand side b); or if we compare Figure 76 left hand side a) with Figure 76 left hand side b)) than the variation of cellular QoS parameter (if we compare for example Figure 75 left hand side a) with Figure 76 right hand side a); or if we compare Figure 75 left hand side b) with Figure 76 left hand side b)). It has been therefore noticed that lower the cellular QoS constraints are, higher the reuse probability P_{UES} is. A good strategy for D2D communication reuse for a given UE-S (as explained when defining P_{UES} reuse probability) is therefore to control cellular QoS parameters rather than to control D2D communication QoS parameters.

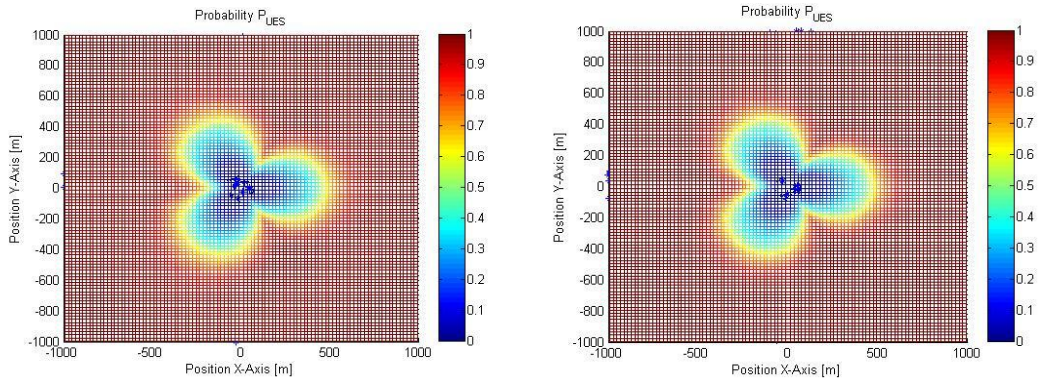

Figure 76. P_{UES} evaluation for cellular UMa, LOS; D2D ITU 1%, 2.6 GHz, 100 m range, a) $\gamma_{b,req}$=-10 dB, $\gamma_{sd,tar}$=0 dB (left hand side); b) $\gamma_{b,req}$=-10 dB, $\gamma_{sd,tar}$=-10 dB (right hand side).

As a general conclusion, we can therefore conclude that for a given UE-S it is easier to find a candidate UE-C if the UE-C QoS constraints are relaxed.

3.2.6 PUES comparison in terms of cellular propagation models

Figure 77 and Figure 78 describe P_{UES} reuse probabilities for 0.7 GHz and 2.6 GHz carrier frequencies, for both NLOS and LOS models. Other parameters such as QoS parameters, D2D channel model and D2D transmission range have been kept constant for comparison purposes. It can be noticed that at 0.7 GHz the P_{UES} reuse probability is slightly better for LOS cellular channel models at the limit of the cell coverage region. However, at 2.6 GHz it can be notice an important difference between LOS and NLOS scenarios, and we can conclude that at higher carrier frequency the P_{UES} reuse probability is higher for LOS cellular propagation environment.

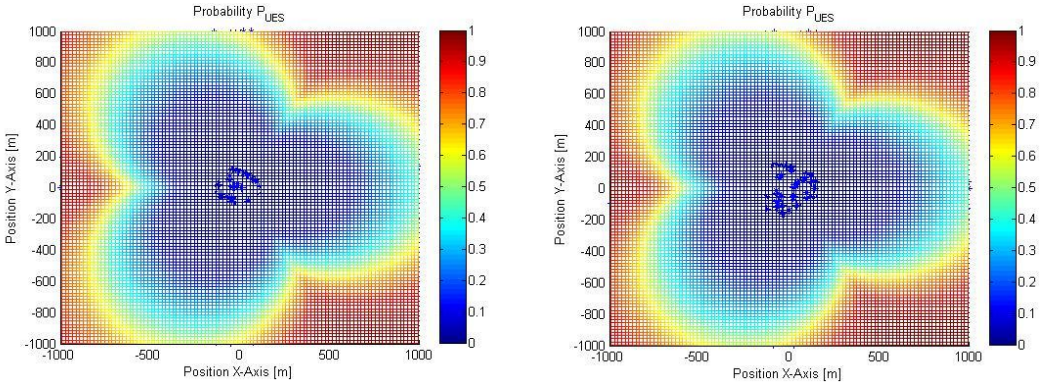

Figure 77. P_{UES} evaluation for $\gamma_{b,req}$=5 dB; $\gamma_{sd,tar}$=0 dB, D2D ITU 10%, 0.7 GHz, 100 m range, a) Cellular UMa, NLOS (left hand side); b) Cellular UMa, LOS (right hand side).

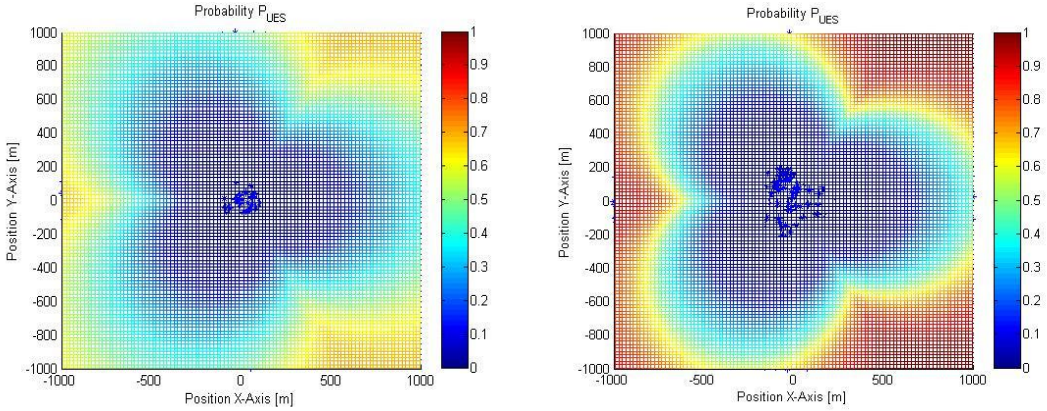

Figure 78. P_{UES} evaluation for $\gamma_{b,req}$=5 dB; $\gamma_{sd,tar}$=0 dB, D2D ITU 10%, 2.6 GHz, 100 m range, a) Cellular UMa, NLOS (left hand side); b) Cellular UMa, LOS (right hand side).

When comparing Figure 77 for cellular UMa, LOS channel model (see right hand side of the figure) with Figure 78 for cellular UMa, LOS channel model (see right hand side of the figure), we can also notice that at higher frequency range the P_{UES} reuse probability is lower with at least 30%.

3.2.7 PUES comparison in terms of D2D propagation models

When comparing P_{UES} reuse probabilities from Figure 79 with Figure 80, we can see that for NLOS cellular models, the D2D channel model (LOS or NLOS) has a minimum impact while a higher carrier frequency will decrease the P_{UES} reuse probability with up to 30%.

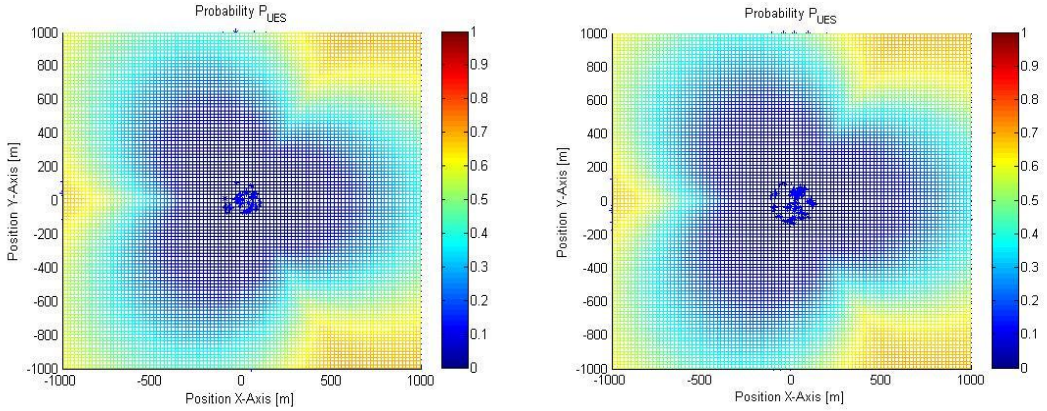

Figure 79. P_{UES} evaluation for $\gamma_{b,req}$=5 dB; $\gamma_{sd,tar}$=0 dB, Cellular UMa, NLOS; 2.6 GHz, 100 m range, a) D2D ITU 10% (left hand side), b) D2D ITU 90% (right hand side).

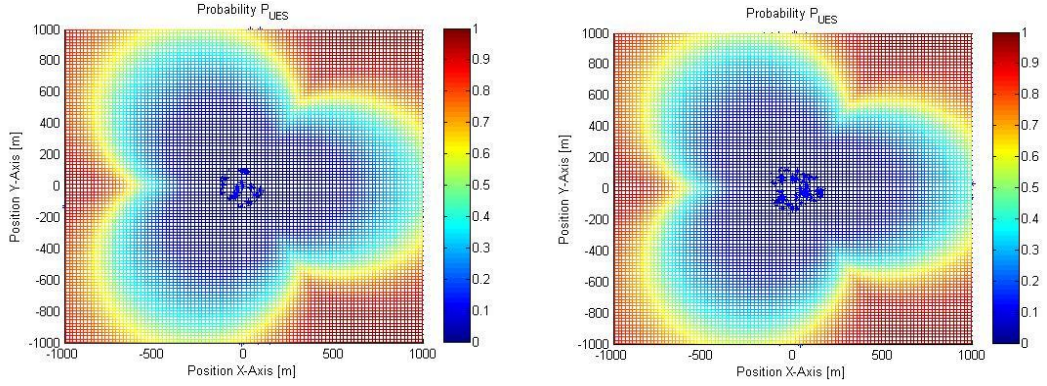

Figure 80. P_{UES} evaluation for $\gamma_{b,req}$=5 dB; $\gamma_{sd,tar}$=0 dB, Cellular UMa, NLOS; 0.7 GHz, 100 m range, a) D2D ITU 10% (left hand side), b) D2D ITU 90% (right hand side).

3.2.8 General conclusions

In order to keep the user experience of the cellular user above a minimum required QoS level, and in order to maintain a certain targeted QoS for the D2D communication, this work shows that there are some necessary requirements which cannot be always fulfilled, and therefore that the D2D reuse of the cellular resources is not always possible. Interference with/from the cellular users and necessary protocols to alleviate interferences are major issues which have to be properly dealt. After deriving the resource reuse conditions, and after presenting practical protocols used to limit the interference produced to the cellular users, feasibility results were presented. These feasibility results were expressed in terms of reuse probability of a cellular resource per D2D communication link, as a function of cellular user position. An operator could use such statistical information to identify if the cellular resource reuse is possible, and also to measure the theoretical gain of reusing cellular resources for D2D communication, depending on the carrier frequency choice, QoS parameters, propagation environment and D2D transmission ranges.

4 CONCLUSIONS

This deliverable compiled the simulation results obtained after the deliveries of D5.1 and D5.2. In addition, it also compared the most promising innovations of each task in WP5 in order to identify the one that would best fit in some specific scenarios.

In the context of Advanced Relaying techniques, we start with the performance of a novel cooperative coding scheme to communicate efficiently over multiple-relay fading channels which relies on non-binary Low Density Parity Check (LDPC) codes at the source, coupled with non-binary repetition codes at the relays. A simple joint decoding strategy is used at the receiver end, so that the decoding complexity is not increased compared to a system without relays, while preserving the coding gain brought by re-encoding the signal at the relays. We show by simulations that the proposed scheme allows maintaining a constant gap to the outage probability of the cooperative system, irrespective of the number of relays. We then recall a three-message half-duplex single-relay scheme described in D5.1 whose key characteristic, in comparison to the one that is currently standardized by 3GPP for 4G, is firstly the use of physical-layer relaying. The relay station decodes information in a first phase and collaboratively aids the transmission with the source in the second phase. In LTE, multi-round transmission using HARQ is already the standard means for transmission and the method here simply puts the relay into the protocol. The second motivation for using the distributed three-message superposition coding approach used is that it achieves full degrees of freedom with half-duplex relaying. We provided new simulation results for dual-antenna receivers using more realistic channel models in order to draw conclusions on a more representative scenario. We show that capacity is close to double in all cases in comparison to the current relaying strategy standardized (but unused) by 3GPP for 4G. As a main conclusion, we suggest that relaying such as this be reconsidered during the standardization phase of 5G. Lastly, we investigate a code-dependent unequal power allocation method for Gaussian channels using irregular LDPC codes. This method allocates the power for each set of coded bits depending on the degree of their equivalent variable nodes. We propose a new algorithm to optimize the power allocation vector using density evolution algorithm under the Gaussian approximation. We show that unequal power allocation can bring noticeable gains on the threshold of some irregular LDPC codes with respect to the classical equal power allocation method depending on the code and the maximum number of decoding iterations.

In terms of clustered mesh networks for Professional Mobile Radio (PMR) systems, which is the particular case of rapidly-deployable systems e.g. for crisis management, there can be absence of wired backhaul between the cells, called here clusters, and hence inter-cluster communications are taken in charge by some relay nodes called bridging mesh routers (MR). A two-way relaying (TWR) technique was investigated and compared with a traditional Decode-and-Forward strategy for two main deployment scenarios:

- A scenario with a smaller frequency bandwidth for MR, a larger inter-site distance (ISD) and a lower location variability (corresponding to a smaller city for example, with lower number of users and lower roof-top height);
- A scenario with a larger frequency bandwidth for MR, a smaller ISD and a higher location variability (corresponding to a more populated city for example, with higher number of users and higher roof-top height – predominant NLOS scenario).

These categories have been defined by taking into account architecture opportunities and real-deployment situations. Real 3GPP and ITU parameters and system constraints have been also considered: the 700 MHz band was considered for simulations since it is one of the main candidate bands for deployment of the future broadband PMR networks. Scenarios A and B show that TWR provides better throughput than DF, for any possible position of a MR. TWR typically doubles the throughput at the best MR position. In scenario A, TWR achieves significant throughput gains only for certain distances (typically the MR must be placed in between the served nodes). However, for more dense urban deployments like scenario B, throughput gains are weakly sensitive to the MR position, which is a desired feature in rapidly deployable PMR systems. It is also shown that DF is more robust than TWR in terms of end-to-end PER (e.g. DF has better or equal PER than TWR, depending on the MR position). A best-case scenario for a PMR deployment in the case of voice services is also considered. In this case it is showed that for long-distance robust communications (e.g. up to 5 km) where maximum limit for the achievable throughput is not of interest, the DF technique is an interesting approach.

Resource allocation for multi-hop communications inside a cell or cluster is considered for applications to PMR context and the work extends three traditional scheduling policies to this new framework. In order to differentiate the impact of relaying on performance a comparison is made among the case when all the communications pass mandatorily through the base station (also named cluster head in mesh deployments), which is the standard cellular configuration, the case in which also direct communications between users are allowed, and finally the case in which any user can be a relay.

We compared the performance of relay-assisted communication in terms of throughput with the capacity of the direct link using empirical path loss models and measured values. The measurements are based on an extensive campaign extracted previously. One set of measurements is focused on the backhaul link whereas another on the access link. The comparison between relay-assisted and direct communication is performed for different relay antenna heights and positions. The work is divided in main parts, firstly we described the simulation setup and secondly reported on simulation results to provide significant conclusions on relay deployment with decode-and-forward relaying namely that the direct link capacity can be improved by a relay-assisted communication when a full-duplex relay technology is used. No significant improved with simple decode-and-forward half-duplex relays. The capacity gain provided by the relay reaches more than 30 % depending on the antenna relay height and location. The analysis assumed omnidirectional antenna at RS and was performed at 2.2 GHz. Future work will analyse the frequency dependency of relay performances. Higher frequencies would allow the use of antenna array with a limited physical size but able to generate high gain directional beam enhancing the backhaul and access link capacities. But the actual benefits of directional antennas depend on the received signal spatial distribution.

We provided extensive simulation results for some of the resource allocation strategies described in D5.2 with respect to D2D communications. We also provided a feasibility study of cellular-D2D reuse of radio resource, i.e. simultaneous use for cellular and D2D links, in the context of an LTE network. This work investigated the conditions for such an allocation scheme to serve the expected Quality of Service (QoS) on both cellular and D2D links, and the simulation results were based on real constraints from recent 3GPP standardization activities. As conclusion, interference constraints have to be identified and new interference control techniques have to be implemented along with a possible associated LTE system design.

5 LIST OF ABBREVIATIONS

3GPP	3rd Generation Partnership Project
AF	Amplify-and-Forward
AWGN	Additive White Gaussian Noise
BER	Bit Error Rate
BLER	BLock Error Rate
BP	Belief Propagation
BS	Base Station
CB	Circular Buffer
CDF	Cumulative Distribution Function
CF	Compress-and-Forward
CFS	CDF Fair Scheduling
CH	Cluster Head
CRC	Cyclic Redundancy Check
CSI	Channel State Information
D2D	Device-to-Device
DeNB	Donor evolved NodeB
DF	Decode-and-Forward
DL	DownLink
DL-SCH	DownLink Shared CHannel
eNB	Evolved NodeB
EPA	Equal Power Allocation
EPA	Extended Pedestrian A
ETU	Extended Typical Urban
FD	Full Duplex
FER	Frame Error Rate
FDD	Frequency Division Duplex
FS	Free Space
gDoF	generalized Degree of Freedom
HD	Half Duplex
IMT	International Mobile Communications
IST	Inter-Site Distance
ITU	International Telecommunication Union
ITU-R	International Telecommunication Union-Radio
JFI	Jain Fairness Index
KPI	Key Performance Indicator
LDPC	Low Density Parity Check
LLR	Log-Likelihood Ratio
LOS	Line of Sight

LTE	Long Term Evolution
LTE-A	Long Term Evolution - Advanced
MAC	Medium Access Control
MCS	Modulation and Coding Scheme
MF	Matched Filter
MIMO	Multiple Input Multiple Output
MPFS	Maximum Proportional Fair Scheduling
MR	Mesh Router
MS	Mobile Station
MUDS	Multi User Diversity Scheduling
MWBM	Maximum Weighted Bipartite Matching
NB-LDPC	Non-Binary Low Density Parity Check
NC	Network Coding
NLOS	Non Line of Sight
NNC	Noisy Network Coding
OFDM	Orthogonal Frequency-Division
PD&F	Partial Decode-and-Forward
PDF	Probability Density Function
PDSCH	Physical Downlink Shared CHannel
PER	Packet Error Rate
PFS	Proportional Fair Scheduling
PHY	Physical
PL	Path Loss
PMR	Private Mobile Radio
PPDR	Public Protection and Disaster Relief
PRB	Physical Resource Block
QAM	Quadrature Amplitude Modulation
QPSK	Quadrature Phase Shift Keying
QoS	Quality of Service
RAN	Radio Access Network
RB	Resource Block
RE	Resource Element
RN	Relay Node
RS	Relay Station
RV	Redundancy Version
SDMA	Spatial Division Multiple Access
SIC	Successive Interference Cancellation
SINR	Signal to Interference plus Noise Ratio
SNR	Signal to Noise Ratio

TB	Transport Block
TBS	Transport Block Size
TDD	Time Division Duplex
TTI	Transmission Time Interval
TWR	Two-Way Relaying
UE	User Equipment
UHF	Ultra High Frequency
UL	UpLink
UMTS	Universal Mobile Telecommunications System
UPA	Unequal Power Allocation
WiFi	Wireless Fidelity
WINNER	Wireless World Initiative New Radio
WP	Work Package

6 REFERENCES

[1] J.J. Boutros, A. Guillén i Fabregas, E. Biglieri, and G. Zémor, "Design and analysis of Low-Density Parity-Check codes for block-fading channels," in IEEE Inf. Theory and App. Workshop, 2007, pp. 54–62.

[2] M. Cardone, D. Tuninetti, R. Knopp, U. Salim, "Gaussian half-duplex relay networks: improved gap and a connection with the assignment problem," IEEE International Information Theory Workshop, September 2013.

[3] M. Cardone, D. Tuninetti, R. Knopp, U. Salim, "Gaussian half-duplex relay networks: improved constant gap and connections with the assignment problem," IEEE Transactions on Information Theory, vol. 60, no. 6, pp. 3559 – 3575, June 2014.

[4] M. Cardone, D. Tuninetti, R. Knopp, U. Salim, "The capacity to within a constant gap of the Gaussian half-duplex relay channel," IEEE International Symposium on Information Theory, July 2013.

[5] M. Cardone, D. Tuninetti, R. Knopp, U. Salim, "Gaussian half-duplex relay channels: generalized degrees of freedom and constant gap result," IEEE International Conference on Communications, June 2013.

[6] M. Cardone, D. Tuninetti, R. Knopp, U. Salim, "On the Gaussian half-duplex relay channel," IEEE Transactions on Information Theory, vol. 60, no. 5, pp. 2542-2562, May 2014.

[7] R. Thomas, M. Cardone, R. Knopp, D. Tuninetti, B.T. Maharaj, "An LTE implementation of a novel strategy for the Gaussian half-duplex relay channel," IEEE International Conference on Communications, June 2015.

[8] M. Cardone, D. Tuninetti, R. Knopp, "The approximate optimality of simple schedules for half-duplex multi-relay network,'' submitted to IEEE International Information Theory Workshop, April 2015 (available at http://arxiv.org/abs/1410.7174).

[9] M. Cardone, D. Tuninetti, R. Knopp, "On user scheduling for maximum throughput in K-user MISO broadcast channel'', IEEE International Conference on Communications, June 2015.

[10] T.J. Richardson, M.A. Shokrollahi, R.L. Urbanke: "Design of capacity-approaching irregular low-density parity-check codes". IEEE Trans. on Information Theory, vol. 47, no. 2, pp 619–637, Feb. 2001

[11] H. Qi, D. Malone, V. Subramanian: "Does every bit need the same power? An investigation on unequal power allocation for irregular LDPC codes". WCSP, 1–5, Nanjing, Nov. 2009

[12] S.Y. Chung, T. Richardson, R.L. Urbanke "Analysis of sum-product decoding of low-density parity-check codes using a Gaussian approximation" IEEE Trans. on Information Theory, vol. 47, no. 2, pp 657–670, Feb. 2001

[13] 3GPP, "Further advancements for E-UTRA physical layer aspects," http://www.3GPP.org, vol. TR 36.814 V9.0.0, March 2010 2010.

[14] A. B. Saleh, S. Redana, B. Raaf, T. Riihonen, J. Hamalainen, and R. Wichman, "Performance of Amplify-and-Forward and Decode-and-Forward Relays in LTE-Advanced," in Vehicular Technology Conference Fall (VTC 2009-Fall), 2009 IEEE 70th, 2009, pp. 1-5.

[15] L. Gang, F. R. Yu, J. Hong, V. C. M. Leung, and L. Xi, "In-Band Full-Duplex Relaying: A Survey, Research Issues and Challenges," Communications Surveys & Tutorials, IEEE, vol. 17, pp. 500-524, 2015.

[16] N. Wiberg. Codes and decoding on general graphs. PhD thesis, Likoping University, Sweden, 1996.

[17] T. Doumi, M. F. Dolan, S. Tatesh, A. Casati, G. Tsirtsis, K. Anchan, and D. Flore, "LTE for Public Safety Networks", IEEE Communications Magazine, p: 106 - 112, February 2013.

[18] ICT-LOLA project: Achieving Low Latency in wireless communications: http://www.ict-lola.eu/

[19] Z. Lin, P. Xiao, B. Vucetic, and M. Sellathurai, "Analysis of Receiver Algorithms for LTE SC-FDMA Based Uplink MIMO Systems", IEEE Trans. on Wireless Comm., vol 9, no 1, pp. 60-65, January 2010.

[20] R. Knopp and P.A. Humblet, "Information capacity and power control in single-cell multiuser communications", in Proc. IEEE In. Conf. Communications (ICC), Seattle, WA, Jun. 1995, pp. 331-335

[21] P. Bender, P. Black, M. Grob, R. Padovani, N. Sindhushyana, and A. Viterbi, "A bandwidth efficient high speed wireless data service for nomadic users", IEEE Communications Magazine, Jul. 2000.

[22] A. Jalali, R. Padovani, and R. Pankaj, "Data throughput of CDMA HDR: a high efficiency-high data rate personal communication wireless system", in Proc. IEEE Vehicular Technology Conference, May 2000.

[23] H. Anouar "Queue Maximum Proportional Fair Scheduling for Saturated and Non-Saturated Regimes", IEEE WCNC 2014.
[24] R. Jain R, D.M. Chiu and W. Hawe, "A Quantitative Measure of Fairness and Discrimination for Resource Allocation in Shared Computer Systems", DEC Research Report TR-301, 1984.
[25] X. Qin and R. Berry, "Opportunistic Splitting Algorithms for Wireless networks with Heterogenous users", Proc. Conf. Inform. Sciences Systems (CISS), March 2004.
[26] Nokia Networks, "LTE-Advanced: The advanced LTE toolbox for more efficient delivery of better user experience," 2014, White Paper, pp. 1-19 [Online], Available: http://networks.nokia.com/system/files/document/nokia_lte-advanced_white_paper.pdf.
[27] E. Lang, S. Redana and B. Raaf, "Business Impact of Relay Deployment for Coverage Extension in 3GPP LTE-Advanced," in ICC Workshops 2009,Jun. 2009, pp. 1-5.
[28] A. Papadogiannis, M. Farber, A. Saadani, M. D. Nisar, P. Weitkemper, T. M. de Moraes, J. Gora, N. Cassiau, D. Ktenas, J. Vihriala, M. Khanfouci, and T. Svensson, "Pass It on: Advanced Relaying Concepts and Challenges for Networks Beyond 4G," Vehicular Technology Magazine, IEEE, vol. 9, pp. 29-37, 2014.
[29] G. Weisi and T. O'Farrell, "Relay Deployment in Cellular Networks: Planning and Optimization," Selected Areas in Communications, IEEE Journal on, vol. 31, pp. 1597-1606, 2013.
[30] A. Bou Saleh, S. Redana, J. Hämäläinen, and B. Raaf, "On the Coverage Extension and Capacity Enhancement of Inband Relay Deployments in LTE-Advanced Networks," Journal of Electrical and Computer Engineering, vol. Article ID 894846, 2010.
[31] Q. Yu, H. Asplund, J. E. Berg, and G. Zhiheng, "Non-Line-of-Sight 2.6GHz Relay Backhaul Channel Performance: Field Test and Analysis," in Vehicular Technology Conference (VTC Fall), 2012 IEEE, 2012, pp. 1-5.
[32] J. M. Conrat, C. Quang Hien, I. Maaz, and J. C. Cousin, "Path loss model comparison for LTE-Advanced relay backhaul link in urban environment," in European Conference on Antennas and Propagation (EuCAP), The Hague, 2014.
[33] I. Maaz, J. M. Conrat, and J. C. Cousin, "Path loss models in LOS conditions for relay mobile channels," in European Conference on Antennas and Propagation (EuCAP), The Hague, 2014.
[34] I. Maaz, J. M. Conrat, and J. C. Cousin, "Path Loss Models in NLOS Conditions for Relay Mobile Channels," in Vehicular Technology Conference (VTC Fall), Vancouver, 2014.
[35] I. Maaz, J. M. Conrat, and J. C. Cousin, "Channel Model Validation for the Relay-Mobile Link in Microcell Environment," in Vehicular Technology Conference (VTC Fall), Boston, 2015.
[36] M. Grech, "Metro cells: A cost effective option to meeting growing capacity demand," Alcatel Lucent, Bell Labs Business Modelling, Mar., 2012.
[37] http://www.3gpp.org/Release-12
[38] D. Feng, L. Lu, Y. Yuan-Wu, G. Y. Li, S. Li and G. Feng, "Device-to-Device Communications in Cellular Networks," IEEE Commun. Mag., vol. 52, no. 4, pp.49-55, April 2014.D. Feng, L. Lu, Y. Yuan-Wu, G. Y. Li, S. Li and G. Feng, "Device-to-Device Communications in Cellular Networks," IEEE Commun. Mag., vol. 52, no. 4, pp.49-55, April 2014.
[39] G. Fodor, E. Dahlman, G. Mildh, S. Parkvall, N. Reider, G. Miklos, and Z. Turanyi, "Design aspects of network assisted device-to-device communications," IEEE Commun. Mag., vol. 50, no. 3, pp. 170–177, 2012.
[40] K. Doppler, M. Rinne, C. Wijting, C. B. Ribeiro and K. Hugl, "Device-to-Device Communication as an Underlay to LTE-Advanced Networks", IEEE Communications Magazine, Dec. 2009.
[41] L. Lei, Z. Zhong, C. Lin and X. S. Shen, "Operator Controlled Device-to-Device Communications in LTE-Advanced Networks", IEEE Wireless Communications, June 2012.
[42] D.-Q. Feng, L. Lu, Y. Yuan-Wu, G. Y. Li, G. Feng, and S.-Q. Li, "Device-to-device communications underlaying cellular networks," IEEE Trans. Commun., vol. 61, no. 8, pp. 3541-3551, 2013.
[43] C.-H. Yu, K. Doppler, C. Ribeiro, and O. Tirkkonen, "Resource sharing optimization for device-to-device communication underlaying cellular networks," IEEE Trans. Wireless Commun., vol. 10, no. 8, pp. 2752 –2763, 2011
[44] B. Kaufman and B. Aazhang, "Cellular networks with an overlaid device to device network," in Proc. IEEE 42nd Asilomar Conf. on Signals, Syst. and Comput., 2008, pp. 1537–1541.

[45] T. Chen, G. Charbit, and S. Hakola, "Time hopping for device-to-device communication in LTE cellular system," in Proc. IEEE Wireless Commun. and Networking Conf. (WCNC' 10), Apr. 2010, pp. 1 –6.

[46] H. Min, W. Seo, J. Lee, S. Park, and D. Hong, "Reliability improvement using receive mode selection in the device-to-device uplink period underlaying cellular networks," IEEE Trans. Wireless Commun., vol. 10, no. 2, pp. 413–418, 2011.

[47] M. Zulhasnine, C. Huang, and A. Srinivasan, "Efficient resource allocation for device-to-device communication underlaying lte network," in Proc. IEEE 6th Int. Conf. on Wireless and Mobile Computing, Networking and Commun. (WiMob' 10), 2010, pp. 368–375.

[48] M. Wellens, "Evaluation of spectrum occupancy in indoor and outdoor scenario in the context of cognitive radio", CrownCom 2007, Aug. 2007, Orlando, Florida.

[49] D. West et al., Introduction to graph theory. Upper Saddle River, NJ: Prentice Hall, 2001.

[50] H. Min, W. Seo, J. Lee, S. Park, and D. Hong, "Reliability improvement using receive mode selection in the device-to-device uplink period underlaying cellular networks," IEEE Trans. Wireless Commun., vol. 10, no. 2, pp. 413–418, 2011.

[51] D.-Q. Feng, L. Lu, Y. Yuan-Wu, G. Y. Li, G. Feng and S.-Q. Li, "User selection based on limited feedback in Device-to-Device Communications", Proc. IEEE PIMRC'13, London, UK, Sept., 2013.

[52] D.-Q. Feng, L. Lu, Y. Yuan-Wu, G. Y. Li, G. Feng and S.-Q. Li, "Optimal resource allocation for Device-to-Device communications in fading channels", Proc. IEEE GLOBECOM'13, Dec., Atlanta, 2013.